Optimization for Integrated Electricity and Gas Systems Considering Uncertainties (Alternative Format Thesis)

Zhao, Pengfei

Award date:
2021

Awarding institution:
University of Bath

Optimization for Integrated Electricity and Gas Systems Considering Uncertainties

By
Pengfei Zhao

Thesis submitted for the degree of

Doctor of Philosophy

in

Department of Electronic and Electrical Engineering

University of Bath

December 2020

Signature …… Date ……

Contents

Abstract

In recent years, there is an increasing need for the integration of multi-energy vectors with the traditional power systems due to energy decarbonization and the booming coupling technologies. Integrated electricity and gas system (IEGS) plays a vital part in the modern energy provision through coordinating supply, conversion, storage and consumption. Although the interaction between electricity and gas systems facilitates the economic performance and security, it raises computational and modelling challenges for analysis and accurate modelling of the emerging IEGS. The optimal operation of IEGS is one most significant research topic to ensure the economic and reliable perspectives of IEGS. Nevertheless, the uncertainties introduced from renewable energy resources (RES), integration of smart grid technologies and natural disasters will affect the economic operation and destroy the energy infrastructures. For instance, underestimated uncertain renewable generation could cause network congestion and overestimated renewable generation will lead to a lack of energy supply. Accordingly, non-optimal and even infeasible solutions will be yielded.

This thesis studies the centralized and coordinated operation of IEGS under different types of uncertainties which contributes to optimal operation schemes of IEGS for the economic, reliable, resilient and sustainable perspectives. The proposed studies will greatly contribute to efficient and economic-effective IEGS operation schemes and related industrial applications in the presence of inevitable uncertainties and disasters. The main achievements of this research can be summarized as follows:

(1) This work proposes a two-stage distributionally robust operation model for integrated water-energy systems in a distribution level considering wind uncertainty. The optimization aims to minimize the total operation cost of the overall system. The presence of wind uncertainty inevitably leads to risks in decision making. Accordingly, a coherent risk measure, i.e., conditional value-at-risk, is combined with the optimization objective to determine risk-aversion operation schemes.

(2) To alleviate the impacts of seismic events on both power lines and gas pipelines of IEGS. A two-stage distributionally robust optimization (DRO) model is proposed to enhance the resilience for an IEGS, where the damage on both power lines and gas pipelines are considered. The seismic activities are regarded as uncertain events and the random damage on power lines and pipelines are regarded as uncertainties, which are handled by DRO. A novel model to assess the performance of IEGS against seismic attacks is developed. This damage quantification builds a probabilistic model and estimated by damage scenarios. The proposed novel DRO framework avoids specifying uncertainty distributions but only uses moment information, which is more practical considering that it is normally not possible to gather a sufficiently large amount of distributional information for extreme events.

(3) To address the adverse impact caused by the high integration of intelligent data technologies in IEGS, a two-stage risk mitigation strategy to address the uneconomic operation of IEGS under false data injection attacks (FDIA) considering renewable

generation uncertainties. The FDIA mitigation scheme conducts the day-ahead and real-time operation, which is more powerful and convenient to be used by system operators to ensure the efficiency and security of the IEGS. FDIA is assumed to attack both electricity and gas meter readings, including i) load measurement of electricity and gas systems and ii) gas density measurement. Uncertainties of renewable resources are considered in the proposed model as they can worsen system operation conditions during FDIA.

(4) The high penetration of renewable generation poses severe challenges to Volt/VAR optimization because of its output uncertainties, leading to voltage deviation and fluctuation. To resolve unacceptable voltage deviation under energy system interdependency, a novel coordinated two-stage multi-objective optimization is proposed for voltage control in the operation of IEGS, considering uncertain renewable generation and multi-vector energy system integration. The optimal voltage is achieved through efficiently coordinating the operation of on-load tap changers (OLTC), photovoltaic systems, and shunt capacitor banks. A conic tractable form with the dual formulation is transformed from the original problem and solved by constraint generation algorithm (CGA).

(5) To investigate the optimal coordinated operation of energy infrastructures in IEGS meanwhile ensure the gas quality, a co-optimization for both gas quality and system operation in an IEGS is proposed. The renewable uncertainty is captured by DRO approach with Kullback-Leibler (KL) divergence-based ambiguity set to ensure both the system robustness and tractability. The key indices to quantify the gas quality include gross calorific value (GCV), specific gravity (SG), Wobbe Index (WI), and Combustion Potential (CP). Apart from ensuring the indices to meet the related standards, the injected gas from power-to-gas (P2G) facility to gas system is mixed with nitrogen and Liquid Petroleum Gas (LPG) for maintaining the overall gas quality.

Keywords: **Cyber-attacks; distributionally robust optimization; integrated electricity and gas system; gas quality; renewable energy resources; resilience; uncertainty.**

Acknowledgements

First and foremost, I would like to express my respectful gratitude to my supervisors, Dr. Chenghong Gu, Dr. Ignacio Hernando-Gil and Dr. Kang Ma, for the patience and consistent support they have shown to me.

I would like to take this opportunity to thank my colleagues, Prof. Furong Li, Dr. Ran Li, Dr. Xiaohe Yan, Dr. Da Huo, Dr. Yuankai Bian, Dr. Hantao Wang for their willingness to share knowledge with me and provide me useful resources.

I would also like to thank all my colleagues and friends in the University of Bath, including Miss Wangwei Kong, Mr. Xinhe Yang, Mr. Haiwen Qin, Miss Lanqing Shan, Mr. Yichen Shen, Mr. Mike Brian Ndawula and Mr. Shuangqi Li. I am sincerely grateful for their support over years.

In addition, special thanks should be given to the lovely people in my life, which are listed below:

I appreciate the academic support from **Dr. Xi Lu** (academic visitor from Hong Kong Polytechnic University) on distributionally robust optimization (DRO). He has provided enormous and selfless help to me based on his innovative research outcome. He contributes significantly on the economic dispatch model via adopting the innovative DRO. Honestly, it would take me years to master this cutting-edge DRO approach without him. Hopefully I can be an outstanding researcher like him in the future, i.e., hard-working, critical-thinking and never give up.

As my senior colleagues, **Dr. Xiaohe Yan** and **Dr. Da Huo** are also supervised by Dr. Chenghong Gu. I would like to thank for their encouragement and experience shared with me on my research. They are always my role model since the first day I became a PhD student. I will still follow the research spirit and life attitude from them.

I would like to express my gratitude to **Mr. Zhe Lin, Mr. Kaixuan Chen, Mr. Likai Liu, Mr. Yan Cui, Mr. Yingtian Chi, Dr. Pengwei Cong, Dr. Tao Zhang, Dr. Xuetao Xing, Dr. Haocheng Luo, Dr. Xiaoyu Duan and Dr. Yiwei Qiu** for their help when I was an academic visitor in 2019, Smart Grid Operations and Optimization

Laboratory (SGOOL) at Tsinghua University. They are the top researchers in the world and each of them are the absolute expert on specific areas. However, they are really humble and willing to spend so much time with me. They took me to explore every corner of Tsinghua University and helped me with my lunch and workout every single day. I have learned so much from each of them and I will definitely go back to SGOOL when I am available in Beijing.

Great appreciate should be given to **Dr. Zechun Hu** who has given me the opportunity to visit and work in Tsinghua University. He is an experienced professor with the most research outcomes among all the researchers I know. He is also a kind senior colleague who has given me advice on my research ideas and career plans. Definitely I hope to be an extrordinary professor like him in the future. He is always my role model.

I would like to thank for **Dr. Yue Xiang** for inviting me to participate in the 'Young Scholar Forum' hosted by Sichuan University. I have got to know what is the real working conditions for a young professor in one of the top universities. Apart from that, he always shared with me his suggestions on my career. If I am qualified, I am looking forward to collaborate with him in the future when I am settled down in Shanghai.

I would also like to thank for **Dr. Jianwei Li**, who has given me so much advice on career plans. His previous research experience in Beijing Institute of Technology and University of Oxford provides me a very useful guideline on my career decision between UK, Beijing and Shanghai.

Even if **Dr. Ignacio Hernando-Gil** (Nacho) has left Bath and cannot supervise me anymore, I will never forget his warm smile and patient supervision on my PhD. His warm smile is like the bright sunshine in the early morning. In addition to the study, I learned so much on greetings, etiquette and how to treat friends well and sincerely from him. I have to mention that his clothing style is absolutely awesome! Before I know him, I have never seen a researcher like him who is handsome, gentlemanly and all-rounded. Without him, I cannot be accepted as a PhD student. He is willing to permit my application when I was helpless and hopeless. Also, the research topic he assigned to me, i.e., optimization of microgrid, is the basis of my success on research. Genuinely, him and Dr. Gu give me the biggest support. I will always miss Nacho and thank him for everything he has done.

Without **Dr. Zhidong Cao**, I cannot fully concentrate on my research. He offered me with the most ideal, satisfied and decent research position before my graduation. I am so thankful and hornored to be a member of Chinese Academy of Sciences. In particular, I am delighted to join his team. I cannot wait to head to the lab and start my career. And I promise I will be dedicated to the work and contribute all of me to our lab.

Life cannot be only fulfilled by research. **Miss Xiaoyu Feng,** who is an expert on psychology and finance has greatly changed my attitude on life, study and career. She is my senior classmate in Chenjinglun High School. I learned a lot from her on who am I, where I am from and where I am going to, as well as how to enjoy life. She drove me every time when we hang out and I realized how grateful your friends will be if you treat them genuinely. I am so grateful to her and definitely we are friends for ever.

In addition, I sincerely thank for my dear friends **Yue Wang**, **Naixuan Li**, **Jiawen Dan**, and **Huan Lai** for their help and concern on my spare time apart from work, which enriches my life and is accordingly effective for my research.

My dear parents, **Mr. Jianzhong Zhao** and **Ms. Hongxia Wang**. You are the two most thankful people in my entire life. You do not know how much I miss you and how much I wish I could stay with you. You gave me a happy childhood, an enviable family and so many enviable opportunities on everything. You always say the smartest decision we made together is my PhD study at University of Bath. And you hope to make another wise decision on my marriage. You always urge me to have my own family and have a smart baby. I promise that is also my biggest wish and my next generation will be a better researcher. I know you miss me more as you always do. And I swear after this virus outbreak and my graduation, we will always be together. I will treat you much better as you did to me. Please be patient and your son will come back to you.

Most importantly, thank you to my best friend and beloved girlfriend **Yixuan Zhao**, for always being there for me. She is the perfect girl I could ever dream of having as my girlfriend. She is beautiful, passionate, optimistic and unique, always wearing a sweet smile. In particular, we have spent happy moments together, studying in libraries and café. The majority of the thesis is proposed with her company. Arriving at this point would not have been possible without the stability and love she provided me, and thus, I will be forever grateful to her.

Dr. Chenghong Gu is the last and most wanted person I want to show my gratitude. I am so lucky to be his student. I believe everything is under destiny as I was not his student from the very beginning. He was willing to accept me when I lost supervisor Nacho. He treated me much better than any other students. I have more than five times of publications than a normal PhD student. And he still gave me enough patience on modifying every single word on my papers. Besides, he helped me to connect with many Chinese senior researchers, study in Tsinghua University, join in the research forum in Sichuan University and even help with my career. The biggest effort from him is the innovative topic he has chosen to me and he was so selfless that he taught the 'gas quality management' to me, which further generates the 'VVP/VPO'. This is able to contribute numerous papers and I am lucky to develop a new concept. Every day I work hard since I do not want to let him down. Sir, you are my biggest motivation which stimulates all my publications. Tears flowing down my cheeks once again and all the acknowledgement words cannot fully express my appreciation to Dr. Gu. Dear Sir, I wish I could be an excellent researcher and a responsible supervisor like you. You are always my respectful and beloved mentor.

List of Figures

List of Tables

List of Abbreviations

Renewable energy sources	RES
Combustion potential	CP
Conditional value-at-risk	CVaR
Coefficient of Performance	CoP
Chance-Constrained Programming	CCP
Combined Heat and Power	CHP
Distributionally robust optimization	DRO
Distributed generation	DG
Demand Response	DR
Distributed Energy Resources	DER
Energy Storage Systems	ESS
Electric Vehicle	EV
Energy internet	EI
False data injection attack	FDIA
Gas Furnace	GF
Ground Source Heat Pump	GSHP
Gross calorific value	GCV
Integrated energy system	IES
Integrated electricity and gas system	IEGS
Information and communication technology	ICT
Integrated water-energy nexus systems	IWENS
Kullback-Leibler	KL
Liquid Petroleum Gas	LPG
Mixed Integer Linear Programming	MILP
On-load tap changer	OLTC

Power-to-gas	P2G
Peer-to-Peer	P2P
Probability Density Function	PDF
Particle Swarm Optimisation	PSO
Robust optimization	RO
Stochastic optimization	SO
Semidefinite programming	SDP
Second-order cone program	SOCP
State of Charge	SOC
Specific gravity	SG
Time-of-use	TOU
Volt-var optimization	VVO
Wobbe index	WI

List of Publications

First-authored papers

1. P. Zhao, Y. Shen, C. Gu, F. Teng, X. Xu and S. Li, ”Data-Driven Moment-Based Multi-Energy Investment and Management under Earthquakes”, in ***IEEE Transactions on Industrial Informatics,*** doi: 10.1109/TII.2020.3043086.
2. P. Zhao, C. Gu, Z. Hu, X. Zhang, X. Chen, I. Hernando-Gil and Y. Ding, " Economic-Effective Multi-Energy Management with Voltage Regulation Networked with Energy Hubs,” in ***IEEE Transactions on Power Systems***, doi: 10.1109/TPWRS.2020.3025861.
3. P. Zhao, X. Lu, C. Gu, Q. Ai, H. Liu, Z. Cao, Y. Bian and S. Li. " Volt-VAR-Pressure Optimization of Integrated Energy Systems with Hydrogen Injection," in ***IEEE Transactions on Power Systems***, doi: 10.1109/TPWRS.2020.3028530.
4. P. Zhao, C. Gu, Q. Ai, Y. Xiang, T. Ding and S. Li. “ Water-Energy Nexus: A Mean-Risk Distributionally Robust Co-Optimization of District Integrated Energy Systems,” in ***IEEE Transactions on Power Systems***, doi:10.1109/TPWRS.2020.3038076 .
5. P. Zhao, C. Gu, Z. Hu, D. XIE, I. Hernando-Gil and Y. Shen, "Distributionally Robust Hydrogen Optimization with Ensured Security and Multi-Energy Couplings," in ***IEEE Transactions on Power Systems***, doi: 10.1109/TPWRS.2020.3005991.
6. P. Zhao, C. Gu and D. Huo, "Two-Stage Coordinated Risk Mitigation Strategy for Integrated Electricity and Gas Systems under Malicious False Data Injections," in ***IEEE Transactions on Power Systems***, doi: 10.1109/TPWRS.2020.2986455.
7. P. Zhao, C. Gu, D. Huo, Y. Shen and I. Hernando-Gil, "Two-Stage Distributionally Robust Optimization for Energy Hub Systems," in ***IEEE Transactions on Industrial Informatics***, vol. 16, no. 5, pp. 3460-3469, May 2020.
8. P. Zhao, C. Gu, Z. Cao, D. Xie, F. Teng, J. Li, X. Chen, C. Wu, D. Yu, X. Xu and S. Li, "Designing a Cyber-Secured Water-Energy Nexus," in ***IEEE Transactions on Power Systems***, doi: 10.1109/TPWRS.2020.3043757.
9. P. Zhao, C. Gu, Y. Ding, Y. Bian and S. Li. “Cyber-Resilience Enhancement and Protection for Uneconomic Power Dispatch under Cyber-Attacks,” in ***IEEE Transactions on Power Delivery***, doi:10.1109/TPWRD.2020.3038065.
10. P. Zhao, C. Gu, Y. Xiang, X. Zhang, Y. Shen and S. Li, "Reactive Power Optimization in Integrated Electricity and Gas Systems," in ***IEEE Systems Journal***, doi: 10.1109/JSYST.2020.2992583.
11. P. Zhao, H. Wu, C. Gu, and I. H. Gil, "Optimal Home Energy Management under Hybrid PV-Storage Uncertainty: A Distributionally Robust Chance-Constrained Approach," ***IET Renewable Power Generation***, vol. 13, no. 11, pp. 1911-1919, 19 8 2019.
12. Zhao, P., Gu, C., Cao, Z., Xiang, Y., Yan, X. and Huo, D., 2020, September. A two-stage data-driven multi-energy management considering demand response. In Adjunct Proceedings of the 2020

ACM International Joint Conference on Pervasive and Ubiquitous Computing and Proceedings of the 2020 ACM International Symposium on Wearable Computers (pp. 588-595).

13. P. Zhao, I. Hernando-Gil and H. Wu, "Optimal Energy Operation and Scalability Assessment of Microgrids for Residential Services," 2018 IEEE International Conference on Environment and Electrical Engineering and 2018 IEEE Industrial and Commercial Power Systems Europe (EEEIC / I&CPS Europe), Palermo, Italy, 2018, pp. 1-6, doi: 10.1109/EEEIC.2018.8493765.

Co-authored papers

14. S. Li, C. Gu, P. Zhao, S. Cheng, 'Adaptive energy management for hybrid power system considering fuel economy and battery longevity', ***Energy Conversion and Management***, Volume 235, 2021, 114004, ISSN 0196-8904.

15. Y. Shen, C. Gu, X. Yang and P. Zhao, "Impact Analysis of Seismic Events On Integrated Electricity and Natural Gas Systems," in IEEE Transactions on Power Delivery, doi: 10.1109/TPWRD.2020.3017050.

16. S. Li and P. Zhao, 'Big data driven vehicle battery management method: A novel cyber-physical system perspective', ***Journal of Energy Storage***, Volume 33, 2021, 102064, ISSN 2352-152X.

17. Cao Z, Zhao P, Liu J, et al. A spatial point pattern analysis of the 2003 SARS epidemic in Beijing[C]//Proceedings of the 3rd ACM SIGSPATIAL Workshop on Emergency Management using. ACM, 2017: 1.

18. Y. Shen, C. Gu, Z. Ma, X. Yang and P. Zhao, "A Two-Stage Resilience Enhancement for Distribution Systems Under Hurricane Attacks," in IEEE Systems Journal, vol. 15, no. 1, pp. 653-661, March 2021, doi: 10.1109/JSYST.2020.2997186.

19. Zhu, F, Fu, J, Zhao, P, Xie, D. Robust energy hub optimization with cross-vector demand response. ***Int Trans Electr Energ Syst***. 2020; 30:e12559. https://doi.org/10.1002/2050-7038.12559.

20. S. Li, H. He, C. Su, and P. Zhao, "Data driven battery modeling and management method with aging phenomenon considered," Applied Energy, vol. 275, p. 115340, 2020/10/01/ 2020, doi: https://doi.org/10.1016/j.apenergy.2020.115340.

21. M. B. Ndawula, P. Zhao and I. Hernando-Gil, "Smart Application of Energy Management Systems for Distribution Network Reliability Enhancement," *2018 IEEE International Conference on Environment and Electrical Engineering and 2018 IEEE Industrial and Commercial Power Systems Europe (EEEIC / I&CPS Europe)*, Palermo, 2018, pp. 1-5.

22. Shen Y, Gu C, Zhao P. Structural Vulnerability Assessment of Multi-energy System Using a PageRank Algorithm[J]. Energy Procedia, 2019, 158: 6466-6471.

Chapter 1

Introduction

This chapter introduces the background, motivation, objectives, and contributions of the research. The structure of the thesis is also outlined.

1.1 Research background

1.1.1 Transition to 'Net Zero Emissions' Target

The environmental challenges are becoming unignorable with the increasing usage and depletion of traditional energy resources. Global warming and greenhouse gas emissions have become the two most serious and concerning issues in the 21st century, which arouse the attention of the public and government all around the world. The average temperature of the global surface has increased by 0.74 degrees in the last 50 years according to [1]. As is shown in Fig. 1-1, global carbon emission has significantly increased by 90% since 1970 [2]. Paris Agreement [3] has been agreed and signed by many countries, which was the first full global agreement to deal with climate change, aiming at controlling the temperature increase below 2 degrees.

To limit the increasing trend of temperature, the UK has led the global effort and become the first major country to achieve the 'Net Zero Emissions' target by 2050 [4]. Net zero is referred as the emission can be balanced via offset measures [5], e.g., planting trees, applying advanced energy technologies and strategies. In 2020, the greenhouse gas emissions were 51% below the level of 1990. This milestone was achieved after a dramatic 11% decrease of greenhouse gas emissions compared with 2019, which is largely owing to the outbreak of COVID-19 [6]. Fig. 1-2 presents the opposite trend of the economy and emissions [4]. In Fig. 1-3, the progress of emission

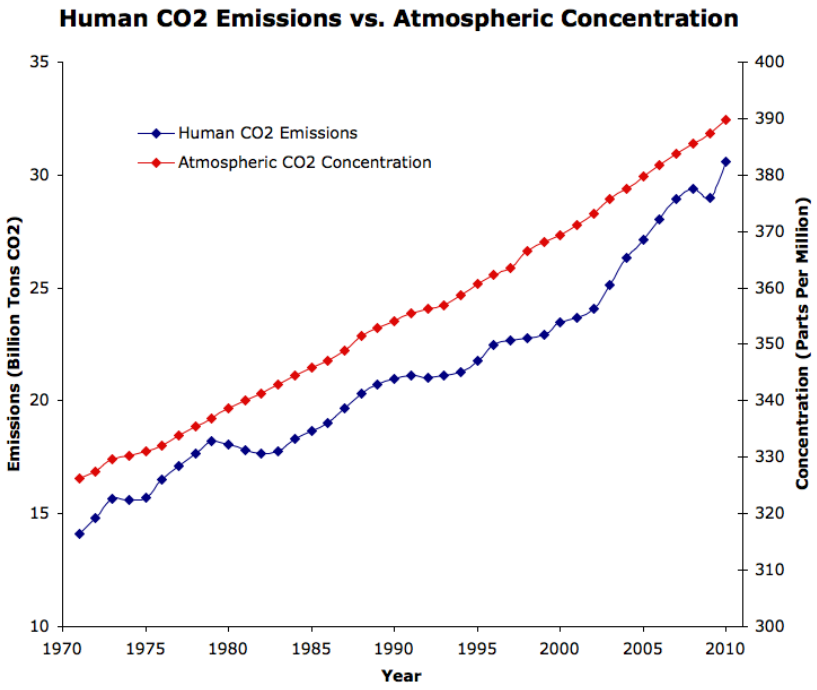

Fig. 1-1. The emission level of carbon dioxide [2].

reduction in different sectors is given. [5] To achieve the 'Net Zero Emissions' target, the UK government has taken the measures including:

Reducing coal-fired power generation: The UK government aims to eliminate all thermal power plants by 2025 to achieve carbon reduction targets [7]. Alternative energy sources include solar, wind, nuclear, natural gas and hydropower. An emission reduction test was designed in May 2019. During the two weeks, on average, nearly 40% of the electricity supply in the UK was from natural gas, 20% from nuclear power generation, 13% from wind power generation, and the rest came from other generations. It is estimated that the last coal-fired power plant will be closed by 2022 [8].

Carbon capture technology: The government provides strong support for the promotion of carbon capture technologies such as carbon capture and storage (CCS),

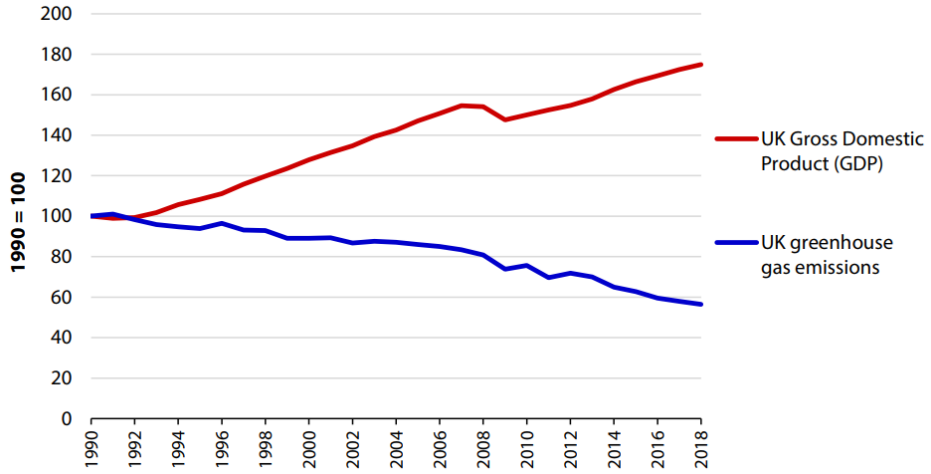

Fig.1- 2. UK realizes falling emissions with a growing economy [4].

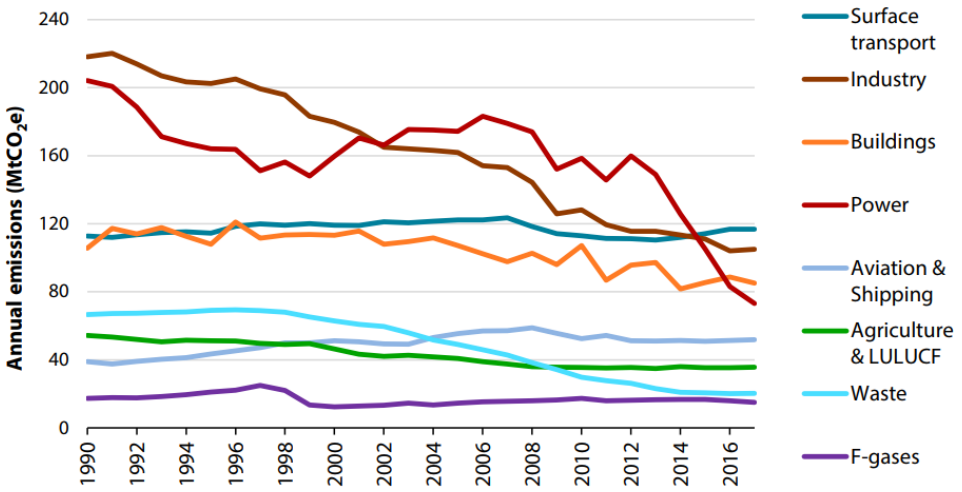

Fig.1- 3. The progress of emissions reduction in different sectors [4].

carbon capture and utilisation (CCU) and carbon capture, utilisation and storage (CCUS). The industries have received government funding of 26 million pounds for carbon capture projects. CCUS aims to encourage industries to capture up to 70,000 tons of carbon dioxide each year, which is used for industrial applications [8].

Renewable energy adoption: In the last five years, one-third of the UK's fossil fuel-based power generation capacity has been decommissioned. However, the installed capacity of wind, solar, biomass, and hydropower have been tripled to 42GW. Renewable energy accounts for the largest share of the UK's installed power generation capacity, surpassing the 40.6GW installed capacity of fossil fuels. Wind power accounts for the largest share of renewable energy, with more than 20GW; solar power comes second with more than 13GW; biomass energy ranks third with 3.2GW [9].

1.1.2 Renewable Curtailment

Based on the global energy statistics [10], it anticipates that the share of renewable power generation will be nearly doubled globally, i.e., from 26% in the current level to 44% by 2040. And it is possible to overpass coal before 2026. Particularly, the share of combined wind and solar generation could potentially increase from 7% to 24% in the world. In comparison with the renewable generation share, the traditional generation share falls sharply from 67%. In particular, the share of coal's generation, which surges 5 times from 1970 to 2013, would decline from the current 38% to 25% by 2040. And the gas-fired generation is predicted to increase rapidly to approximately 50% by 2040 due to the increasingly cheap price of gas sources [11].

In the UK, the large deployment of renewable energy resources causes curtailment problems, which causes the waste of renewable generation and economic losses. The wind curtailment is 3.6TWh in 2020 in the UK [12]. The potential reasons for renewable energy curtailment can be listed:

- The congestion of power systems affects the feed of power to users.
- The inflexible plants such as nuclear plants cannot be flexibly controlled to provide renewable energy.
- The growth of renewable capacity will lead to over-capacity issues when the demand is low.

1.1.3 Energy Internet

The concept of Energy Internet (EI) has been put forward by Jeremy Rifkin in 2011, which aims to make full use of the distributed renewable energy resources and thus improve the energy utilization efficiency [13]. The report pointed out that the final aim of the EI is to establish the realization of interdependent energy systems which facilitate the penetration of distributed renewable energy resources [14]. The achievement of EI requires the strong integration of power, gas, heating, cooling and water systems, with the supplement of energy storage technologies. The UK National Energy and Climate Plan strengthens the importance of developing and creating modern, integrated and low carbon energy systems [15]. In 2018, the Chinese government put forward a guideline for developing EI-based integrated energy systems and encouraged the applications and constructions of modern energy platforms [16]. Overall, the rising research and application attention on EI has motivated the associated modelling and operation research of EI.

1.1.4 Integrated Energy Systems

The power system is the most vital part of EI, facilitated by the smart grid and multi-energy technologies to achieve the coordination and complementation of each subsystem. Meanwhile, interdependent energy converters are also increasingly gaining attention, such as combined heat and power (CHP), power-to-gas (P2G) and gas turbine, etc. These conversion technologies enhance the couplings of subsystems and aggregate them into an efficient energy entity incorporating energy production, transmission, distribution, conversion, storage and usage. Integrate energy system (IES) is composed of multi-energy systems and renewable energy sources which are interconnected by coupling devices [17-19]. It improves energy efficiency compared with independent energy systems. Accordingly, the system economy, security, reliability and flexibility are strengthened. In addition, the excessive renewable generation can be accommodated within the IES. The aforementioned energy conversion technologies can tighten the couplings of different subsystems. For instance, CHP facilitates the interconnection between gas, power and heating systems [20]; P2G facilitates the interconnection between power and gas systems [21], and electric vehicles (EVs) enhance the interconnection between power and transportation systems [22]. Apart from the energy infrastructures, the optimal coordination between each energy vector also depends on

the advanced energy management schemes. The operation algorithm of IES will further improve the system economic efficiency and reliability through comprehensively coordinating the energy infrastructures.

Gas-fired generation has gradually taken the place of coal-fired generation due to the lower price, lower emission and high reliability of natural gas [23]. In addition, the advancing techniques in the gas industry further impact the electric power industry. The high integration of renewable resources brings security issues to power systems due to its variability and fluctuation. However, the integration of a gas system counteracts the resulted negative effects thanks to the slow inertia characteristic of natural gas [24]. Accordingly, the high integration of natural gas is becoming the trend of IES, which introduces the concept of integrated electricity and gas system (IEGS). In the UK, granted by the government, modelling and building real IEGS is given sufficient attention by Supergen, HubNet and other research associations for the energy transition [25]. The Adaptation and Resilience in Energy Systems (ARIES) project conducted by the University of Edinburgh aims to develop new methods to model the system vulnerabilities under the climate change for IEGS [26]. The project Horizon 2020 MAGNITUDE is expected to identify flexibility options from synergies between power, gas, heating and cooling systems and also support the integration of renewable energy sources to achieve a cost-effective energy system [27]. CHP and gas turbines are widely utilized for coupling the power and gas systems in the existing IEGS projects. However, the energy flow is unidirectional, i.e., from a gas system to the power system. P2G is a promising technology, which enables to convert excessive renewable power output from the power system to the gas system and thus achieve the bidirectional energy flow in IEGS [28, 29]. However, most P2G projects are at the experimental stage and the application is few.

1.1.5 Research Motivation

Due to the energy crisis, pollution issues and the encouragement of governments' policies, renewable industry witnesses a rapid development. The wide deployment of renewable energy sources leads to power systems facing more challenges on secure system operation and power-load balance. IEGS is considered and planned to resolve the new challenges based on the significant coordination and complementation between

power and gas systems. Accordingly, accurate and feasible mathematical modelling, strengthening energy integration, facilitating renewable integration are the key elements.

This thesis focuses on investigating the benefits and challenges of economic efficiency, security and sustainability due to the integration of power and gas systems. This thesis aims to resolve the following five problems:

i) The renewable uncertainty turns the operation of IEGS into a stochastic and complicated optimization problem. The economic performance of the IEGS operation needs to be guaranteed pertaining to the variation of renewable power generation.

ii) Natural disasters can cause huge power losses of energy systems that threaten the economy. Enhancing resilience to withstand seismic hazards and mitigate resulting damages is of great value for IEGS.

iii) With the extensive deployment of digital communication technologies, IEGS is under extensive exposure to information and communication technology (ICT). The adversary can launch false data injection attacks (FDIA) to tamper critical data and inject falsified data, which brings serious challenges to state estimators, indirectly affecting system operation and control.

iv) Due to the variable and intermittent nature renewable energy penetration, it poses operational and security challenges to voltage profile by affecting normal operations of on-load tap changer (OLTC) and capacity banks in IEGS.

v) P2G enables the conversion from electric energy to hydrogen and synthetic natural gas, accordingly achieving bidirectional energy flows for tighter couplings in IEGS. However, the injection of hydrogen could impact gas quality since gas composition fundamentally changes, adversely effecting the combustion, safety and lifespan of appliances.

1.2 Research Contributions

This thesis contains research contributions as follows:

- *Energy structure:* The innovative energy structures of IEGS and IWENS designed for economic effective, resilient, reliable and sustainable

functionalities are extensively modelled. It aggregates considerable interconnections and converters among subsystems, e.g., gas turbines, P2G facilities, CHP, GF, GSHP, water pumps and electric boilers. The enormous interdependencies and interactions between energy sectors are beneficial for improving economic efficiency and sustainability.

- *Uncertainty modelling*: Two-stage DRO models are applied to optimize operation and planning schemes. It is the first attempt to combine DRO with mean-risk optimization. The benefits are in threefold: i) it overcomes the shortages of SO and RO by using partial distributional information with moderate robustness, ii) the KL divergence-based ambiguity set can flexibly shape the considered candidate distributions compared with moment-based ambiguity sets and accordingly yields less-conservative results and iii) the trade-off between economic performance and risk can be realized based on the incorporation of Conditional Value at Risk (CVaR) on the objective function.

- *Resilience enhancement:* A two-stage earthquake-resilient co-optimization model is established, incorporating both planning and operation schemes, is for the first time proposed to enhance IES resilience, considering the worst-distributed seismic attack. A novel model to assess the performance of IES against seismic attacks is developed. This damage quantification builds a probabilistic model and estimated by damage scenarios. This assessment model can be easily combined with the proposed two-stage DRO model to determine the optimal enhancement plan for IES.

- *Cyber resilience*: This work models FDIA in an IEGS for the first time, particularly on natural gas load and density measurement, where existing research only focuses on FDIA on electricity systems.

- *Voltage regulation*: This paper is the first such effort to investigate VVO in an IEGS. The strong coupling of power and gas infrastructure and tight interdependency between the two systems are considered.

- *Gas quality improvement*: Four key indices are used in the economic operation of IEGS to quantify the impact of hydrogen injection from P2G on gas quality. A novel co-optimization model is developed to minimize system operation costs and maintain gas quality within an acceptable range, achieved by a mixture of nitrogen and LPG.

1.3 Thesis Layout

The rest of the thesis is organised as follows:

Chapter two is devoted to the DRO approach, where the moment-based DRO and discrepancy-based DRO are introduced, respectively. This chapter summarizes the methodology of handling uncertainties for chapters 3-7. The formulations and solution algorithms of each method are explicitly discussed.

Chapter three provides a two-stage economic operation scheme for an integrated electricity, gas and water system under the water-energy nexus with enormous interdependencies. The tight couplings and interactions between each subsystem enable the reliable and economic operation for the entire IES. Renewable uncertainty is captured by mean-risk DRO. The coherent risk measure, CVaR provides the trade-off to system operators with flexible alternatives on choosing between economic efficiency and risk. A tractable Bender's decomposition is employed to solve the problem.

Chapter four proposes a two-stage DRO method to enhance the resilience of an IEGS under seismic attacks with combined planning and operation strategies. The proposed method provides optimal hardening plans for specific power lines and gas pipelines under different seismic intensity levels and investment budgets. This method can help system operators to make economical hardening and operation strategies to improve the resilience of the IES under seismic attacks.

Chapter five designs a risk mitigation scheme for IEGS against FDIA with a two-stage DRO model. The hierarchical two-stage framework can determine both day-ahead and real-time system optimal operation schemes considering the impact of FDIA and renewable uncertainties on electricity load, gas load and gas density. A tractable semidefinite programming formulation is built for the original problem, which is solved

by constraint generation algorithm (CGA) in an iterative manner. The proposed mitigation scheme ensures the economic performance of IEGS by providing a two-stage risk mitigation scheme by implementing efficient load shedding under FDIA and renewable uncertainty.

Chapter six proposes a multi-objective optimization for minimizing both operation cost and voltage deviation of IES considering renewable power uncertainty. A two-stage data-driven DRO approach is used to solve the voltage management with dual and semidefinite (SDP) formulations to ensure computational tractability. The reformulated two-stage voltage management is solved by CGA with master and subproblems. This work can benefit integrated system operators with powerful operation tool to manage the systems with fewer costs but integrate more renewable energy.

Chapter seven presents a coordinated optimization for gas quality management and operation of IEGS in the presence of wind uncertainty is proposed. The wind uncertainty is handled by DRO with Kullback-Leibler divergence for controlling the conservatism of numerical performance. A tractable deterministic formulation is obtained and the resulted linear programming model can be efficiently solved. The proposed co-optimization for IEGS ensures both the economic performance and gas quality via coordinating traditional DGs, natural gas resources and P2G facility, which can benefit system operators with economic benefits through saving operation cost and secure gas distribution with gas quality guaranteed.

Chapter eight concludes the main findings of the thesis and the major contributions.

Chapter nine presents some potential research topics in future work.

Chapter 2

Distributionally Robust Optimization

This chapter describes the application of distributionally robust optimization method on IEGS optimization problems. The problem formulations, mathematical reformulations and solution algorithms are explicitly discussed.

Distributionally robust optimization (DRO) is developed to bridge between stochastic optimization (SO) and robust optimization (RO) [30]. In terms of uncertainty modelling, SO either relies on a vast number of samples to approximate distributions or fits data into an empirical distribution, which could be overly optimistic. RO also considers the worst case via uncertainty sets, potentially resulting in over-conservative solutions. By contrast, DRO avoids assuming a specific uncertainty distribution and yields less-conservative results [31]. DRO has simpler requirements of uncertainties and is mathematically tractable, which accommodates distributions via an ambiguity set [30]. Additionally, DRO performs better in making the best use of limited statistical data and produces less-conservative results by considering the worst expectation over all possible distributions, compared to the traditional worst-case oriented RO.

Ambiguity set is used to characterize the distributional information of uncertainties. DRO can be generally categorized into moment-based DRO and discrepancy-based DRO with respect to different types of ambiguity sets. Moment-based DRO applies the moment information, e.g., mean vectors, covariance matrices, to shape the uncertain distribution [32]. Discrepancy-based DRO measures the closeness between the reference distribution and the candidate distributions [33]. This chapter presents i) the modelling of the moment-based DRO constructed via Markov and Chebyshev ambiguity sets; ii) the modelling of discrepancy-based DRO relies on the KL-divergence. The main technical chapters, i.e., chapters 3-7, utilize DRO to handle the uncertainty modelling.

2.1 Moment-Based DRO

2.1.1 Markov Ambiguity Set

Markov ambiguity set contains all distributions with known mean information. This section proposes the modelling and solution of a two-stage DRO problem based on the Markov ambiguity set. Assume that the abstract forms of matrices and vectors are used to describe the constraints and variables. Then the ambiguity set modelling is proposed followed by Bender's decomposition as the solution algorithm.

The compact form of a two-stage optimization model can be reformulated as (2-1). The first-stage objective function is represented by $c'x$. And the expected second-stage objective function is represented by $Q(x,\xi)$. x and y are the variables of the first and second stages. The uncertain variable is denoted as ξ. The 'min-sup' structure allows

the model to make decision under the worst-case scenario. The first and second stage constraints are represented by (2-1) and (2-4), respectively.

$$\min_{x\in X} c'x + \sup_{P\in D} E_P[Q(x,\xi)] \tag{2-1}$$

$$\text{s.t. } Ax \le b, \tag{2-2}$$

$$Q(x,\xi) = \min_{y} f'y \tag{2-3}$$

$$\text{s.t. } Ex + Fy + G\xi \le h, \tag{2-4}$$

The ambiguity set containing the mean vector information is presented as (2-5).

$$D_{Markov} = \left\{ f(\xi) \middle| \begin{matrix} \mathrm{P}\{\xi \in \Xi\} = 1 \\ \mathrm{E}\{\xi\} = \mu \end{matrix} \right\} \tag{2-5}$$

In some occasions, the support Ξ is required for accommodating the uncertainties, i.e., the total number of a uncertain binary variable is fixed.

$$\Xi = \left\{ \sum \xi = N \right\} \tag{2-6}$$

The variables of the optimization problem are the probability densities in (2-5). The optimization problem contains a finite number of constraints and an infinite number of variables, which is non-tractable. By transforming it from the primal form into the dual form, the problem becomes tractable.

The second-stage objective function $\sup_{P\in D_{EL}, D_{PL}} E_P[Q(x,\xi)]$ can be represented by *S(x)*, where $P(\xi)$ is the probability density function.

$$S(x)^{primal} = \max_{P(\xi)\in D_{EL}, D_{PL}} \int_{\Xi} Q(x,\xi)\, P(\xi) d\xi \tag{2-7}$$

$$\text{s.t. } P(\xi) \ge 0, \forall \xi \in \Xi \tag{2-8}$$

$$\int_{\Xi} P(\xi) d\xi = 1 \tag{2-9}$$

$$\int_{\Xi} \xi P(\xi) d\xi = \mu \tag{2-10}$$

Based on dual theory [30], when the strong duality holds, the dual form of (2-7) is transformed to (2-11). Accordingly, the results of (2-11) are equal to those of (2-7) [34, 35]. Now, the dual form has an infinite number of constraints and a finite number of variables after the dual formulation, which is easier to solve. The dual variables Ψ and ψ_0 are associated with constraints (2-9) and (2-10).

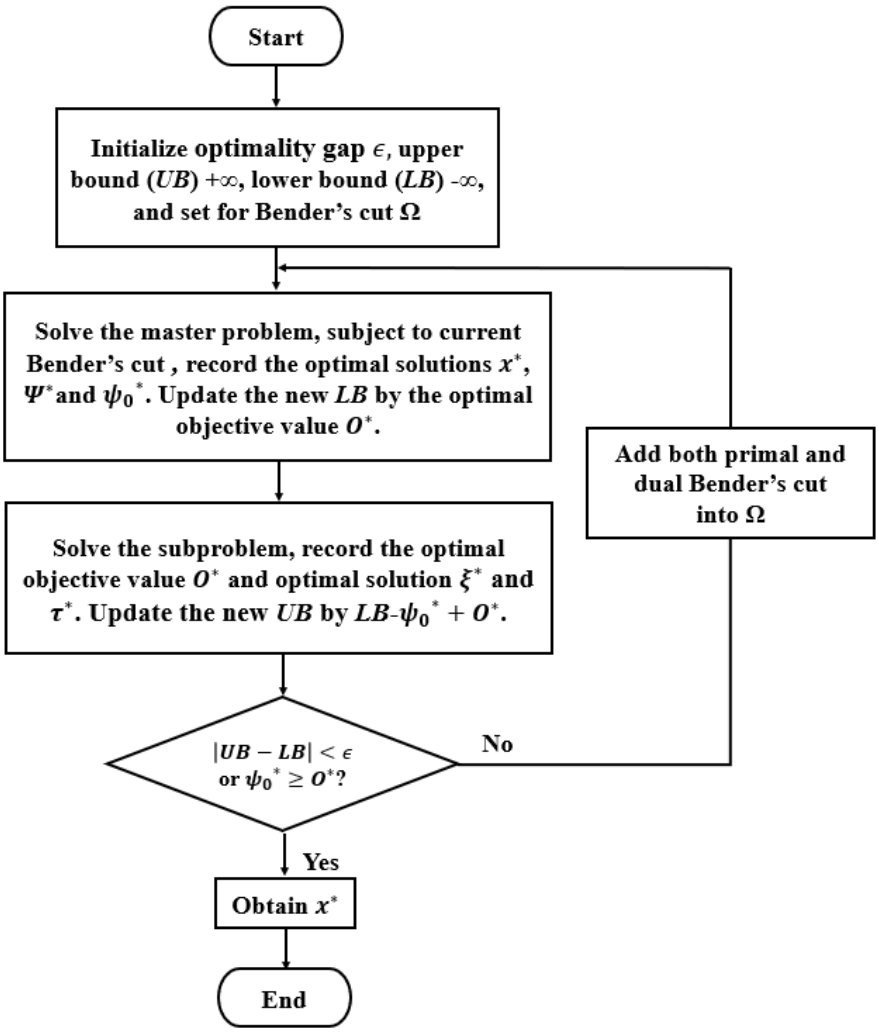

Fig. 2-1. Flow chart of bender's decomposition method.

$$S(x)^{dual} = \min_{\Psi,\psi_0} \Psi\,\mu + \psi_0 \tag{2-11}$$

$$\text{s.t. } \Psi\xi + \psi_0 \geq Q(x,\xi) \quad \forall \xi \in \Xi \tag{2-12}$$

Then, the dual formulation (2-11) is substituted into (2-1) and the following reformulations can be obtained:

$$\min_{\Psi,\psi_0} c'x + \Psi\,\mu + \psi_0 \tag{2-13}$$

$$\text{s.t. } Ax \leq b, \tag{2-14}$$

$$\Psi\xi + \psi_0 \geq Q(x,\xi), \forall \xi \in \Xi \tag{2-15}$$

Bender's decomposition is applied to solve the overall model in a master-subproblem framework, summarized in the flowchart in Fig. 2-1. Under the acceptable optimality gap, the master problem and subproblem are solved separately with the update of upper

and lower bounds. A Bender's cut is formulated and added to the set in each iteration. The set of Bender's cut becomes larger until the real gap between lower and upper bounds is smaller than the optimality gap. The master problem and primal subproblem are shown in (2-16)-(2-17) and (2-18).

$$\min_{\Psi,\psi_0} c'x + \Psi\,\mu + \psi_0 \tag{2-16}$$

$$\text{s.t. } Ax \le b, \tag{2-17}$$

$$\max_{\Psi} Q(x^*, \xi) - \Psi^*\xi \tag{2-18}$$

The new dual variable τ is introduced to represent the dual form of (2-3). Accordingly, (2-3) and (2-4) can be represented in the following closed form:

$$\max \tau'(b - Ex - G\xi_s) \tag{2-19}$$

$$\text{s.t. } F'\tau \le f, \tau \ge 0 \tag{2-20}$$

Equation (2-18) is recast as (2-21) based on the new dual variable.

$$\max \tau'(b - Ex - G\xi_s) - \Psi^*\xi \tag{2-21}$$

$$\text{s.t. } F'\tau \le f, \tau \ge 0 \tag{2-22}$$

It is worth noting that the term $\Psi^*\xi$ in (2-21) is nonlinear because it contains the product of dual variable Ψ^* and binary variable ξ. Although it can be solved by some nonlinear solvers, linearization is still required to ensure a more efficient and global solution. McCormick inequality is used to relax this nonconvex problem, where ϑ_{ij} is used to represent $\tau_i G_{ij} \xi_j$.

$$\vartheta_{ij} \ge G_{ij}\tau_i - M\left(1 - \xi_j\right) \tag{2-23}$$

$$\vartheta_{ij} \ge - M\xi_j \tag{2-24}$$

Therefore, the dual subproblem can be written as:

$$\max \tau'(b - Ex) - \vartheta - \Psi^*\xi \tag{2-25}$$

$$\text{s.t. } F'\tau \le f, \tau \ge 0 \tag{2-26}$$

$$\vartheta_{ij} \ge G_{ij}\tau_i - M\left(1 - \xi_j\right) \tag{2-27}$$

$$\vartheta_{ij} \ge - M\xi_j \tag{2-28}$$

Based on the obtained ξ^*, the primal and dual Bender's cuts can be presented in (2-29) and (2-31) respectively.

$$\psi_0 \geq f'y^* - \Psi \xi^* \tag{2-29}$$

$$Ex + Fy^* + G\xi^* \leq h, \tag{2-30}$$

$$\psi_0 \geq \tau'^*(b - Ex - G\xi^*) - \Psi \xi^* \tag{2-31}$$

2.1.2 Chebyshev Ambiguity Set

Based on the Markov ambiguity set, Chebyshev ambiguity set models the distributional ambiguity utilizing the mean and covariance matrix. The original problem can be recast as a semidefinite programming (SDP). First of all, the linear DRO problem can be epresented by a compact matrix form. Then, the family of possible uncertainty distributions is defined by an ambiguity set. Finally, the dual problem is formulated and solved by a column generation algorithm (CGA) efficiently.

Matrices and vectors are used to represent the original problem for notation abbreviation. The objective function (2-32) is to minimize the sum of the first-stage objective $c'x$ and the expected second-stage objective $E_{Pf}[Q(x,\xi)]$. The random parameter ξ is sampled from a family of distributions Pf.

$$\min_{x \in X} c'x + \sup_{Pf \in D_\xi, \xi = \Delta P_k, \xi_j} E_{Pf}[Q(x,\xi)] \tag{2-32}$$

$$\text{s.t. } Ax \leq b, \tag{2-33}$$

$$Q(x,\xi) = \min_y f'y \tag{2-34}$$

$$\text{s.t. } Ex + Fy + G\xi \leq h, \tag{2-35}$$

The first-stage constraints are shown in (2-33). Equations (2-34) and (2-35) represent the recourse function.

The uncertainties can be captured by ambiguity sets that define a family of distributions. Based on limited historical data, moment information, i.e., mean and covariance can be obtained for constructing empirical point-estimates. The proposed ambiguity set is given in (2-36) which guarantees i) the integral of distribution of ξ is 1, and ii) the second moments are known.

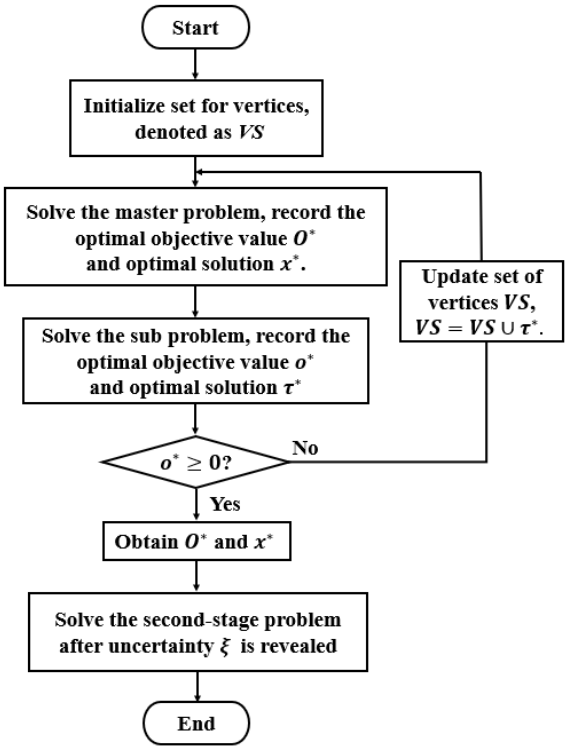

Fig. 2-2. Flowchart of constrained generation algorithm.

$$D = \left\{ f(\xi) \left| \begin{array}{c} \mathrm{P}\{\xi\} = 1 \\ \mathrm{E}\{\xi\} = \mu \\ \mathrm{E}\{\xi\,(\xi)'\} = \Sigma + \mu\,(\mu)' \end{array} \right. \right\} \tag{2-36}$$

The ambiguity set used to characterize uncertain variables is composed of mean and covariance information. Intuitively, a certain set of mean vector and covariance matrix contains all possible probability distributions. To obtain a 'min' form of the second-stage problem, dual reformulation is required for the inner problem 'min sup $E_{Pf}[Q(x,\xi)]$'. The second-stage problem $E_{Pf}[Q(x,\xi)]$ is an infinite-dimensional linear problem and the primal form is given in (2-37)-(2-41).

$$S(x)^{primal} = \max_{Pf \in D_\xi} \int_{\Xi} Q(x,\xi)\, Pf(\xi) d\xi \tag{2-37}$$

$$\text{s.t. } Pf(\xi) \geq 0, \forall \xi \in \Xi \tag{2-38}$$

$$\int_{\Xi} Pf(\xi) d\xi = 1 \tag{2-39}$$

$$\int_{\Xi} \xi^m Pf(\xi) d\xi = \mu_m,\ m=1,2,\ldots,\Xi \tag{2-40}$$

$$\int_{\Xi} \xi^m \xi^n Pf(\xi) d\xi = \Sigma_{mn} + \mu_m \mu_n,\ m, n=1,2,\ldots,\Xi \tag{2-41}$$

For tractability, the primal form needs to be recast as (2-42) and (2-43), where ψ_0, ψ_j and Ψ_{jk} are dual variables associated with the second-stage constraints and Θ represents $\Sigma + \mu\,(\mu)'$. When the weak duality holds, $S(x)^{primal} \leq S(x)^{dual}$. However, (2-41) ensures that the strong duality holds when Θ is strictly positive definite and thus $S(x)^{primal} = S(x)^{dual}$ [30]. Accordingly, now the problem with an infinite number of variables is transformed into one with a finite number of variables (2-42)-(2-43), which is easier to solve.

$$S(x)^{dual} = \min_{\Psi,\psi,\psi_0} \langle \Psi'\Theta \rangle + \psi'\,\mu + \psi_0 \tag{2-42}$$

$$\text{s.t. } (\xi)'\Psi\xi + \psi'\xi + \psi_0 \geq Q(x,\xi) \quad \forall \xi \in \Xi \tag{2-43}$$

The new compact form is:

$$\min_{x \in X} c'x + S(x)^{dual} \tag{2-44}$$

Problem (2-44) is a semi-infinite-dimensional program which contains an infinite number of constraints. Thus, it is required to be transformed into a closed form [36]. By introducing the new dual variable τ, a positive quadratic function in (2-45) can be obtained from (2-34). VS denotes the polyhedral set of extreme points and N_v is the set of vertices of feasible region in VS.

$$\max_{u \in VS} \tau'(b - Ex - G\xi\,) \tag{2-45}$$

$$VS = \{\tau | F'\tau = f, \tau \leq 0\} \tag{2-46}$$

$$(\xi)'\Psi\xi + \left(\psi + G'\tau^i\right)'\xi\ + \psi_0 - (h - Ex)\tau^i \geq 0 \quad \forall \xi \in \Xi,\ i = 1,2,\ldots,N_v \tag{2-47}$$

In summary, the SDP form is as follow, which is the master problem.

$$\min_{x,\Psi,\psi,\psi_0} c'x + \langle \Psi'\Theta \rangle + \psi'\mu + \psi_0$$

$$\begin{bmatrix} \xi \\ 1 \end{bmatrix}' \begin{bmatrix} \Psi & \frac{1}{2}\left(\psi + G'\tau^i\right) \\ \frac{1}{2}\left(\psi + G'\tau^i\right)' & \psi_0 - (h - Ex)'\tau^i \end{bmatrix} \begin{bmatrix} \xi \\ 1 \end{bmatrix} \geq 0 \quad \forall \xi \in \Xi,\ i = 1,2,\ldots,N_v,\ x \in X, \forall \tau^i \in VS \tag{2-48}$$

A large number of constraints with infinite cardinality of VS cause high computational burden. CGA initially enumerates a subset of vertices and incorporates

more vertices step by step. This relaxation method can efficiently solve the proposed problem, which is separated into a master and sub problem in (2-48) and (2-49). The flowchart of the CGA is given in Fig. 2-2.

$$(\xi_s)'\Psi\xi_s + \psi'\xi_s + \psi_0 - (h - Ex - G\xi_s)'\tau \geq 0 \quad \text{(2-49)}$$

$$\text{s.t. } \forall \xi \in \Xi, \tau \in VS$$

2.2 KL-Divergence-Based DRO

Discrepancy-based ambiguity set use more distributional information to shape real distributions compared with moment-based ambiguity set [33]. It measures the discrepancy between the candidate distribution and reference distribution. The discrepancy can be controlled to either decrease or increase the conservatism depending on the reliability requirement of the optimization. KL divergence is a common ϕ-divergence to measure the distance between two distributions. Estimation of uncertainty distributions can be obtained by statistical fitting [33, 37]. KL divergence-based ambiguity set models uncertainty requiring the candidate distribution within a predefined distance from the nominal distribution.

2.2.1 Risk-Based Ambiguity Set

Firstly, the linear problem is represented by a compact form for notation brevity. Secondly, the KL divergence-based ambiguity set is used to define the uncertainty. Then, CVaR is derived. The final step incorporates the mathematical reformulation and decomposition methods for solving the problem.

The original problem can be represented by vectors and matrices to represent the objective function and constraints for notation simplicity. Compared to the proposed risk-averse model, the traditional risk-neutral DRO model does not consider risk factor, which is given in (2-50). In (2-50), the first-stage objective function is represented by $c'x$. And the expected second-stage objective function is represented by $Q(x, \xi)$. x and y are the variables of the first and second stages. The uncertain variable is denoted as ξ. The ‘min-sup’ structure allows the model to make decision under the worst-case scenario.

$$\min_{x\in X} c'x + \sup_{p\in D_\xi} E_p[Q(x,\xi)] \tag{2-50}$$

Based on the traditional risk-neutral DRO model, the risk measure can be included in the second stage problem, shown below:

$$\min_{x\in X} c'x + \sup_{p\in D_\xi} \{(1-\alpha)E_p[Q(x,\xi)] + \alpha R\big(Q(x,\xi)\big)\} \tag{2-51}$$

$$\text{s.t. } Ax \le b, \tag{2-52}$$

$$Q(x,\xi) = \min_y f'y \tag{2-53}$$

$$\text{s.t. } Ex + Fy + G\xi \le h, \tag{2-54}$$

The risk-averse objective function (2-51) is to minimize the sum of the first-stage objective $c'x$, the weighted expected second-stage objective$(1-\alpha)E_p[Q(x,\xi)]$, and the weighted risk measure $\alpha R\big(Q(x,\xi)\big)$. D_ξ denotes the ambiguity set, containing distribution p. The weighting factor α ranges between 0 and 1. When α=0, (2-51) degrades to the traditional risk-neutral DRO. Equation (2-51) presents the first-stage constraints. The recourse process is represented by (2-53) and (2-54), where *f* denotes the coefficient of (2-53).

The discrepancy-based ambiguity set is constructed based on measuring the distance between probability distributions, i.e., the divergence tolerance η in (2-55). The true and reference probability distribution are represented by p and p_{ref}, respectively. The KL divergence between p and p_{ref} is defined in (2-55), where $p\,(\xi)$ and $p_{ref}(\xi)$ are the probability density functions.

$$Dis = \{p \in D_{\xi,} | D_{\xi,}\big(p \| p_{ref}\big) \le \eta\} \tag{2-55}$$

$$D_{\xi,}\big(p \| p_{ref}\big) = \int f(\xi)\, log \frac{p\,(\xi)}{p_{ref}(\xi)}\, d\xi \tag{2-56}$$

KL-divergence function of variable *a* is in (2-57), which will be used in the dual formulation to solve the inner maximization problem in section *D*.

$$\varphi_{KL}(a) := a \log a - a + 1 \tag{2-57}$$

The probability of the second-stage objective function $Q(x,\xi)$, i.e., the corrective operation cost including load shedding lost, is restricted by the threshold ζ. As an

emerging risk measure method, CVaR is a coherent risk measure, which is convex, transition-equivalent, and monotonic. The original expression of CVaR is in (2-58), which can be further approximated by (2-59) to avoid the computation of multiple integral [38]. $[Q(x,\xi)-\zeta]^+$ represent determining the larger value between $Q(x,\xi)-\zeta$ and 0.

$$CVaR_\beta\big(Q(x,\xi)\big):=\frac{1}{1-\beta}\int_{Q(x,\xi)\geq VaR_\beta(x,\xi)} Q(x,\xi)p\,(\xi)d\xi \tag{2-58}$$

$$CVaR_\beta\big(Q(x,\xi)\big):=\min_{\zeta\in\mathbb{R}}\left\{\zeta+\frac{1}{1-\beta}E_p[Q(x,\xi)-\zeta]^+\right\} \tag{2-59}$$

The proposed FMS is formulated as (2-60) with weighted CVaR. Equation (2-61) can be derived by substituting CVaR in (2-62) with (2-61).

$$\min_{x\in X} c'x+\sup_{p\in D_\xi,\xi=\Delta P_k,\xi_j}\left\{(1-\alpha)E_p[Q(x,\xi)]+\alpha CVaR_\beta\big(Q(x,\xi)\big)\right\} \tag{2-60}$$

$$\min_{x\in X}\left\{c'x+\sup_{p\in D_\xi,\xi=\Delta P_k,\xi_j}\min_{\zeta\in\mathbb{R}}\left\{\alpha\zeta+E_p[G(x,\xi)]\right\}\right\} \tag{2-61}$$

$$G(x,\xi):=(1-\alpha)[Q(x,\xi)]+\frac{\alpha}{1-\beta}\tilde{a}$$

$$\text{s.t.}Q(x,\xi)-\tilde{a}-\zeta\leq 0,\ \tilde{a}\geq 0$$

Based on the proof in [39] on the strong duality, (2-61) can be reformulated to (2-62) and (2-63) with a further step, where

$$\min_{x\in X}\left\{c'x+\min_{\zeta\in\mathbb{R}}\sup_{p\in D_\xi,\xi=\Delta P_k,\xi_j}\left\{\alpha\zeta+E_p[G(x,\xi)]\right\}\right\} \tag{2-62}$$

$$\min_{x\in X}\left\{c'x+\alpha\zeta+\max_{p\in D_\xi,\xi=\Delta P_k,\xi_j}\left\{\sum_{i=1}^{m}p_iG_i(x,\xi)\right\}\right\} \tag{2-63}$$

The inner maximization problem can be handled by the Lagrange function (2-64) with its dual formulation (2-70).

$$\mathcal{L}(p,\tau,\mu)=\sum_{i=1}^{m}p_iG_i(x,\xi)+\tau\left(1-\sum_{i=1}^{m}p_i\right)+\mu\left(\eta-\sum_{i=1}^{m}p_{ref,i}\,\varphi_{KL}\left(\frac{p_i}{p_{ref,i}}\right)\right) \tag{2-64}$$

$$\max\ \mathcal{L}(p,\tau,\mu)=\tau+\eta\mu+\mu\sum_{i=1}^{m}p_{ref,i}\left[\exp\left(\frac{G_i(x,\xi)-\tau}{\mu}\right)-1\right] \tag{2-65}$$

According to Slater's condition [40], when η is larger than 0, the below reformulation can be made:

$$\max_{p\in D_{\xi},\tilde{\xi}=\Delta P_k,\xi_j}\left\{\sum_{i=1}^{m}p_iG_i(x,\xi)\right\}=\min_{\tau,\mu\geq 0}\max\ \mathcal{L}(p,\tau,\mu) \tag{2-66}$$

$$=\min_{\tau,\mu\geq 0}\left\{\tau+\eta\mu+\mu\sum_{i=1}^{m}p_{ref,i}\left[\exp\left(\frac{G_i(x,\xi)-\tau}{\mu}\right)-1\right]\right\} \tag{2-67}$$

Substituting the inner maximization in (3-57) with (3-61), the below derivation can be obtained.

$$\min_{\zeta,\tau,\mu\geq 0}\left\{c'x+\alpha\zeta+\tau+\eta\mu+\mu\sum_{i=1}^{m}p_{ref,i}\left[\exp\left(\frac{G_i(x,\xi)-\tau}{\mu}\right)-1\right]\right\} \tag{2-68}$$

s.t. $x\in X$, $Q(x,\xi)-\tilde{a}-\zeta\leq 0$, $\tilde{a}\geq 0$,$G(x,\xi):=(1-\alpha)[Q(x,\xi)]+\frac{\alpha}{1-\beta}\tilde{a}$

However, the optimization problem (3-62) is nonlinear, which needs to be linearized before decomposition. For a given $x=x^k$, when $Q(x^k,\xi)<\infty$, then $Q(x^k,\xi)$ is subdifferentiable [41] and equation (3-63) can be obtained, where $Dual(x^k)=arg\max\{\pi'(h-Ex^k):F'\pi\leq f\}$ is the set of optimal solutions of dual problem for (3-47) and $\pi^{k,i}\in Dual(x^k)$ is optimal solution for *i*th and *k*th iterations.

$$\partial Q(x^k,\xi)=-E'Dual(x^k) \tag{2-69}$$

Let $s^k:=\frac{G_i(x^k,\xi)-\tau^k}{\mu^k}$ and $F_i^k:=\mu^k[\exp(s^k)-1]$, the subgradient of F_i^k can be described as:

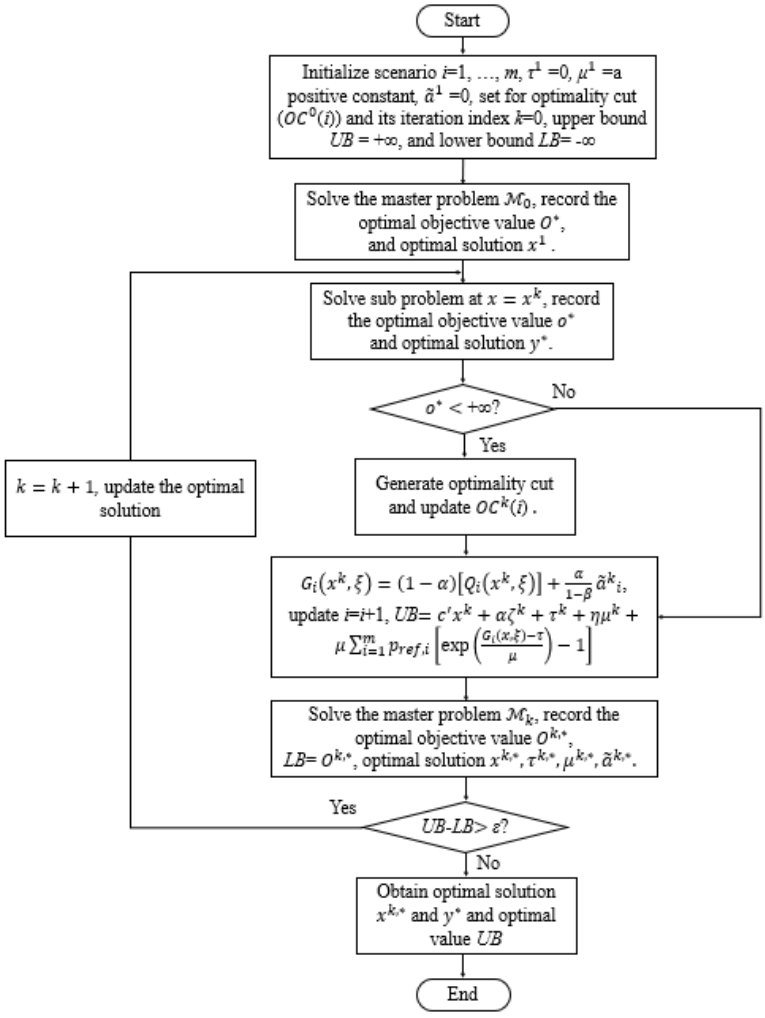

Fig. 2- 3. Flowchart of Bender's decomposition approach.

$$\partial F_i^k = \Big[(1-\alpha)\exp(s^k)E'\pi^{k,i}, (1-s^k)\exp(s^k) - 1, -\exp(s^k), \frac{\alpha}{1-\beta}\exp(s^k)\Big] \tag{2-70}$$

Based on the subgradient inequality of convex function, the below equation can be obtained. The optimality cut can be defined in (3-66).

$$F_i(x,\mu,\tau,\tilde{a}_i) \geq F_i\left(x^k,\mu^k,\tau^k,\tilde{a}_i^k\right) + \partial F_i^k \cdot \left(x - x^k, \mu - \mu^k, \tau - \tau^k, \tilde{a}_i - \tilde{a}_i^k\right) \tag{2-71}$$

$$F_i(x,\mu,\tau,\tilde{a}_i) \geq \left[G_i(x^k,\xi) + (1-\alpha)\left(\pi^{k,i}\right)'Ex^k - \frac{\alpha\tilde{a}_i^k}{1-\beta}\right] + \partial F_i^k(x,\mu,\tau,\tilde{a}_i) \tag{2-72}$$

A Bender's decomposition is employed to solve the problem and the flowchart is given in Fig. 2-3.

2.2.2 Kernel Density Estimation-Based Ambiguity Set

The uncertainty in a equality constraint can be represented by two inequality constraints. For instance, the original equality constraint in (2-73) can be represented by (2-75) and (2-76), where $\omega_{j,t}^{s}$ is the real-time wind power output and ξ is the uncertain wind power forecast error.

$$\sum_{i_e \in I_e} P_{i_e,t} + \sum_{j \in J} \omega_{j,t}^{s} + \sum_{l_e \in L_e} f_{l_e,t}^{a,ini} - \sum_{l_e \in L_e} f_{l_e,t}^{a,ter} - \sum_{k_e \in K_e} P_{k_e,t} = 0 \tag{2-73}$$

$$\omega_{j,t}^{s} = \omega_{j,t}^{f} + \xi \tag{2-74}$$

$$\sum_{i_e \in I_e} P_{i_e,t} + \sum_{j \in J} \omega_{j,t}^{s} + \sum_{l_e \in L_e} f_{l_e,t}^{a,ini} - \sum_{l_e \in L_e} f_{l_e,t}^{a,ter} - \sum_{k_e \in K_e} P_{k_e,t} \geq 0 \tag{2-75}$$

$$\sum_{i_e \in I_e} P_{i_e,t} + \sum_{j \in J} \omega_{j,t}^{s} + \sum_{l_e \in L_e} f_{l_e,t}^{a,ini} - \sum_{l_e \in L_e} f_{l_e,t}^{a,ter} - \sum_{k_e \in K_e} P_{k_e,t} \leq 0 \tag{2-76}$$

Constraint (2-75) is used as the representative of reformulations in the later section, which is transformed into (2-77) since DRO considers the worst distribution of uncertain forecast error.

$$\min_{P \in} \sum_{i_e \in I_e} P_{i_e,t} + \sum_{j \in J} \omega_{j,t}^{s} + \sum_{l_e \in L_e} f_{l_e,t}^{a,ini} - \sum_{l_e \in L_e} f_{l_e,t}^{a,ter} - \sum_{k_e \in K_e} P_{k_e,t} \geq 0 \tag{2-77}$$

Equation (2-78) measures the discrepancy between two probability distribution P and reference distribution P_{ref} based on *φ-divergence* through the divergence tolerance η. Equation (2-79) defines the KL divergence between P and P_{ref}, where $\mathrm{f}(\xi)$ and $\mathrm{f_{ref}}(\xi)$ are the probability density functions.

$$P = \left\{ P \in D \middle| D\left(P \middle\| P_{ref}\right) \leq \eta \right\} \tag{2-78}$$

$$D\left(P \middle\| P_{ref}\right) = \int f(\xi) \, log \, \frac{f(\xi)}{f_{ref}(\xi)} d\xi \tag{2-79}$$

DRO considers the worst distribution scenario and thus the expectation of constraint (2-75) is based on all the possible uncertainty distributions are considered, which is given in (2-80).

$$\min_{P \in D} Ep\left[H(x, \xi)\right] \geq 0 \tag{2-80}$$

Based on the change-of-measure method, (2-81) can be obtained according to [33], where $L(\xi) = f(\xi)/f_{ref}(\xi)$. By applying the change-of-measure method to constraint (2-80), equation (2-82) can be obtained.

$$D\left(P\middle\|P_{ref}\right) = \int f(\xi)\, log\, \frac{f(\xi)}{f_{ref}(\xi)}\, d\xi = E_{P_{ref}}[L(\xi)\, log\, L(\xi)] \tag{2-81}$$

$$E_P[H(x,\xi)] = \int H(x,\xi)\ \frac{f(\xi)}{f_{ref}(\xi)} f_{ref}(\xi)\, d\xi = E_{P_{ref}}[H(x,\xi)L(\xi)] \tag{2-82}$$

To incorporate uncertainty within the constraint (2-77), it needs to be treated as an inner optimization problem with sub-objectives and constraints.

$$min\ E_{P_{ref}}[H(x,\xi)L(\xi)] \tag{2-83}$$

$$s.t.\ E_{P_{ref}}[L(\xi)\, log\, L(\xi)] \le \eta$$

The original optimization problem is reformulated into (2-84) as follows with the expectation of the constraints.

$$\min\ \ \Gamma \tag{2-84}$$

$$\text{s.t. Constraints (5)-(31)}$$

$$\text{s.t. } \min_{P\in P} E_{P_{ref}}\left[H(x,\xi)\right] \ge 0$$

$$P = \left\{P \in D \middle| D\left(P\middle\|P_{ref}\right) \le \eta\right\}$$

According to [33], when strong duality holds, (2-84) can be transformed into (2-85).

$$\min\ \ \Gamma \tag{2-85}$$

$$\text{s.t. Constraints (5)-(31)}$$

$$\text{s.t. } \max_{P\in P} \alpha\, log\, E_{P_{ref}}\left[e^{H(x,\xi)/\alpha} + \alpha\eta\right] \ge 0$$

Then, the explicit expression of constraints of (2-85) according to (2-71) can be obtained in (2-86).

$$\max_{P\in P} \alpha\, log\, E_{P_{ref}}\left[e^{\sum_{i_e\in I_e} P^s_{i_e,t} + \sum_{j\in J}\omega^s_{j,t} + \sum_{l_e\in L_e} f^{a,s,ini}_{l_e,t} - \sum_{l_e\in L_e} f^{a,s,ter}_{l_e,t} - \sum_{k_e\in K_e} P_{k_e,t}/\alpha} + \alpha\eta\right] \ge 0 \tag{2-86}$$

The logarithmic expression under expectation is a moment generating function with distribution P_{ref}, which can be transformed into a deterministic formulation. In this

paper, kernel density estimation (KDE) in (2-87) is used to estimate the reference distribution, where ξ^i represents error data, N is the number of error data, h_N is a positive smoothing parameter, and H( ) is the kernel function (non-negative and the integral of the probability distribution is 1) [42]. Assuming H( ) follows the normal distribution, (2-88) is formulated from (2-87) with mean value ξ^i and variance ${h_N}^2$.

$$f_N(\xi) = \frac{1}{Nh_N}\sum_{i=1}^{N} H\left(\frac{\xi - \xi^i}{h_N}\right) \tag{2-87}$$

$$f_N(\xi) = \frac{1}{N}\sum_{i=1}^{N} \frac{1}{h_N\sqrt{2\pi}} e^{-\left((\xi-\xi^i)^2/2h_N^2\right)} \tag{2-88}$$

Finally, (2-73) can be transformed into (2-89) based on [33].

$$\sum_{i_e\in I_e} P^s_{i_e,t} + \sum_{j\in J} \omega^f_{j,t} + \sum_{l_e\in L_e} f^{a,s,ini}_{l_e,t} - \sum_{l_e\in L_e} f^{a,s,ter}_{l_e,t} - \sum_{k_e\in K_e} P_{k_e,t} + \max_{\alpha\geq 0}\left\{\alpha\eta + \frac{h^2_{N,P}}{2\alpha} + \alpha\, ln\frac{1}{N_{P,t}}\sum_{i=1}^{N_{P,t}} e^{\left((\xi^i_P(t)/\alpha)\right)}\right\} \geq 0 \tag{2-89}$$

Chapter 3

Mean-Risk Distributionally Robust Co-Optimization of District Integrated Electricity-Gas-Water Systems

This chapter proposes a hierarchical mean-risk two-stage distributionally robust optimization (DRO) method to optimally coordinate the multi energy infrastructures in integrated power, gas and water systems. This two-stage mean-risk DRO is solved by Bender's decomposition method.

Statement of Authorship

This declaration concerns the article entitled:			
Water-Energy Nexus: A Mean-Risk Distributionally Robust Co-Optimization of District Integrated Energy Systems			
Publication status: Accepted			
Publication details (reference)	P. Zhao, C. Gu, Q. Ai, Y. Xiang, T. Ding and S. Li. " Water-Energy Nexus: A Mean-Risk Distributionally Robust Co-Optimization of District Integrated Energy Systems," in ***IEEE Transactions on Power Systems***, doi:10.1109/TPWRS.2020.3038076 .		
Candidate's contribution to the paper	The candidate proposed the idea of the paper, he designed the methodology, and predominantly executed the coding to derive the experimental results. Other authors helped the candidate with the design of case studies, format of the paper, and improvement of academic writing. The percentage of the candidate did compared with the whole work is indicated as follows: Formulation of ideas: 100% Design of methodology: 90% Experimental work: 90% Presentation of data in journal format: 80%		
Statement from candidate	This paper reports on original research I conducted during the period of my Higher Degree by Research candidature.		
Signed	Pengfei Zhao	Date	18/11/2020

3.1 Abstract

Integrated energy system (IES) is a viable and effective solution for improving the energy utilization efficiency and promoting the renewable penetration via aggregating independent systems into an integrated management scheme. The water system management problem has been widely investigated. However, the interdependencies between water and energy systems are significant and the effective co-optimization is required considering strong interconnections. For instance, around 80% of the power consumed in water systems is used for pumping and distributing water. In power systems, surplus water resources significantly contribute to the generation and conversion in power systems. This paper proposes a two-stage distributionally robust operation model for integrated water-energy nexus systems (IWENS) including power, gas and water systems networked with energy hub systems in a distribution level considering wind uncertainty. The presence of the wind uncertainty inevitably leads to the risks in decision-making process. Accordingly, a coherent risk measure, i.e., conditional value-at-risk, is combined with the optimization objective to determine risk-aversion operation schemes. This two-stage mean-risk distributionally robust optimization is solved by Bender's decomposition method. Case studies focus on investigating the strong interdependencies among the four interconnected energy systems. Numerical results validate the economic effectiveness of IES through optimally coordinating the multi-energy infrastructures. This work aims at jointly optimizing the IWENS in a distribution level considering the extensive water-energy nexus and renewable variation. To the end, the overall operational efficiency can be improved.

3.2 Nomenclature

Due to space limitation, the variables defined in section *C* represents both the scheduled variables in the first stage optimization and the regulated variables in the second stage. The superscript '*s*' and '*re*' representing 'scheduled' and 'regulated' respectively are omitted in section *C*. The full expression of variables is given in section II. In addition, the superscript '*ini*' and '*ter*' representing initial and terminal nodes of power bus, gas and water nodes are also omitted in this section to save space.

A. Indices and sets

t, T	Index and set of time periods.

b , B	Index and set of electricity buses.
n , N	Index and set of gas nodes.
w , W	Index and set of water nodes.
i_e, I_e	Index and set of traditional distributed generators (DG).
i_g, I_g	Index and set of natural gas sources.
wr, WR	Index and set of water reservoirs.
j, J	Index and set of renewable DGs.
gt, GT	Index and set of gas turbines.
wp, WP	Index and set of water pumps.
l_e, L_e	Index and set of power lines.
l_g, L_g	Index and set of gas pipelines.
l_w, L_w	Index and set of water pipelines without pumps.
l_{wp}, L_{wp}	Index and set of water pipelines with pumps.
k_e, K_e	Index and set of power loads.
k_g, K_g	Index and set of gas loads.
k_w, K_w	Index and set of water loads.

B. Parameters

$P_{k_e,t}, Q_{k_e,t}, G_{k_g,t}, P_{k_w,t}$	Demand of active power, reactive power, gas and water.
$P_{m,max}, P_{wr,max}$	Maximum active power purchase from upper level market and water purchase from reservoir.
$R_{i_e}^{+}$, $R_{i_e}^{-}$, R_{gt}^{+}, R_{gt}^{-}, R_{wp}^{+}, R_{wp}^{-}	Maximum up and down reserve capacity of traditional DGs, the gas turbine and water pumps.
$P_{i_e,max}$, $P_{i_e,min}$, $P_{gt,max}$, $P_{gt,min}$, $P_{wp,max}$,$P_{wp,min}$	Maximum and minimum limits for active power output of traditional DGs, gas turbine output and water pump power consumption.
$Q_{i_e,max}$, $Q_{i_e,min}$	Maximum and minimum reactive power output of traditional DG i_e.
$V_{b,max}$,$V_{b,min}$	Maximum and minimum voltage limits.
x_{l_e}, r_{l_e}	Reactance and resistance of power line l_e.
V_0	Reference voltage magnitude.
$f_{l_e,max}$,$qf_{l_e,max}$	Maximum active and reactive power flow of line l_e.
c_{eb}, c_{gt}	Conversion coefficient for electric boilers and the gas turbine.
$\omega_j^s(t)$	Forecasted output of renewable DG j at time t.
$G_{i_g,max}$,$G_{i_g,min}$	Maximum and minimum output of gas source i_g.

$Pr_{l_g,max}, Pr_{l_g,min}$	Maximum and minimum gas pressure of gas pipeline l_g.
γ_{l_g}	Coefficient for Weymouth equation.
$f_{l_g,max}$,	Maximum gas flow of line l_g.
CF_{l_g}	Gas compressor coefficient.
η_e	Electrical efficiency for electrolyser.
$\eta_{hy-ca}, \eta_{hy-me}$	Reaction coefficients for required carbon dioxide and methanation output.
$h_{w,max}^{l_{wp}}, h_{w,min}^{l_{wp}}$, $h_{w,max}^{l_w}, h_{w,min}^{l_w}$	Maximum and minimum limits for head pressure of water node connected with or without water pump.
$a_{l_{wp}}, b_{l_{wp}}$	Water pump characteristic coefficients.
$R_{l_{wp}}, R_{l_w}$	Head gain and loss coefficients.
π_{wp}	Water pump efficiency.
$f_{l_{wp},max}^{s}, f_{l_w,max}^{s}$	Water flow for water pipeline with and without pump.
η_{cp^e}, η_{cp^e}	Electric and heating efficiency for combined heat and power (CHP).
$\eta_{COP,}\eta_{GF}$	Coefficient of performance of ground source heat pump (GSHP) and efficiency of gas furnace (GF).
$P_{cp,max}^{i}, P_{cp,min}^{i}, P_{HP,max}^{i}$, $P_{HP,min}^{i}, P_{GF,max}^{i}, P_{GF,min}^{i}$	Maximum and minimum input limits of CHP, GSHP and GF.
$P_{BS,max}^{ch}, P_{BS,min}^{ch}$, $P_{BS,max}^{dch}, P_{BS,min}^{dch}$	Maximum and minimum charging and discharging power for battery storage.
$P_{HS,max}^{ch}, P_{BS,min}^{ch}$, $P_{HS,max}^{dch}, P_{HS,min}^{dch}$	Maximum and minimum charging and discharging heat for heat storage.
$\eta_{BS}^{ch}, \eta_{BS}^{dch}, \eta_{HS}^{ch}, \eta_{HS}^{dch}$	Charging and discharging efficiency for battery and heat storage.
$E_{BS,max}, E_{BS,min}$, $E_{HS,max}, E_{HS,min}$,	Maximum and minimum remaining energy limits of battery and heat storage.
$L_{e,t}, L_{h,t}$	Electricity and heat load ofenergy hub system.
$\lambda_{i_e}^{a}, \lambda_{i_e}^{b}, \lambda_{i_e}^{c}$	Cost coefficients for generation of traditional DG i_e.
λ_{i_g}	Cost coefficient for output of natural gas source i_g.
$\lambda_{m,}\lambda_{wr}$	Cost coefficient of power and water purchase.
$\lambda_{i_e}^{+}, \lambda_{i_e}^{-}, \lambda_{GT}^{+}, \lambda_{GT}^{-}, \lambda_{wp}^{+}$, λ_{wp}^{-}	Cost coefficient for up and down reserve of traditional DGs, the gas turbine and water pumps.

$\lambda_m^{re}, \lambda_{i_e}^{re}, \lambda_j^{re}, \lambda_{i_g}^{re}, \lambda_{wr}^{re}$	Regulation cost coefficient of power purchase, traditional DGs i_e, wind turbines, natural gas sources and water reservoir.

C. Variables

$P_{m,t}, P_{wr,t}$	Active power and water purchase.
$r_{i_e,t}^{+}, r_{i_e,t}^{-}, r_{gt,t}^{+}, r_{gt,t}^{-}, r_{wp,t}^{+}, r_{wp,t}^{-}$	Up and down reserve capacity of traditional DGs, the gas turbine and water pumps.
$P_{i_e,t}, P_{gt,t}, P_{wp,t}$	Active power output of traditional DGs, gas turbine output and water pump power consumption.
$Q_{i_e,t}$	Reactive power output of traditional DGs.
$P_{i_g,t}$	Output of natural gas source.
$V_{b,t}^{s}, V_{b,t}^{re}$	Scheduled and regulated voltage of bus b at time t.
$f_{l_e,t}, qf_{l_e,t}, f_{l_g,t}$	Active and reactive power flow and gas flow.
$f_{l_e,eb,t}, P_{eb,t}$	Injected power flow and output of electric boiler.
$G_{i_g,t}$	Output of natural gas sources.
$Pr_{n,t}$	Pressure of gas node *n*.
$f_{l_g,GT,t}, P_{gt,t}$	Injected gas flow and output of gas turbine.
$P_{n,t}^{P2G}$	Power consumed by the electrolyser.
$G_{n,t}^{hy}, G_{n,t}^{hy\_me}, G_{n,t}^{hy\_d}, G_{n,t}^{me}$	Gas output for overall P2G process, direct hydrogen injection, hydrogen during methanation process and methanation.
$G_{n,t}^{ca}$	Required gas of carbon dioxide during methanation process.
$h_{w,t}^{l_{wp}}, h_{w,t}^{l_w},$	Water pressure of pipe with and without water pump.
$\bar{h}_{w,t}^{l_w}, \bar{h}_{w,t}^{l_{wp}}$	Elevation of water node connected with and without pump.
$\tilde{h}_{w,t}^{l_w}, \tilde{h}_{w,t}^{l_{wp}}$	Head loss and gain of water node.
$f_{l_{wp},t}, f_{l_w,t}$	Water flow of pipe with and without water pump.
$f_{l_e,t}^{inj}, f_{l_g,t}^{inj}$	Power and gas flow injection to EHSs.
$P_{COP,t}^{i}, P_{COP,t}^{o},$	Power input and heat output of GSHP.
$P_{GF,t}^{i}, P_{GF,t}^{o}$	Gas input and output of gas furnace.
$P_{cp,t}^{s,i}, P_{cp^e,t}^{s,o}, P_{cp^h,t}^{s,o}$	Gas input and power and heat output of CHP.
$P_{BS,t}^{ch}, P_{BS,t}^{dch},$ $P_{HS,t}^{ch}, P_{HS,t}^{dch}$	Charging and discharging power and heat of battery and heat storage.
$E_{BS,t}, E_{HS,t}$	Remaining energy of battery and heat storage.

$v_{e,t}, v_{g,t}$	Dispatch factors of power and gas.
x, y	Vectors of first and second stage variables.

3.3 Introduction

Integrated energy system (IES) is an interdependent configuration and management solution to coordinate multiple energy vectors. It can be realised by the utilization of energy converters, e.g., power-to-gas (P2G), combined heat and power (CHP), heat pumps and gas turbines, etc, further intensify the operational interdependency of IES. Through optimally coordinating multiple energy infrastructures, system efficiency can be significantly improved, renewable energy penetration can be highly facilitated, and environmental targets can be achieved.

Much effort has been focused on the optimization of IES, mainly achieving economic and environmental targets. A robust optimization (RO) model is proposed for an integrated power-gas-heat system in smart districts [43]. This model is demonstrated on a real multi-energy district and real-world physical limitations of energy infrastructures are examined. Paper [44] designs an optimal operation model for a regional IES considering energy price variations. Both system cost and environmental pollutions can be reduced through this optimization model. In [45], an energy sharing framework for multiple interconnected microgrids in an integrated power and heat system is proposed. This model comprehensively optimizes energy generation cost, trading cost with the utility grid and other microgrids, and discomfort cost. Paper [19] presents a decentralized optimization framework for an integrated power and gas system with networked energy hubs. A distributed algorithm based on Bender's decomposition is used to solve this mixed-integer second-order cone programming problem. In [46], a consumption-based carbon pricing method is combined with an optimization model for IES. Accordingly, energy customers are given proper incentives to use low-carbon energy.

Traditionally, water and power systems are designed and operated separately. Nevertheless, water and energy systems are mutually interdependent [47]. According to [48], 3% of the U.S. electricity is facilitated by water distribution systems and approximately 80% of the water consumed electricity is used for distributing and pumping water. The abundant water resources largely contribute to power generation and conversion in power systems.

The existing work on joint optimization of water and power systems mainly focus on reducing system operation cost and gas emissions. Paper [49] proposes an optimal water-power usage by controllable assets considering the couplings in an integrated water and power system (IWPS). A distributed algorithm based on the alternating direction method of multipliers helps pursue individual objectives. In [50], a coordinated day-ahead optimization model for IWPS is proposed considering the hydraulic constraints of water systems. An energy flexibility model for water systems is designed to offer the feasible energy flexibility capacity to the system operator. Paper [51] proposes an optimization model for the demand-side management of IWPS. The water system is treated as an effective resource to manage renewable generation. Stochastic programming (SP) based multi-stage fuzzy optimization is developed for a combined operation and planning problem in an IWPS considering uncertain power demand [52].

The inherent interdependencies between subsystems in IES have been promoted due to increasing energy demand growth, lower prices of gas resources, and emerging conversion technologies for interconnecting subsystems. The aforementioned literature review in the IES demonstrates the benefits of interdependencies. Moreover, the integration of multiple energy systems and water systems will further strengthen the couplings and interdependencies.

However, research on the integration of multi-energy systems and water system is very limited until very recent work in[53], which proposes a robust optimization model (RO) for a multi-energy water-energy nexus system (MEWENS) considering wind uncertainty based on a box-like uncertainty set. The multi-energy flow of power, gas, heat and water systems is analysed in a two-stage optimization framework and solved by column-and-constraint generation algorithm.

In the existing literature, the uncertainty pertaining to renewable generation in IES operation is commonly handled by SP [54, 55] and RO [43, 53]. SP assumes that the distribution of uncertain variables is known. However, obtaining explicit distributions is impractical and the scenario approach will lead to computational burden in optimization. RO copes with uncertainty considering all realizations, including the worst-case renewable fluctuation scenario, which ensures system robustness but sacrifices system cost effectiveness. Distributionally robust optimization (DRO) , which employs partial distributional information to capture the ambiguous uncertainty

distributions, can overcome the limitations and deficiencies of SP and RO. Recently, DRO has been applied in the operation of IES. An optimal gas-power flow model is established in [56] and wind power uncertainty is characterized by Wasserstein-based ambiguity set. Paper [57] proposes distributionally robust scheduling for integrated electricity and gas systems considering demand response. The revenue from demand response is maximized and expected load shedding cost is minimized.

DRO employs ambiguity sets to capture the uncertainties pertaining to known distributional information. The optimization results will be intractable or over-conservative if the ambiguity set is not chosen appropriately. There are two common methods to characterize ambiguity sets, moment-based ambiguity set and discrepancy-based ambiguity set. The former one has simple tractable reformulations, e.g., semidefinite program (SDP) or second-order cone program (SOCP). Nevertheless, different distributions might have the same moment information, which introduces challenges for determining the worst-case distribution. Discrepancy-based ambiguity set measures the statistical distance between the reference distribution and candidate distributions. Kullback-Leibler (KL) divergence is widely applied in operation problems in the area of power systems [58, 59].

The uncertainties bring risks into economic operation. Intuitively, risks in the proposed IES operation model can lead to abnormal high operation cost. Mean-risk optimization considers a coherent trade-off between system economic performance and risk, which has been applied with SP on energy system operation [60-62]. Paper [60] develops a mean-risk stochastic programming model for unit commitment considering renewable energy uncertainty. A conditional value-at-risk (CVaR) is incorporated to assess the risk from renewable energy uncertainty. In [62], a day-ahead operational planning model for a regional energy service provider with electricity price uncertainty is proposed. The CVaR criterion is employed to hedge against the uncertainty.

This paper aims at constructing a two-stage mean-risk DRO model, which is helpful for providing system operators the trade-off operation scheme between operation cost and risk mitigation. Based on the common IES, this paper proposes a coordinated optimization for integrated water-energy nexus system (IWENS) with the connection of multiple energy hub systems (EHSs) containing power, gas, heat and water systems. This paper proposes a two-stage mean-risk distributionally robust optimization (TSMR-DRO) for IWENS considering the uncertainty of wind power generation. The two-stage

model includes day-ahead and real-time operation schemes, prior to and after wind uncertainty realization. The ambiguity set for capturing wind uncertainty is constructed using KL divergence. The coherent risk measure, i.e., CVaR is employed to model the trade-off between expected computational performance and risk. Bender's decomposition is applied to solve the problem in an iterative manner. The proposed IWENS can provide system operators a two-stage operation scheme aiming at minimizing the system operation cost and a new perspective when dealing with enormous interdependencies.

Compared with the existing MEWENS [53], this paper makes further improvements: i) the proposed IWENS is in distribution level, which further considers the voltage at each bus, and both active and reactive power; ii) IWENS is connected with multiple EHSs, which supplies residential energy customers. It also brings about more conversions and interdependencies and accordingly enhances the overall energy utilization efficiency; iii) The proposed KL divergence-based DRO offers less-conservative results than RO; iv) compared with the risk-neutral optimization, TSMR-DRO offers the system operators with decision makings between the economic efficiency and the risk.

The main contributions of this paper are as follows:

1) *Energy structure:* It is the first attempt to model an innovative IWENS structure networked with EHSs and renewable distributed generators (DGs) in a distribution level. The intricate nexus between power, gas and water is extensively modelled. The high renewable penetration in the IWENS can be effectively facilitated by the energy conversions and thus the excessive power flow caused by renewable fluctuation can be compensated by other subsystems.

2) It aggregates considerable interconnections and converters among subsystems, e.g., gas turbines, P2G facilities, CHP, GF, GSHP, water pumps and electric boilers. The enormous interdependencies and interactions between energy sectors are beneficial for improving economic efficiency and sustainability.

3) A two-stage DRO model is applied to optimize both day-ahead and real-time operation schemes. The day-ahead stage determines the initial operation scheme with reserve capacity from traditional DGs and CHPs and water pumps.

4) *Optimization method*: It is the first attempt to combine DRO with mean-risk optimization. The benefits of the proposed DR-MRO is in threefold: i) it overcomes the

shortages of SO and RO by using partial distributional information with moderate robustness, ii) the KL divergence-based ambiguity set can flexibly shape the considered candidate distributions compared with moment-based ambiguity sets and accordingly yields less-conservative results and iii) the trade-off between economic performance and risk can be realized based on the incorporation of CVaR on the objective function.

The remainder of this paper is organized as follows. Section 3.4 presents the objective function and constraints for both day-ahead and real-time stages. Section 2.2.1 proposes the method for solving KL divergence-based TSMR-DRO considering the incorporation of CVaR. The case studies for demonstrating the advantages of IWENS and TSMR-DRO are given in Section 3.5. Finally, section 3.6 concludes the entire paper.

3.4 IWENS Structure

The enormous interdependencies among each subsystem are realized by the strong couplings for subsystems with multiple energy converters facilitated. CHP enables the conversion from gas to both heat and electricity to supply the heating and electricity loads of energy hubs. P2G facilities can convert excessive renewable power generation to synthetic natural gas; The conversion from gas to power is mainly realized by utilizing gas turbines; Ground source heat pump (GSHP) and gas furnace (GF) enable the heat conversion from power and gas respectively; The electrolyses in the P2G facilities consume the water from water system; The energy conversion from CHP relies on the water supply; Water pumps consume electricity from power system; The electricity boiler in the water system requests the electricity supply to convert the water to heat. Consequently, modelling and optimizing all the subsystems as an entity can facilitate the economy and security of IWENS.

The proposed IWENS structure is given in Fig. 3-1. The power and gas systems have three interconnection points: i) bus 6 and 15 in power system is connected with node 2 and 6 in gas system via gas turbines and P2G facility on bus 10 is connected with gas node 3. The two EHSs are sourced from both power and gas systems. The water distribution system interconnects with all the other subsystems: i) water node 11 is connected with the P2G facility for the water electrolysis process, ii) water node 2 connects with EHS 1 and 2 for CHP conversion; iii) water pump at node 1, 2 and 6 consume electricity from EHS 1 and iv) water system is connected with EHS via an electric boiler. The IWENS contains two EHSs. Each EHS contains a CHP, a GSHP, a

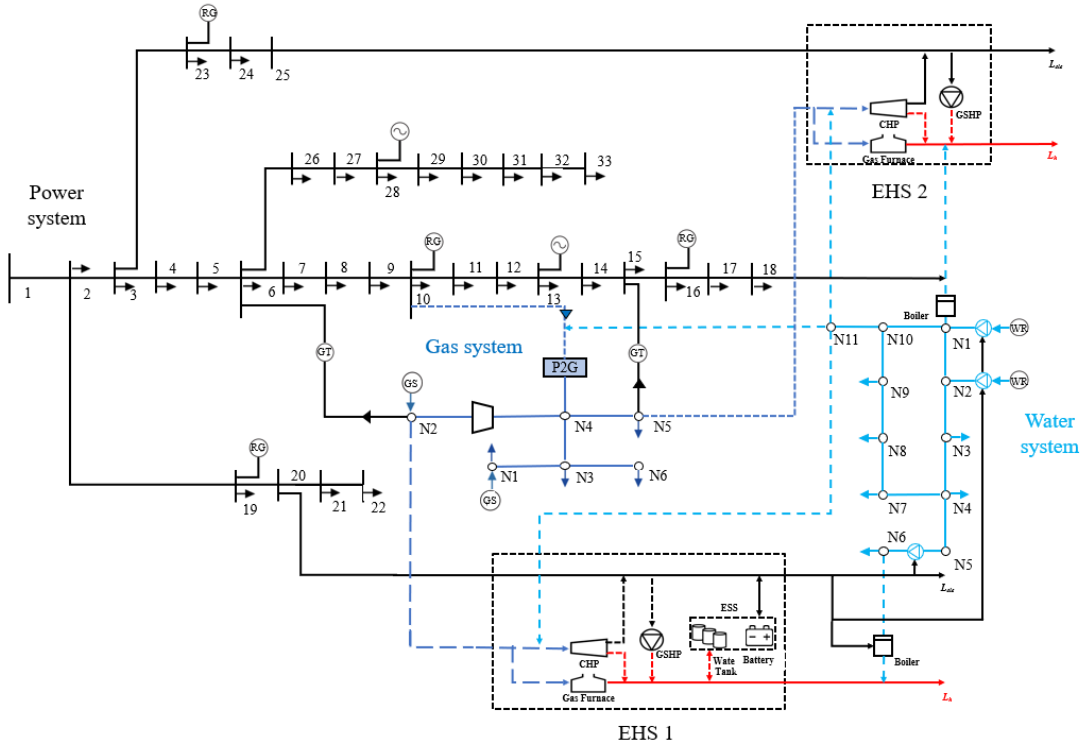

Fig. 3-1 . Proposed structure of IWENS.

GF. EHS 1 contains an energy storage system (ESS). The ESS is composed of a battery storage and a water tank for storing excessive electricity and heating respectively.

3.5 Problem Formulation

This section proposes the mathematical modelling for IWENS including both day-ahead and real-time operation schemes. Then the risk measure is given. Finally, the objective function is illustrated. The assumption is made that the entire IWENS is owned by a single entity who controls all the energy infrastructures and there is no trading between each subsystem.

3.5.1. Day-ahead Operation

The day-ahead optimization schedules power generation plan of traditional DGs and the reserve capacity dispatch from traditional DGs, gas turbines and water pumps considering the operation status of other energy infrastructures. The constraints are in (3-1)-(3-40). The power purchase from upper-level market is given in (3-1). The reserve capacity from traditional DGs, gas turbines and water pumps are shown in (3-2) and (3-3), followed by their output limits in (3-4) and (3-5). Constraint (3-6) limits the reactive power output of traditional DGs. In power distribution systems, linearized

DistFlow equations are commonly used in optimization problems, given in (3-7)-(3-9). Constraint (3-10) is the output of electric boiler. The balancing conditions for active and reactive power are in (3-11) and (3-12).

The output of natural gas source is constrained in (3-13). Constraints (3-14) and (3-15) are used to limit the gas pressure. Note that the gas pressures of initial nodes are always higher than terminal nodes due to the unidirectional gas flow. Initial and terminal nodes exist at the same pipeline. The initial node represents the origin of the gas flow and the terminal node represents the end of the gas flow. Accordingly, constraint (3-15) is used to ensure unidirectional gas flow. Equation (3-16) is the Weymouth gas flow equation that characterizes the relationship between gas pressure and flow. The gas flow of gas pipelines is constrained in (3-17). The output of gas turbine is in (3-18). Equation (3-19) presents the relationship between the gas pressure of initial and terminal nodes of gas compressors. The excessive renewable generation can be converted into gas via P2G. The electrolyser splits water into hydrogen and oxygen. The output of electrolyser is given in (3-20). The nodal gas balance is given in (3-21).

In water distribution systems, constraint (3-22) limits the output of reservoir. Equation (3-23) is the constraint of water pressure limit for pipes installed with and without water pumps. In (3-24)-(3-27), the hydraulic characteristics of water pipes are given for pipes installed with and without water pump in terms of head gain and loss. The pressure head gain of water pump is in (3-26). Equation (3-27) describes the hydraulic characteristic of pipes without pumps using Darcy-Weisbach equation [63]. The power consumption of water pump is in (3-28). Constraint (3-29) limits the water flow magnitude. The mass balance for the water system is in (3-30).

In EHSs, the energy conversion of CHP, GF and GSHP are in (3-31)-(3-33). The input limit for all converters is given in (3-34). Equation (3-35) is the constraint of the charging and discharging power and heat for ESSs. Constraint (3-36) and (3-37) limit the remaining energy for battery storage and water tank. Constraint (3-38) presents the coupling relationship for the EHSs, which is the energy balance constraint of EHSs.

$$0 \le P^{s}_{m,t} \le P_{m,max} \tag{3-1}$$

$$0 \le r^{+}_{\{\cdot\},t} \le R^{+}_{\{\cdot\}}, \{\cdot\} = i_e, gt, wp \tag{3-2}$$

$$0 \le r^{-}_{\{\cdot\},t} \le R^{-}_{\{\cdot\}}, \{\cdot\} = i_e, gt, wp \tag{3-3}$$

$$P^{s}_{\{\cdot\},t} + r^{+}_{\{\cdot\},t} \le P_{\{\cdot\},max}, \{\cdot\} = i_e, gt, wp \tag{3-4}$$

$$P_{\{\cdot\},min} \le P^{s}_{\{\cdot\},t} - r^{-}_{\{\cdot\},t}, \{\cdot\} = i_e, gt, wp \tag{3-5}$$

$$Q_{i_e,min} \le Q^{s}_{i_e,t} \le Q_{i_e,max} \tag{3-6}$$

$$V_{b,min} \le V^{s}_{b,t} \le V_{b,max} \tag{3-7}$$

$$V_b^{s,ini} - V_b^{s,ter} = \left(f^{s}_{l_e,t} r_{l_e} + q f^{s}_{l_e,t} x_{l_e}\right)/V_0 \tag{3-8}$$

$$0 \le \{\cdot\}^{s}_{l_e,t} \le \{\cdot\}^{s}_{l_e,max}, \{\cdot\} = f, qf \tag{3-9}$$

$$P^{s}_{eb,t} = c_{eb} f^{s}_{l_e,eb} \tag{3-10}$$

$$\sum_{i_e \in I_e} P^{s}_{i_e,t} + \sum_{j \in J} \omega^{s}_{j,t} + \sum_{l_e \in L_e} f^{s,ini}_{l_e,t} - \sum_{l_e \in L_e} f^{s,ter}_{l_e,t} + P^{s}_{gt,t} = \sum_{k_e \in K_e} P_{k_e,t} + \sum_{l_e \in L_e} f^{s,inj}_{l_e,t} + \sum_{eb \in EB} P^{s}_{eb,t} + \sum_{n \in N} P^{s,P2G}_{n,t} + \sum_{wp \in WP} P^{s}_{wp,t} \tag{3-11}$$

$$\sum_{i_e \in I_e} Q^{s}_{i_e,t} + \sum_{l_e \in L_e} q f^{s,ini}_{l_e,t} - \sum_{l_e \in L_e} q f^{s,ter}_{l_e,t} = \sum_{k_e \in K_e} Q_{k_e,t} \tag{3-12}$$

$$G_{i_g,min} \le G^{s}_{i_g,t} \le G_{i_g,max} \tag{3-13}$$

$$Pr^{2}_{l_g,min} \le Pr^{s^2}_{l_g,t} \le Pr^{2}_{l_g,max} \tag{3-14}$$

$$Pr^{s,ini}_{l_g,t} \ge Pr^{s,ter}_{l_g,t} \tag{3-15}$$

$$f^{s}_{l_g,t}{}^{2} = \gamma_{l_g}\left(Pr^{s,ini^2}_{l_g,t} - Pr^{s,ter^2}_{l_g,t}\right) \tag{3-16}$$

$$0 \le f^{s}_{l_g,t} \le f^{s}_{l_g,max} \tag{3-17}$$

$$P^{s}_{gt,t} = c_{GT} f^{s}_{l_g,gt,t} \tag{3-18}$$

$$Pr^{ter}_{l_g,t} \le CF_{l_g} Pr^{ini}_{l_g,t} \tag{3-19}$$

$$G^{s,hy}_{n,t} = \eta_e \frac{P^{s,P2G}_{n,t}}{\Omega_{hy}} \tag{3-20}$$

$$\sum_{i_g \in I_g} G_{i_g,t}^{s} + \sum_{n \in N} G_{n,t}^{s,hy} + \sum_{l_g \in L_g} f_{l_g,t}^{s,ini} - \sum_{l_g \in L_g} f_{l_g,t}^{s,ter} = \sum_{k_g \in K_g} G_{k_g,t} + \sum_{l_g \in L_g} f_{l_g,gt,t}^{s} + \sum_{l_g \in L_g} f_{l_g,t}^{s,inj} \tag{3-21}$$

$$0 \le P_{wr,t}^{s} \le P_{wr,max} \tag{3-22}$$

$$h_{w,min}^{\{\cdot\}} \le h_{w,t}^{s,\{\cdot\}} \le h_{w,max}^{\{\cdot\}}, \{\cdot\} = l_w, l_{wp} \tag{3-23}$$

$$\tilde{h}_{\{\cdot\},t}^{s} = \left(h_{w,t}^{s,\{\cdot\},ini} + \bar{h}_{w,t}^{s,\{\cdot\},ini}\right) - \left(h_{w,t}^{s,\{\cdot\},ter} + \bar{h}_{w,t}^{s,\{\cdot\},ter}\right), \{\cdot\} = l_w, l_{wp} \tag{3-24}$$

$$\tilde{h}_{l_{wp},t}^{s} \ge 0 \tag{3-25}$$

$$\tilde{h}_{l_{wp},t}^{s} + a_{l_{wp}} f_{l_{wp},t}^{s} + b_{l_{wp}} = R_{l_{wp}} {f_{l_{wp},t}^{s}}^{2} \tag{3-26}$$

$$\tilde{h}_{l_w,t}^{s} = R_{l_w} {f_{l_{wp},t}^{s}}^{2} \tag{3-27}$$

$$P_{wp,t}^{s} = \left(a_{l_{wp}} {f_{l_{wp},t}^{s}}^{2} + b_{l_{wp}} f_{l_{wp},t}^{s}\right)/\pi_{wp} \tag{3-28}$$

$$0 \le f_{\{\cdot\},t}^{s} \le f_{\{\cdot\},max}^{s}, \{\cdot\} = l_w, l_{wp} \tag{3-29}$$

$$\sum_{wr \in WR} P_{wr,t}^{s} + \sum_{\{\cdot\} \in L_w, L_{wp}} f_{\{\cdot\},t}^{s,ini} - \sum_{\{\cdot\} \in L_w, L_{wp}} f_{\{\cdot\},t}^{s,ter} = \sum_{k_{pg} \in K_{pg}} \sigma_{k_{pg}} P_{n,t}^{s,P2G} + \sum_{k_{cp} \in K_{cp}} \sigma_{k_{cp}} P_{cp,t}^{s,i} + \sum_{eb \in EB} \sigma_{eb} P_{eb,t}^{s} + \sum_{k_w \in K_w} P_{k_w,t} \tag{3-30}$$

$$P_{\{\cdot\},t}^{s,o} = \eta_{\{\cdot\}} P_{\{\cdot\},t}^{s,i}, \{\cdot\} = COP, GF \tag{3-31}$$

$$P_{cp^e,t}^{s,o} = \eta_{cp^e} P_{cp,t}^{s,i} \tag{3-32}$$

$$P_{cp^h,t}^{s,o} = \eta_{cp^h} P_{cp,t}^{s,i} \tag{3-33}$$

$$P_{\{\cdot\},min}^{i} \le P_{\{\cdot\},t}^{i} \le P_{\{\cdot\},max}^{i}, \{\cdot\} = cp, COP, GF \tag{3-34}$$

$$P_{\{\cdot\},min}^{s,ch/dch} \le P_{\{\cdot\},t}^{s,ch/dch} \le P_{\{\cdot\},max}^{s,ch/dch}, \{\cdot\} = BS, HS \tag{3-35}$$

$$E_{\{\cdot\},t}^{s} = E_{\{\cdot\},t-1}^{s} + \sum\nolimits_{1}^{t} P_{\{\cdot\},t}^{s,ch} \eta_{\{\cdot\}}^{ch} - P_{\{\cdot\},t}^{s,dch}/\eta_{\{\cdot\}}^{dch}, \{\cdot\} = BS, HS \tag{3-36}$$

$$E_{\{\cdot\},min} \le E^s_{\{\cdot\},t} \le E_{\{\cdot\},max}, \{\cdot\} = BS, HS \tag{3-37}$$

$$\begin{bmatrix} L_{e,t} + P^s_{BS,t} \\ L_{h,t} + P^s_{HS,t} \end{bmatrix} = \begin{bmatrix} 1 - v^s_{e,t} & v^s_{g,t}\eta_{CHP^e}(1 - v^s_{e,t}) \\ v^s_{e,t}\eta_{COP} & v^s_{g,t}(\eta_{CHP^h} + \eta_{CHP^e} v^s_{e,t}\eta_{COP} + \eta_{GF} - v^s_{g,t}\eta_{GF}) \end{bmatrix} \times \begin{bmatrix} f^{s,inj}_{l_e,t} \\ f^{s,inj}_{l_g,t} \end{bmatrix} \tag{3-38}$$

3.5.2. Real-time Operation

In the second stage, corrective operation schemes are deployed based on the realization of wind uncertainty. Equation (3-39) is the constraint for the regulated power output of traditional DGs and gas turbine. And (3-40) is the new power balance constraint considering wind uncertainty. Apart from (3-39) and (3-40), the rest second-stage constraints are the same as the first-stage constraints, where the superscript '*s*' on each variable is changed to '*re*'. '*s*' represents the scheduled decision variables in the first stage and '*re*' represents the regulated decision variables in the second stage. The regulated decision variables are summarized in (3-41).

$$P^s_{\{\cdot\},t} - r^-_{\{\cdot\},t} \le P^{re}_{\{\cdot\},t} \le P^s_{\{\cdot\},t} + r^+_{\{\cdot\},t}, \{\cdot\} = i_e, gt, wp \tag{3-39}$$

$$\sum_{i_e \in I_e} P^{re}_{i_e,t} + \sum_{j \in J} \xi_{j,t} + \sum_{l_e \in L_e} f^{re,ini}_{l_e,t} - \sum_{l_e \in L_e} f^{re,ter}_{l_e,t} + P^{re}_{GT,t} = \sum_{k_e \in K_e} P_{k_e,t} + \sum_{l_e \in L_e} f^{re,inj}_{l_e,t} + \sum_{eb \in EB} P^{re}_{eb,t} + \sum_{n \in N} P^{re,P2G}_{n,t} + \sum_{wp \in WP} P^{re}_{wp,t} \tag{3-40}$$

$$y = \left\{ \begin{array}{c} P^{re}_{m,t}, P^{re}_{i_e,t}, P^{re}_{gt,t}, Q^{re}_{i_e,t}, V^{re}_{b,t}, f^{re}_{l_e,t}, qf^{re}_{l_e,t}, G^{re}_{i_g,t}, Pr^{re}_{l_g,t}, f^{re}_{l_g,t}, P^{re}_{gt,t}, P^{re,P2G}_{n,t}, \\ G^{re,hy}_{n,t}, P^{re,P2G}_{n,t}, G^{re,hy_{me}}_{n,t}, G^{re,hy_d}_{n,t}, G^{re,ca}_{n,t}, G^{re,me}_{n,t}, P^{re}_{wr,t}, h^{re}_{l_w,t}, h^{re}_{l_{wp},t}, \\ \tilde{h}^{re}_{l_w,t}, \tilde{h}^{re}_{l_{wp},t}, f^{re}_{l_w,t}, f^{re}_{l_{wp},t}, P^{re}_{wp,t}, P^{re,i}_{COP,t}, P^{re,i}_{GF,t}, P^{re,i}_{cp,t}, P^{re,o}_{COP,t}, P^{re,o}_{GF,t}, P^{re,o}_{cp^e,t}, \\ P^{re,o}_{cp^h,t}, P^{re,ch}_{BS,t}, P^{re,dch}_{BS,t}, P^{re,ch}_{HS,t}, P^{re,dch}_{HS,t}, E^{re}_{BS,t}, E^{re}_{HS,t}, v^{re}_{e,t}, v^{re}_{g,t} \end{array} \right\} \tag{3-41}$$

3.5.3. Objective Function

In the first stage, the day-ahead objective in (3-42) is to minimize total operation cost, including i) generation cost of traditional DGs and natural gas sources, ii) power purchase cost from day-ahead upper-level market, iii) water purchase cost from water

reservoirs, iv) cost for reserve capacity from traditional DGs, gas turbines and water pumps.

$$\begin{aligned} \Gamma_1 = \min \sum_{i_e \in I_e, i_g \in I_g, t \in T, wr \in WR, gt \in GT} & \lambda_m P_{m,t}^s + \lambda_{i_e}^a {P_{i_e,t}^s}^2 + \lambda_{i_e}^b P_{i_e,t}^s + \lambda_{i_e}^c \\ & + \lambda_{wr} P_{wr,t}^s + \lambda_{i_g} P_{i_g,t}^s + \lambda_{\{\cdot\}}^+ r_{\{\cdot\},t}^+ + \lambda_{\{\cdot\}}^- r_{\{\cdot\},t}^-, \{\cdot\} \\ & = i_e, gt, wp \end{aligned} \tag{3-42}$$

The second-stage problem considers real-time redispatch and corrective actions pertaining to wind uncertainty. The objective function contains the penalties due to the overestimation or underestimation of scheduling in the first stage. The first-stage generation decisions include the scheduled power and water purchase, wind generation forecast, scheduled output of traditional DGs and natural gas sources. The penalties for the renewable forecast error is calculated by the multiplication of the penalty coefficient and the forecast error. The renewable forecast error is calculated by the difference of the renewable forecast and the real-time realization, i.e., $\left|\omega_{j,t}^s - \xi_{j,t}\right|$. The minimization of deviation between scheduled and regulated results promotes the utilization of renewable energy [64, 65].

$$\begin{aligned} \Gamma_2 = \min \sum_{i_e \in I_e, i_g \in I_g, t \in T, wr \in WR} & \lambda_m^{re} \left|P_{m,t}^s - P_{m,t}^{re}\right| + \lambda_j^{re} \left|\omega_{j,t}^s - \xi_{j,t}\right| \\ & + \lambda_{i_e}^{re} \left|P_{i_e,t}^s - P_{i_e,t}^{re}\right| + \lambda_{i_g}^{re} \left|P_{i_g,t}^s - P_{i_g,t}^{re}\right| \\ & + \lambda_{wr}^{re} \left|P_{wr,t}^s - P_{wr,t}^{re}\right| \end{aligned} \tag{3-43}$$

3.6 Case Studies

The proposed DR-IWENS is verified on a district water-energy nexus system consisting of a modified IEEE 33-bus system, a 6-node gas system, two EHSs and a 11-node water system [53, 66-68], where generator information is given in TABLEs 3-1, 3-2 and 3-3. The gas pressure is regulated between 105 Psig and 170 Psig. The power system has two traditional DGs and four renewable DGs. The power system is connected with the gas system via two gas turbines and a P2G facility. Two EHSs are supplied by both electricity and gas from buses 20 and 25 of power system and nodes 2 and 5 from gas system. The water consumption from P2G and CHPs are supplied by node 11 of water system. It is assumed that the water is injected into the CHP with

TABLE 3-1 PARAMETERS OF WATER RESERVOIRS

Node No.	$P_{wr,max}$ (m^3/h)	λ_{wr} ($/$m^3$)	Elevation (m)
1	325	6.4	-252.5
2	700	2.6	-255

TABLE 3-2 PARAMETERS OF NATURAL GAS SOURCES

Node No.	$P_{i_g,min}$ (kcf/h)	$P_{i_g,max}$ (kcf/h)	λ_{i_g} ($/kcf)
1	1000	3000	2.2
2	1000	6000	2

TABLE 3-3 GENERATOR PARAMETERS

Bus No.	$P_{i_e,max}$ (MW)	$P_{i_e,min}$ (MW)	R_i^+, R_i^- (MW)	a_i ($/MW^2)	b_i ($/MW)	c_i ($)
13	1.2	0.3	0.2	6000	7100	6200
28	1.0	0.1	0.2	4500	10500	4000

TABLE 3-4 ECONOMIC PERFORMANCE FOR ALL CASES

Economic result	*Case 1*	*Case 2*	*Case 3*	*Case 4*	*Case 5*
Power system operation cost ($)	22900	20400	13275	21472	28925
Gas system operation cost ($)	15512	14485	12044	16324	26140
Water system operation cost ($)	1962	1802	2310	1858	2352
System operation cost ($)	40374	36687	27629	39609	57417

heated outflow, which converts into the heating. The capacity of CHP is 0.35MW. The heat/power ratio is 1.73.

The electric boilers enable the heating conversion from power and water. The following cases are considered:

Case 1: Benchmark case.

Case 2: Risk-neutral optimization without considering CVaR in the objective function.

Case 3: The output of renewable DGs is twice of case 1.

Case 4: No P2G facility.

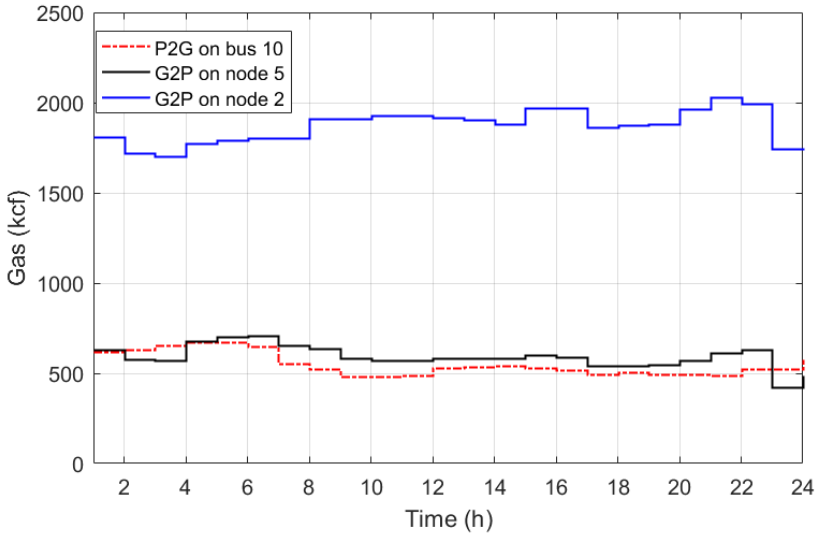

Fig. 3-2. Gas scheduling of gas turbines and P2G.

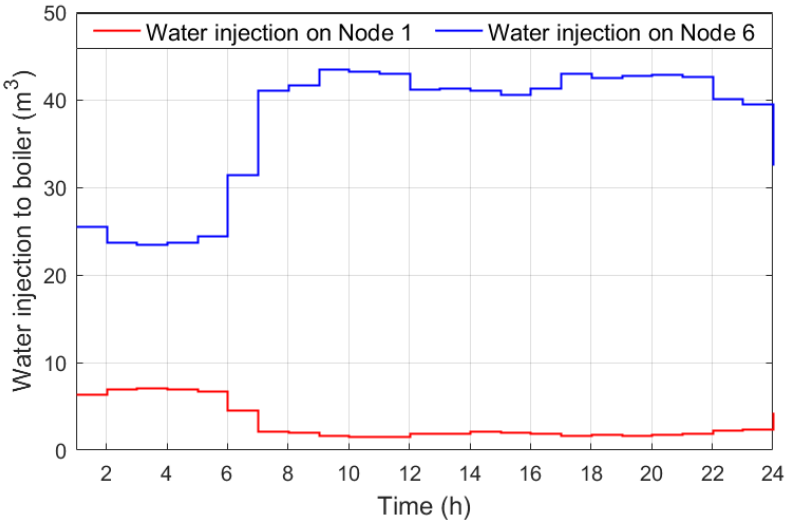

Fig. 3-3. Water injection of boilers.

Case 5: The gas price is twice of case 1.

The economic performance for all the cases is studied firstly in this section, followed by the optimal schedule of interdependent energy converters. The mathematical performance with different risk-aversion parameters is given in section 3.5.3.

3.6.1. Economic Performance of Each Subsystem

The economic performance for all the cases is given in TABLE 3-4, which incorporates the operation cost of power system, gas system, water system and entire IES. Overall, case 3 with twice output of the renewable DGs yields the lowest total operation cost whilst the total operation cost of case 5 is the highest when gas price is twice of case 1. Case 2 is the risk-neutral optimization without considering CVaR in

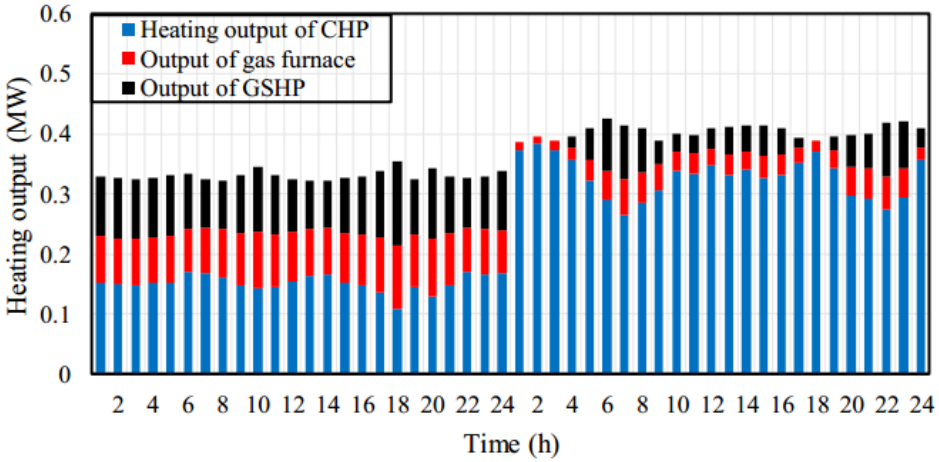

Fig. 3-4. Heating output of CHP, gas furnace and GSHP.

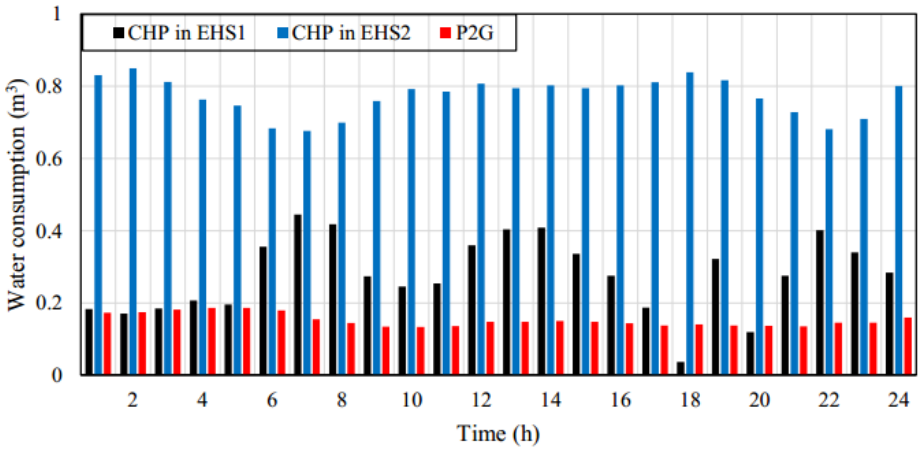

Fig. 3-5. Water consumption of CHPs and P2G.

the objective function. It can be seen that the operation cost of each subsystem is lower than those of case 1. The total operation cost, i.e., \$36687, is 91% of that of case 1. When the output of renewable DGs is doubled in case 3, the most distinct feature is the operation cost of power system, which is only \$13275. Meanwhile, the gas system operation cost is also reduced by \$3468 since the there is more excessive renewable output injecting to the gas system via the P2G facility. However, the water system operation cost is \$348 more than that of case 1. The reason is that the P2G and CHPs cosume more water with increasing renewable output. In case 4, there is no supply from the power system to the gas system, which causes the higher operation cost of gas system since the excessive renewable generation cannot be fully utilized. The operation cost of all the subsystems and the overall system is the highest in case 5. Compared with case 3 with the lowest cost, the total operation cost is 107% higher. Particularly, the gas system operation cost is \$26140, which is \$10628 more than that of case 1.

TABLE 3-5 ECONOMIC PERFORMANCE WITH DIFFERENT CONFIENCE LEVELS

Economic result ($)	β=0.8	β=0.9	β=0.95	β=0.99
Case 1	35635	39573	40374	40652
Case 3	25830	26412	27629	27940
Case 4	38749	39015	39609	40527
Case 5	54119	57087	57417	57906

TABLE 3-6 ECONOMIC PERFORMANCE WITH DIFFERENT WEIGHTING FACTORS

Economic result ($)	α=0	α=0.25	α=0.5	α=0.75
Case 1	36687	38200	40374	42049
Case 3	25872	26412	27629	28950
Case 4	37321	38580	39609	47140
Case 5	50767	51263	57417	62875

3.6.2. Analysis of Energy Conversions

This section investigates the scheduling of coupling devices for interconnecting each system, i.e., gas turbines, P2G facility, electric boilers, CHP, gas furnace and GSHP. To begin with, the operation scheme of gas turbines and the P2G facility is given in Fig. 3-2. Note that it shows the input of gas turbines and output of P2G facility. It can be seen that the gas turbine at node 2 has higher gas consumption than node 5. The average gas consumption of node 2 is 1867kcf and that of node 5 is 591kcf. The potential reason of the higher gas consumption at node 2 are i) node 2 is connected to a natural gas source which has abundant gas supply and ii) the requirement of power transformation at bus 6 is higher as it is connected with more buses. As for P2G, it produces 549kcf averagely. The transformed gas from P2G can supply loads at nodes 3, 5 and 6. In addition, the abundant gas can be converted back to power system at node 5. The scheduling of water injection of electric boilers is shown in Fig. 3-3. The water injection is 3 at node 6m3 and 37m3 at node 1 averagely. Although the heating loads of EHS 1 and 2 have similar amount, the heating supplied by water system at water node 1 is more than 6 times of that at node 6. Since the gas supply of EHS 2 connected to gas node 5 is less but the water supply from water node 1 is sufficient connected to the water reservoir.

In Fig. 3-4, the heating output of converters in EHS 1 and 2 are given, respectively. Overall, the total heating output of converters in EHS 1 is 0.1MW higher than that of

EHS 2. The heating supply composition is different for EHS 1 and 2. The CHP is utilized around 0.15MW for each hour and takes up 50% of the total heating output of converters. While the CHP in EHS 2 outputs approximately 0.33MW, which is 81% of the total heating conversion. The reason is that the supply from power system is not sufficient, which affects the heat conversion of GSHP even though the heating conversion efficiency of GSHP is high. The insufficient electricity consumption needs to be satisfied by CHP conversion, which also increases heating conversion.

The water consumption of CHPs and P2G is in Fig. 3-5. As discussed for Fig. 3-4, the heating conversion from CHP in EHS 2 is higher than that of EHS 1. The water consumption of CHP in EHS 2 is also higher than that of EHS 1, i.e., the average water consumption of CHP in EHS 2 is 0.28m^3 and it is 0.77m3 of CHP in EHS 1. Compared to CHP, P2G consumes less water and its average water consumption is 0.15 m^3.

3.6.3. The Impact of CVaR on Economic Performance

Through adjusting the confidence level and weighting factor for operation cost versus risk trade-off, the overall economic performance varies. TABLEs 3-5 and 3-6 present the economic performance with different beta and alpha, respectively. This paper considers 95% as the benchmark alpha used in TABLE IV. As shown in TABLE V, the total cost increases with the increase of alpha. For case 1, the highest total operation cost is $40652 with beta=0.9 and the lowest total operation cost is $35635 with beta=0.99. When beta is fixed, case 5 which considers twice of the original gas price has the highest total operation cost, followed by cases 4, 1 and 3, which is the same as discussed in section 3.5.1. In TABLE 3-6, the impact of changing beta on the economic performance for all cases is presented. It can be seen that the higher alpha causes higher priority on minimizing the risk, which leads to higher operation cost. When alpha=0, the mean-risk DRO degrades into the risk-neutral DRO. For case 5, the total operation cost is only $50767 compared with the $57417 solved by the benchmark mean-risk DRO.

3.7 Chapter Summary

A mean-risk coordinated optimization for an IES in the water-energy nexus with enormous interdependencies is proposed in this chapter. The tight couplings and interactions between each subsystem enable the reliable and economic operation for the entire IES. The renewable uncertainty is captured by mean-risk DRO. The coherent risk

measure, CVaR provides the trade-off to system operators with flexible alternatives on choosing between economic efficiency and risk. A tractable Bender's decomposition is employed to solve the DR-IWENS problem.

Through the extensive case studies on the economic performance, scheduling of interdependent coupling devices and the risk management via adjusting parameters, the major contributions are tested:

- The coordination of each subsystem with the conversion technologies enhances the energy efficiency.
- The water system is highly required to consider in the IES operation as the water is extensively consumed by energy conversions.

The mean-risk DRO applied in IES operation problem provides system operators with not only economic but risk concerns.

Chapter 4

Resilience Enhancement and Emergency Response for Integrated Energy Systems against Seismic Attacks: A Data-Driven Approach

This chapter proposes to utilise distributionally robust optimization (DRO) to analyse and resolve the resilience-oriented planning problem with uncertain seismic attacks in integrated energy systems (IES). The optimal system hardening plan optimal joint load shedding scheme can be eventually obtained.

Statement of Authorship

<table>
<tr><th colspan="4">This declaration concerns the article entitled:</th></tr>
<tr><td colspan="4">Resilience Enhancement and Emergency Response for Integrated Energy Systems against Seismic Attacks: A Data-Driven Approach</td></tr>
<tr><td colspan="4">Publication status: Accepted</td></tr>
<tr><td>Publication details (reference)</td><td colspan="3">P. Zhao, Y. Shen, C. Gu, F. Teng, X. Xu and S. Li, ”Data-Driven Moment-Based Multi-Energy Investment and Management under Earthquakes”, in IEEE Transactions on Industrial Informatics</td></tr>
<tr><td>Candidate’s contribution to the paper</td><td colspan="3">The candidate and the second author jointly proposed the idea of the paper, and they designed the methodology. The candidate executed all the coding to derive the experimental results. Other authors helped the candidate with the design of case studies, format of the paper, and improvement of academic writing. The percentage of the candidate did compared with the whole work is indicated as follows:
Formulation of ideas: 70%
Design of methodology: 80%
Experimental work: 90%
Presentation of data in journal format: 80%</td></tr>
<tr><td>Statement from candidate</td><td colspan="3">This paper reports on original research I conducted during the period of my Higher Degree by Research candidature.</td></tr>
<tr><td>Signed</td><td>Pengfei Zhao</td><td>Date</td><td>03/12/2020</td></tr>
</table>

4.1 Abstract

Seismic events can severely damage both electricity and natural gas systems, causing devastating consequences. Ensuring the secure and reliable operation of the integrated energy system (IES) is of high importance to avoid potential damage to the infrastructure and reduce economic losses. This paper proposes a new optimal two-stage data-driven optimization to enhance the resilience of IES planning and operation against seismic attacks. In the first stage, hardening investment on the IES is conducted, featuring in preventive measure for seismic attacks. The second stage minimizes the expected operation cost of emergency response. The random seismic attack is modelled as uncertainty, which is realized after the first stage. An explicit damage assessment model is developed to define the budget set of the uncertain seismic activity. Based on the survivability of transmission lines and gas pipelines of IES, an optimal system investment plan is developed. The problem is formulated as a two-stage data-driven distributionally robust optimization (DRO) model, which is tested on an integrated IEEE 30-bus system and 6-node gas network. Case studies demonstrate that the two-stage DRO outperforms robust optimization and single-stage optimization model in terms of minimizing the investment cost and expected economic loss.

4.2 Nomenclature

A. Sets

T	Set for time periods.
I	Set for power lines.
M	Set for gas pipelines.
G_E	Set for electricity distributed generators.
G_G	Set for gas-fired distributed generators.
D_E	Set for electricity loads.
D_G	Set for gas loads.

B. Parameters

CL_{co},CL_{ex}, CL_{mo}, CL_{mi}	Connection loss for complete, extensive, moderate and minor seismic level.
γ	Failure rate constant for gas pipelines.
π_{ij}, π_{mn}	Unit hardening cost for power lines and gas pipelines.
EL_h, PL_h	Maximum number of hardening power lines and pipelines.
IC_{max}	Maximum monetary budget.
x_{ij}	Reactance of power line ij.

$f_{ij,max}$,$f_{mn,max}$	Maximum power flow of line ij and gas flow of pipeline mn.
$P_{ge,min,}P_{ge,max}$	Minimum and maximum power output of electricity generators.
$\delta_{d_e,max,}$ $\delta_{d_g,max}$	Maximum limit for electricity and gas load shedding.
$P_{d_e,t}$, $P_{d_g,t}$	Electricity and gas load demand at time t.
$P_{gg,min,}$ $P_{gg,max}$	Minimum and maximum output of gas-fired generators.
Pr_{min},Pr_{max}	Minimum and maximum pressure.
γ_{mn}	Coefficient for Weymouth equation.
C. Variables	
P_{co}, P_{ex}, P_{mo}, P_{mi}	Probability of being complete, extensive, moderate and minor seismic attacks under a randomly chosen seismic level.
P_{ED}	Expected connection loss.
h_{ij}, h_{mn}	Binary variables indicate if power line (i,j)/pipeline (m,n) is hardened.
$\theta_{i,t}$, $\theta_{j,t}$	Phase angle at electricity bus i and j
x_{ij}	Reactance of power line ij.
$f_{ij,t}$,$f_{mn,t}$,	Power and gas flow of power line ij and gas pipeline mn at time t.
$P_{ge,t}$, $P_{gg,t}$	Electricity and gas-fired distributed generation at time t.
$\delta_{d_e,t}$, $\delta_{d_g,t}$	Electricity and gas load shedding at time t.
Pr_t	Gas pressure at time t.
ξ_{ij}, ξ_{mn}	Binary variable indicates if power line (i,j)/ pipeline (m,n) is damaged.
a_{ij}, a_{mn}	Binary variable indicates if power line (i,j)/pipeline (m,n) is available.

4.3 Introduction

Natural disasters can cause huge power losses of energy systems that threaten the economy. Earthquake is considered as one of the most disruptive natural disasters, which may cause large-scale blackouts without sufficient time for response due to the weak predictability. The Wenchuan earthquake in May 2008 damaged around 270 transmission lines and 900 substations, leaving 46 million people suffered without electricity. A massive power outage was caused in 2010 Chile earthquake.

Approximately 3GW generation capacity became unavailable, 26% of transmission network substations were damaged, where 93% residents suffered from a power outage with two weeks [69]. According to existing research, more than 90% of such damage can be avoided if upgraded seismic preventive measures are adopted [70]. The most powerful earthquake in 20 years damaged the gas transmission and distributions systems in July, 2019, which causes the unavailable gas usage of 13000 customers [71].

To enhance the resilience of power systems against natural disasters, resilience planning has been extensively investigated. Paper [72] proposes a multi-stage and multi-zone based robust optimization (RO) for a bi-level resilience problem considering power line hardening and distributed generation resource placement. Different grid enhancing strategies against extreme weather conditions are considered in [73] in a tri-level framework, which is transformed into an equivalent bi-level problem and solved by a greedy searching algorithm. Paper [74] develops a two-stage stochastic optimization (SO) for resilient planning in a large-scale transmission network to mitigate seismic risk. Optimal capacity expansion is considered as the planning strategy based on explicit damage distribution.

Meanwhile, energy infrastructures are becoming more complex and independent, especially with higher attention on the interdependence of different energy carriers. The rapid growth of gas consumption and mushrooming deployment of gas-fired generation and electrolysis have boosted the synergetic integration of electricity and natural gas systems. The integrated energy system (IES) can significantly increase energy utilization efficiency. Therefore, enhancing resilience to withstand seismic hazards and mitigate resulting damages is of great vitality for IES. A two-stage robust integrated planning of IES is proposed for enhancing the resilience in [75], which is implemented by replacing power lines by a gas transportation system. Paper [76] optimally minimizes the worst-case electricity and gas load shedding through a tri-level robust planning model with network hardening. Paper [77] proposes a resilience assessment for IES including heating, cooling and distributed generation systems. The proposed assessment is quantified through functionality loss and monetary costs.

However, recent IES planning studies consider the impacts of general natural disasters without specifying the types and ignore the attack assessment model, hardly targeting at mitigating seismic risks [75, 76]. This is impractical as the impacts of

natural disasters depend on the grid structure, disaster types, duration and intensity, etc. Different natural disasters could have a very different damage scale that needs specified preventive investment strategies. Thus, it is essential to develop models for assessing seismic risks on IES.

To accommodate the uncertainty of natural disasters, RO and SO have been extensively applied [73-75]. Nevertheless, RO ensures system robustness while inevitably leads to over conservativeness. SO requires the explicit distributions with a large number of samples, which not only produces high computational burden but also is not always practical. Distributionally robust optimization (DRO) bridges the strengths of RO and SO, which relaxes the assumption of specifying a certain distribution and considers the worst distributions compared to the worst-case oriented RO. An optimal gas-power flow is proposed in [78] by DRO with wind uncertainty. Wasserstein metric is used to select candidate distributions. A two-stage DRO model for IES scheduling is proposed in [79] and compared with traditional adjustable robust optimization, proving that DRO generates less conservative and more economical solutions.

This paper targets at alleviating the impacts of seismic events on both power lines and gas pipelines of IES. A two-stage DRO model is proposed to enhance the resilience for an IES, where the damage on both power lines and gas pipelines are considered. For simplicity, the keywords ‘distributionally robust’, ‘seismic’, ‘integrated’ and ‘planning’ are picked and this proposed model is referred to DR-SIP. The seismic activities are regarded as uncertain events and the random damage on power lines and pipelines are regarded as uncertainties, which are handled by DRO. The first stage minimizes the investment cost for hardening IES against seismic attacks. The hardening strategy incorporates strengthening power lines and gas pipelines with earthquake-resistant material and design. After the uncertainty of seismic activities is realized, the second stage minimizes the loss of emergency response through load shedding under the worst potential seismic risks. The Bender’s decomposition is utilized to solve this IES resilience optimization problem, which is then demonstrated through extensive case study. The merits of the proposed model are summarized in the case study section.
The main contributions of this paper are as follows:

1) A two-stage DRO method, incorporating both planning and operation schemes, is for the first time proposed to enhance IES resilience, considering the worst-distributed seismic attack. Compared to existing research, such as [74], [75] and [76], this paper is specifically focused on resilience enhancement for IES.

2) A novel model to assess the performance of IES against seismic attacks is developed. This damage quantification builds a probabilistic model and estimated by damage scenarios. This assessment model can be easily combined with the proposed two-stage DRO model to determine the optimal enhancement plan for IES.

3) It utilizes the novel DRO in IES resilience assessment and enhancement with a tractable reformulation. The historical information of seismic events is efficiently used to reduce the conservativeness, thus producing more economical investment and operation decisions.

4) The proposed novel DRO framework avoids specifying uncertainty distributions but only uses moment information, which is more practical considering that it is normally not possible to gather a sufficiently large amount of distributional information for extreme events.

The rest of this paper is organized as follows. Section 4.4 proposes the damage assessment of seismic events. Section 4.5 designs resilience enhancement strategies. Section 4.6 presents the mathematical formulation for resilience planning and emergency operation. The methodology and solution algorithm are given in section 2.1.1. Section 4.7 demonstrates case studies and performance of DR-SIP. Conclusions are drawn in section 4.8.

4.4 Assessment of Seismic Damage on IES

This section provides the seismic damage modelling for both electricity and natural gas systems, which mainly considers the damages on power lines and gas pipelines. The relationship between damage consequence and seismic level is established in this section. The seismic intensity is described by peak ground acceleration (PGA) and peak ground velocity (PGV), which are mainly related to landslides and surface faulting [80]. The relationship between seismic level, PGA and PGV are summarized in TABLE 4-1 [81].

The concept of connection loss (CL) is adopted to quantify the line failures of

electricity systems [82] due to the damage on pylons and conductors from seismic events. They destroy conductors and shake pylons and consequently damage power lines. For simplicity, this paper considers the number of damaged power lines, which are modelled as CL. Paper [83] concludes four-line damage states, minor, moderate, extensive and complete, which refers to 4%, 12%, 50% and 80% of CL, indicating the number of damaged power lines in percentage. For clarity, the relationship between line damage state and the probability in each damage state is shown in TABLE 4-2.

A random intensity level can cause a certain range of PGA, presented in TABLE 4-1. Based on the fragility curve in Fig. 4-1, a random PGA can cause an earthquake in one or a combination of different line damage states. For example, when PGA is 0.6g, the line damage state of being complete is 0% and being extensive is 60%, while 100% for being moderate and minor. Thus, the expected number of line failures modelled as CL under a specific PGA is described in (4-1).

$$N_{ED} = P_{co}CL_{co} + (P_{ex} - P_{co})CL_{ex} + (P_{mo} - P_{ex})CL_{mo} + (P_{mi} - P_{mo})CL_{mi} \quad (4\text{-}1)$$

The steps to specify seismic damages on electricity lines are summarized as:

1. A random seismic intensity level is sampled from the Monte Carlo approach based on an empirical probability density function of seismic intensity level.
2. Based on TABLE 4-1 and the sampled intensity level, a certain range of PGA is given. Then Monte Carlo approach is used to pick a random PGA from the PGA range.
3. Based on the fragility curve in Fig. 4-1 and obtained PGA, the probability of 4 damage states is obtained.
4. Finally, according to TABLE 4-2 and equation (4-1), the expected number of damaged power lines, N_{ED}, is obtained.

To quantify the damage of the natural gas system due to seismic events, similar to CL of the electricity system, failure rate (*FR*) is defined to represent the number of damage points on gas pipelines [84]. For simplicity, the natural gas system is assumed to operate in the steady state, ignoring the dynamic gas leakage characteristics of pipelines.

FR can be described with PGV:

$$FR = \gamma(PGV)^{2.25}L \quad (4\text{-}2)$$

The steps to acquire *FR* of gas pipelines are as follows:

TABLE 4-1 RANGES OF PGA, PGV AND SEISMIC INTENSITY

Intensity	I	II~III	IV	V	VI	VII	VIII	IX
PGA (%g)	<0.17	0.2-1.4	1.4-3.9	3.9-9.2	9.2-18	18-34	34-65	65-124
PGV (cm/s)	<0.1	0.1-1.1	1.1-3.4	3.4-8.1	8.1-16	16-31	31-60	60-116

TABLE 4-2 LINE DAMAGE OF ELECTRICITY SYSTEMS

Damage state	CL	Probability
Minor	4%	P_{mi}
Moderate	12%	P_{mo}
Extensive	50%	P_{ex}
Complete	80%	P_{co}

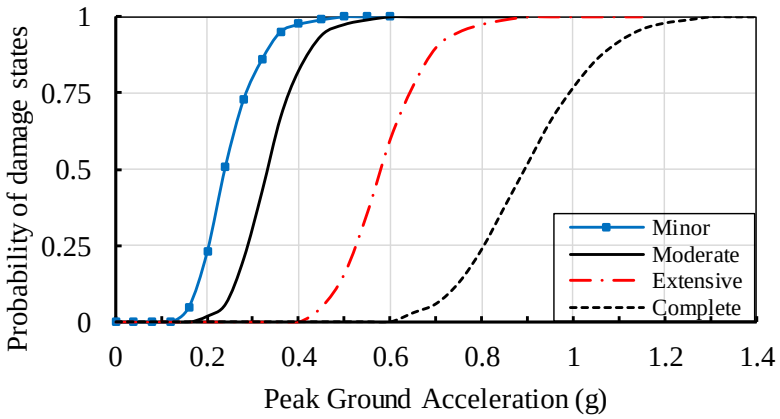

Fig. 4-1. Fragility curve of damage states for seismic attacks.

1. As described in step 1 of section A, the same seismic intensity level is obtained.

2. Based on TABLE 4-1 and obtained seismic intensity level, a certain range of PGV is given. Then Monte Carlo approach is used to pick a random PGV from the PGV range.

3. According to equation (4-2), FR is obtained.

4.5 Seismic Risk Oriented Resilience Enhancement

In terms of resilience-based IES planning, Fig. 4-2 presents the order of widely adopted enhancement steps [85], consisting of adaptation and recovery. The scope of this paper is on resilience planning and emergency response against seismic attacks. The preventive response is ignored as the preventive time after detecting seismic events

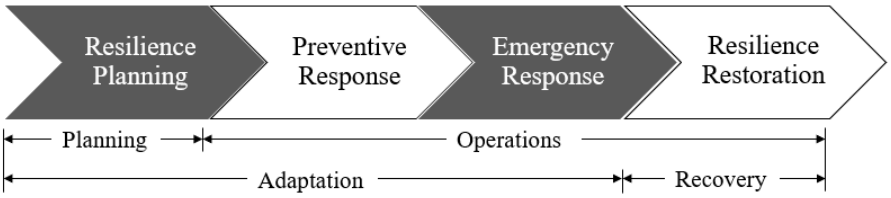

Fig. 4-2. Steps for resilience enhancement under seismic attacks.

is only up to a few seconds, which is too short for seismic preventive actions. In resilience planning, system operators make investment plans for seismic hardening on existing energy infrastructures. After the damage caused by seismic disasters, emergency response is implemented by system operators to mitigate the impact. There are two steps in the proposed DR-SIP: the first stage -resilience planning and the second stage - emergency response:

In the first stage, hardening on power lines is considered as the proposed resilience planning measure. Grid hardening, including constructing new lines and facilities, upgrading damaged poles and burying power lines underground, etc, is the most widely-proposed and effective measure to protect systems against natural disasters [86]. In this paper, reconstruction and upgrade to be earthquake-resistant are considered as the hardening measures for power lines and gas pipelines. It is assumed that the hardened lines will survive from seismic attacks [72, 74, 76]. In the second stage, the daily operation is implemented in the pre-hardened IES. The daily operation is designed instantly after the emergence of the seismic attack with a 24-hour time horizon. To maintain the system balance while suffered from uncertain seismic attacks, load shedding is considered.

4.6 Mathematical Formulation for Resilience Enhancement

Resilience planning and emergency response modelling are illustrated in this section. The seismic hardening strategy is considered for power lines and gas pipelines. Linearized DC power flow and Weymouth gas flow equations are employed with load shedding to meet flow constraints. Finally, a two-stage optimization is proposed to minimize hardening costs in the first stage and operation cost in the second stage.

4.6.1. Overall Objective

It is assumed that the system operator curtails electricity and gas load under the worst-distributed seismic attacks to mitigate damage. The first and second-stage objectives are in (4-3) and (4-4). Γ_P represents hardening investment cost. Γ_R is

emergency response cost, including: 1) shedding costs of electricity and gas loads and 2) generation costs of electricity and gas-fired generators. In the second stage objective, in addition to supplying electricity by gas, gas generation in the gas system is also considered, which is given in ' $\sum_{t\in T,gg\in GG}\lambda_{gg}P_{gg,t}$'.

$$\Gamma_P = \sum_{i,j\in I} h_{ij}\pi_{ij} + \sum_{m,n\in M} h_{mn}\pi_{mn} \tag{4-3}$$

$$\Gamma_R = \sum_{t\in T,d_e\in D_E} \delta_{d_e,t}\pi_{d_e} + \sum_{t\in T,d_e\in D_E} \delta_{d_g,t}\pi_{d_g} + \tag{4-4}$$

$$\sum_{t\in T,ge\in GE} \lambda^a_{ge}P^2_{ge,t} + \lambda^b_{ge}P_{ge,t} + \lambda^c_{ge} + \sum_{t\in T,gg\in GG} \lambda_{gg}P_{gg,t}$$

The overall objective of the proposed DR-SIP is to minimize the planning cost in the first stage and the emergency response cost in the second stage in (4-5).

$$\min \Gamma_P + \sup E_P[\Gamma_R] \tag{4-5}$$

4.6.2. Seismic Risk Oriented Resilience Planning

Here, the feasibility set of hardening strategies for electricity network, gas network and the overall IES are shown in (4-6) to (4-8) respectively. The maximum number of power lines and pipelines to be hardened are constrained by (4-6) and (4-7). Constraint (4-8) means the total hardening investment cannot exceed the maximum monetary budget.

$$\sum_{i,j\in I} h_{ij} \le EL_h \tag{4-6}$$

$$\sum_{m,n\in M} h_{mn} \le PL_h \tag{4-7}$$

$$\sum_{i,j\in I} h_{ij}\pi_{ij} + \sum_{m,n\in M} h_{mn}\pi_{mn} \le IC_{max} \tag{4-8}$$

4.6.3. Emergency Response

Seismic events can have disruptive damage on power lines and gas pipelines, where the damages are considered as uncertainty, represented by binary variables d_{ij} and d_{mn}. In the second stage of DR-SIP, to mitigate the loss of seismic events, electricity and gas

load shedding is identified and implemented accordingly to keep the system balance. The sub-objective is to minimize the cost of load shedding and generation as an emergency response. When considering the effects of hardening strategies against seismic damage, the availability of lines needs to be identified and multiplied with the power and gas flow. Reference [76] considers the availability as $1-\xi+\xi h$, but the term ξh is nonlinear. This paper presents the availability as $\xi+h$ in (4-14) and (4-15), which is linear but may cause $\xi+h$ =2 and thus leads to overloading on power lines. For instance, in (4-14), $(\xi_{ij}+h_{ij})f_{ij,max}$ can be $2f_{ij,max}$. Accordingly, additional constraints are added to ensure the original limits, i.e., $-f_{ij,max} \le f_{ij,t} \le f_{ij,max}$.

The DC linearized power flow and Weymouth gas flow are utilized for modelling power flow and gas flow respectively, which are shown in (4-9) and (4-10).

$$x_{ij}f_{ij,t} = \left(\theta_{i,t}-\theta_{j,t}\right) \tag{4-9}$$

$$f_{mn,t}\left|f_{mn,t}\right| = \gamma_{mn}\left(Pr_{m,t}{}^2 - Pr_{n,t}{}^2\right) \tag{4-10}$$

However, this paper considers the availability of asset that will inevitably lead to the nonlinear term $(\xi+h)\left(\theta_{i,t}-\theta_{j,t}\right)$ and $(\xi+h)\left(Pr_{m,t}{}^2 - Pr_{n,t}{}^2\right)$. This nonlinearity is linearized based on sufficiently large constants M_{ij} and M_{mn}. Thus, the linearized DC power flow and Weymouth gas flow constraints are used in (4-11)-(4-12) and (4-22)-(4-23).

The constraints of electricity and gas-fired generation output are in (4-16) and (4-17). Equations (4-18) and (4-19) show the constraints for electricity and gas load shedding. Equation (4-20) shows the upper and lower bounds for the pressure square of pipelines. Weymouth gas flow is presented in (4-21) and (4-22). The power and gas balance constraints are in (4-23) and (4-24).

$$x_{ij}f_{ij,t} \le \left(\theta_{i,t}-\theta_{j,t}\right) + (1-\xi_{ij}-h_{ij})M_{ij} \tag{4-11}$$

$$x_{ij}f_{ij,t} \ge \left(\theta_{i,t}-\theta_{j,t}\right) - (1-\xi_{ij}-h_{ij})M_{ij} \tag{4-12}$$

$$-\pi \le \theta_{i/j,t} \le \pi \tag{4-13}$$

$$-(\xi_{ij}+h_{ij})f_{ij,max} \le f_{ij,t} \le (\xi_{ij}+h_{ij})f_{ij,max} \tag{4-14}$$

$$0 \le f_{mn,t} \le (\xi_{mn}+h_{mn})f_{mn,max} \tag{4-15}$$

$$P_{ge,min} \le P_{ge,t} \le P_{ge,max} \tag{4-16}$$

$$P_{gg,min} \le P_{gg,t} \le P_{gg,max} \tag{4-17}$$

$$0 \le \delta_{d_e,t} \le \delta_{d_e,max} \tag{4-18}$$

$$0 \le \delta_{d_g,t} \le \delta_{d_g,max} \tag{4-19}$$

$$Pr_{min}{}^2 \le Pr_t{}^2 \le Pr_{max}{}^2 \tag{4-20}$$

$$f_{mn,t} \le \gamma_{mn}\left(\left(Pr_{m,t}{}^2 - Pr_{n,t}{}^2\right) + (1 - \xi_{mn} - h_{mn})M_{mn}\right) \tag{4-21}$$

$$f_{mn,t} \ge \gamma_{mn}\left(\left(Pr_{m,t}{}^2 - Pr_{n,t}{}^2\right) - (1 - \xi_{mn} - h_{mn})M_{mn}\right) \tag{4-22}$$

$$\sum_{d_e \in D_E} P_{d_e,t} - \delta_{d_e,t} = \sum_{ge \in G_E} P_{ge,t} + \sum_{ij \in I(ter)} f_{ij,t} - \sum_{ij \in I(ini)} f_{ij,t} \tag{4-23}$$

$$\sum_{d_g \in D_G} P_{d_g,t} - \delta_{d_g,t} + \sum_{gg \in G_G} P_{gg,t} = \sum_{mn \in M(ter)} f_{mn,t} - \sum_{g \in M(ini)} f_{mn,t} \tag{4-24}$$

The Weymouth gas flow is nonlinear, but $Pr_t{}^2$ is modelled in the squared form in this paper, which does not require linearization. The nonlinear term $f_{mn,t}{}^2$ can be linearized by piecewise linear approximation to convert DR-SIP into a MILP problem [23], which is presented as follows. $h(f_{mn,t})$ represents the nonlinear function, $\Delta f_{mn,k}$ is the segment of gas pipeline mn, and $\chi_{mn,t,k}$ is the auxiliary continuous variable.

$$h\left(f_{mn,t}\right) \approx h\left(\Delta f_{mn,1}\right) + \sum_{k \in K}\left(h\left(\Delta f_{mn,k+1}\right) - h\left(\Delta f_{mn,k}\right)\right)\chi_{mn,t,k} \tag{4-25}$$

$$f_{,t} = \Delta f_{mn,1} + \sum_{k \in K}\left(\Delta f_{mn,k+1} - \Delta f_{mn,k}\right)\chi_{mn,t,k} \tag{4-26}$$

$$0 \le \chi_{mn,t,k} \le 1 \tag{4-27}$$

4.7 Case Studies

This section presents the numerical case studies of the proposed DR-SIP on an integrated electricity and gas system. The IES consists of the standard IEEE 30 busbars

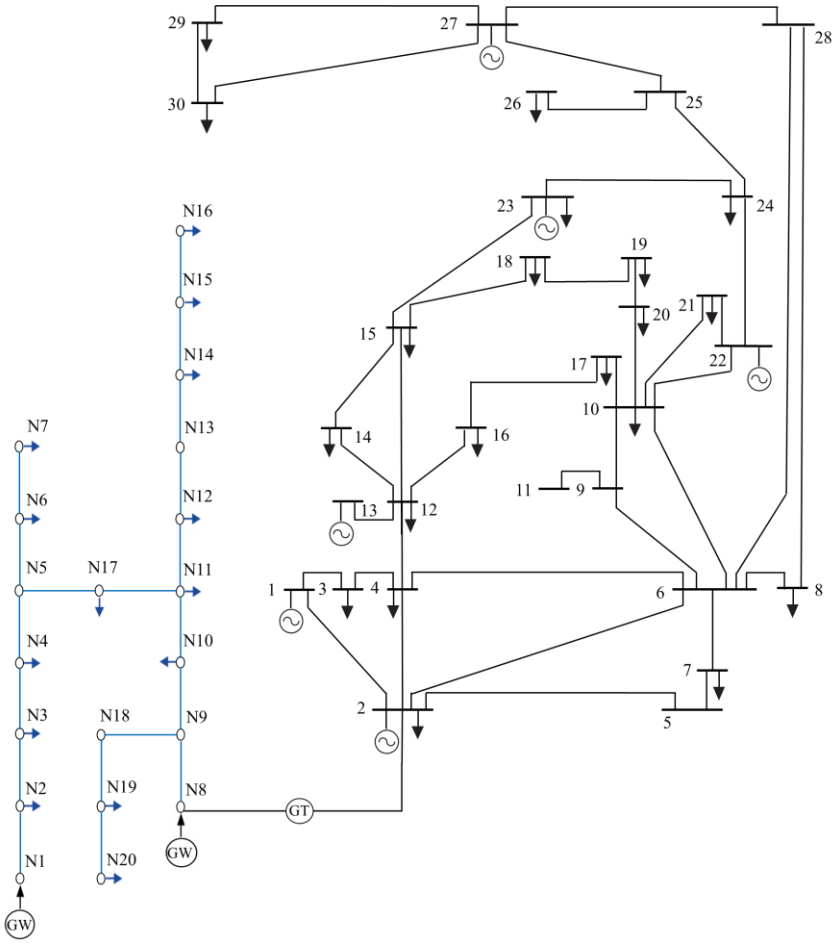

Fig. 4-3. Proposed test system.

electricity system and a 6-node gas network, shown in Fig. 4-3 [57]. The gas network includes a gas-fired generator, 4 gas demands and 7 pipelines. A gas turbine is connected between bus 2 of the electricity network and bus 6 of the gas network. Three cases are performed to optimize DR-SIP. The only difference between cases 2 and 1 is the addition of the planning stage before the seismic attacks.

- Case 1: Single-stage emergency response without considering hardening investment for IES.
- Case 2: Two-stage model including resilience enhancement planning and emergency response for IES.
- Case 3: Two-stage model for IEEE 30-bus system.

Section 4.7.1 presents comparisons of each case. Sections 4.7.2 and 4.7.3 illustrate the optimal hardening plan and computational results for case 2. Section 4.7.4 compares

TABLE 4-3 OPTIMAL HARDENING PLAN UNDER DIFFERENT PLANNING BUDGET

Intensity level	Case 1		Case 2	
	Expected operation cost (10^3\$)	Total cost (10^3\$)	Expected operation cost (10^3\$)	Total cost (10^3\$)
I	30	30	30	362
II~III	30	30	30	362
IV	33	33	30	362
V	43	43	38	370
VI	56	56	42	374
VII	71	71	54	448
VIII	263	263	77	872
IX	402	402	125	920

TABLE 4-4 OPTIMAL HARDENING PLAN UNDER DIFFERENT PLANNING BUDGET

Planning budget	Optimal hardening plan
1	1-2
2	1-2, 1-3
3	1-3, 3-4, 2-6
4	1-2, 2-4, 2-5, 6-9
5	1-2, 2-5, 2-6, 12-13, 12-15
6	1-2, 2-4, 4-12, 12-13, 12-15, 25-27
7	1-2, 2-4, 4-12, 12-13, 12-15, 25-27, 2-g1
8	1-2, 2-4, 2-5, 5-7, 4-12, 12-13, 12-15, 8-28
9	1-2, 2-4, 2-5, 5-7, 4-12, 12-13, 12-15, 8-28, 2-g1
10	1-2, 2-4, 2-5, 5-7, 4-12, 12-13, 12-15, 8-28, 2-g1, g1-g4
15	1-2, 2-4, 2-5, 5-7, 4-12, 12-13, 12-15, 12-16, 16-17, 10-17, 10-21, 27-30, 8-28, 2-g1, g1-g4
20	1-2, 2-5, 2-6, 4-6, 6-7, 6-10, 4-12, 12-13, 12-15, 10-21, 10-22, 15-23, 22-24, 23-24, 28-27, 8-28, 6-28, 2-g1, g1-g4

the numerical performance of case 2 between DRO and RO. Section 4.7.5 highlights the merits of the proposed model.

4.7.1 Case Comparisons

TABLE 4-3 shows the operation and total cost for cases 1 and 2 with the increasing seismic intensity level. For case 1, without hardening investment, the total cost is the same as the operation cost. For case 2, the total cost is the sum of operation and investment cost. The predefined investment budget for case 2 is 10 lines. When the intensity level is under level III, the expected line damage obtained from seismic risk assessment model is around 0, thus the operation cost for both case 1 and 2 is the same as generation cost. When the intensity level is above III, operation cost increases since more load shedding is conducted. The investment cost of case 2 also increases from 332×10^3\$ to 795×10^3\$ even though the investment budget is fixed. The reason is that when more lines are damaged, DR-SIP invests on more important lines, which causes

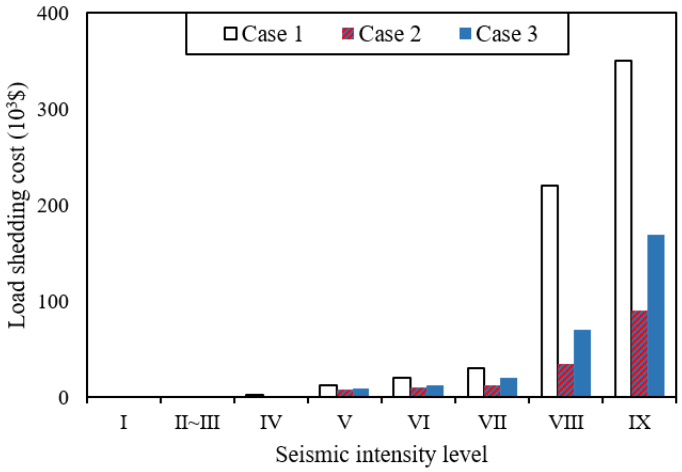

Fig. 4-4. Load shedding cost of three cases.

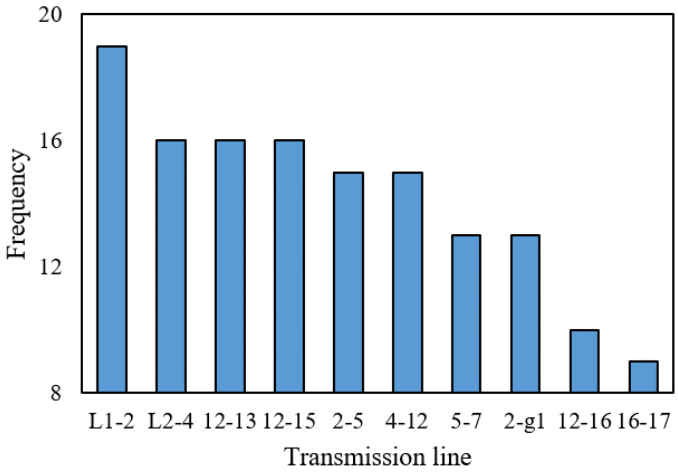

Fig. 4-5. Frequency of line hardened.

139% increase of investment cost when intensity is up to level IX. When the intensity is above level VII, the investment cost remains constant as the 10 most vital lines to be hardened are found.

It is to be noted that the operation cost in case 1 is always higher than that in case 2, i.e., the gap is from 10% under level IV to 220% under level IX, since more load shedding is made without hardening investment to protect lines. With the increasing intensity level, the total cost of case 1 is increasing faster than that of case 2. When the intensity level is I, the total cost of case 1 is only 8% of case 2, which reflects that only implementing load shedding without hardening investment is much more economical. However, under level IX, the ratio is up to 44%, which shows that emergency response under seismic attacks without hardening planning causes huge economic loss.

When generation cannot satisfy all original load due to broken lines caused by seismic attacks, load shedding is made to maintain the system balance, which inevitably

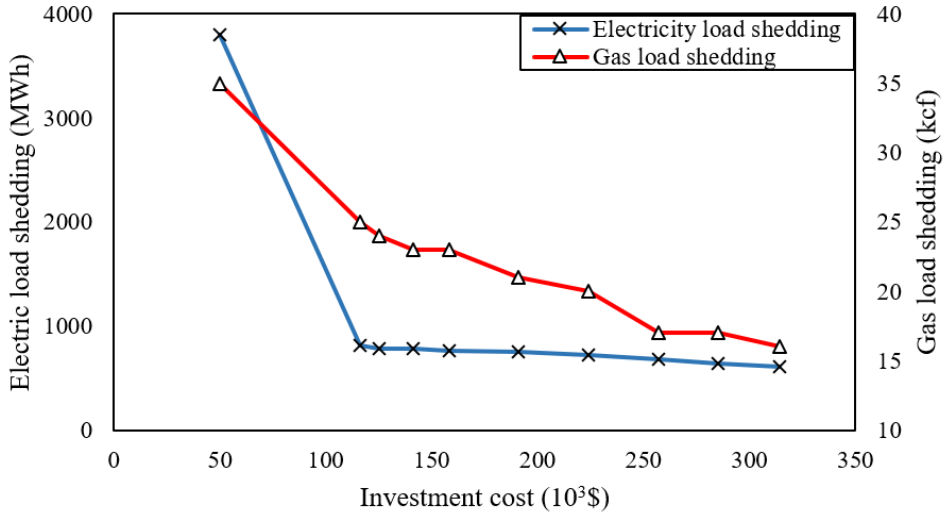

Fig. 4-6. Electricity and gas load shedding under different investment cost.

leads to huge load shedding cost. Fig. 4-4 depicts the load shedding cost for three cases under different seismic intensity levels. Higher load shedding cost is regarded as the system is more vulnerable when facing seismic attacks. It shows that case 1 yields the highest load shedding cost in all intensity levels, which reaches 350×10^3\$. This figure also shows that case 2 requires less load shedding than case 3, with the cost in case 3:169×10^3\$ and in case 2: 90×10^3\$. The potential reason is that: i). Gas-fired generators provide more supplies to the IES; ii) The IES network is more complex that can defend more severe seismic attacks; iii) Underground pipelines are more reliable than power lines, which is pre-set in the mean value vector in ambiguity set.

With increasing intensity level, the cost difference between each case is becoming larger. When intensity level is IX, the cost of case 2 and 3 are only 26% and 48% of case 1 respectively. Overall, it can be observed that the integration of electricity and gas networks makes the system more reliable against seismic attacks.

4.7.2 Optimal Hardening Plan

The impact of increasing the budget on both planning and operation is given in TABLE 4-4 and the intensity level is set as level V. However, when a large number of damaged lines with few hardening lines considered, e.g., budget=1, may probably cause an infeasible solution. Since there are still many lines damaged without previously hardened, causing the congestion and unbalance among transmission lines. Line 1-2 is

TABLE 4-5 COMPUTATIONAL RESULTS UNDER DIFFERENT PLANNING BUDGET

Planning Budget	Investment cost (10^3\$)	Expected operation cost (10^3\$)	Electricity load shedding (MWh)	Gas load shedding (Sm^3)
1	50	132	3800	35
2	116	72	813	25
3	125	72	787	24
4	141	72	779	23
5	158	72	763	23
6	191	71	752	21
7	224	71	727	20
8	257	71	684	17
9	285	65	640	17
10	314	65	612	16
15	446	62	429	12
20	587	55	315	9

TABLE 4-6 COMPARISON WITH ROBUST OPTIMIZATION

Case	Robust optimization		Distributionally robust optimization	
	Expected operation cost (10^3\$)	Total cost (10^3\$)	Expected operation cost (10^3\$)	Total cost (10^3\$)
1	90	90	71	71
2	72	495	54	448
3	102	544	95	516

almost considered in all the budget ranges since both buses 1 and 2 contain the two largest generators and the power can be transmitted to buses 3, 5, 6 and gas bus 1. Line 2-4 is the second most frequent line to harden as the second largest generation of bus 2 needs to be securely transmitted to bus 4, which is connected with buses 3, 6 and 12. Fig. 4-5 shows the times for most frequent lines being hardened when planning budget is under 20. It is concluded that buses 2 and 12 are the most significant buses that involved most frequently. As observed in Fig. 4-3, bus 2 connects with 5 buses with a generator and load. Bus 12 connects with 5 buses with a load.

4.7.3 Computational Results Under Different Planning Budgets

In TABLE 4-5, it shows that a larger planning budget directly leads to more investment cost, but also improves the resilience and accordingly reduces load shedding cost. When the budget increases from 1 to 2, the investment cost increases dramatically by 66×10^3\$. The reason is that when the budget is extremely insufficient, e.g., budget=1 or 2, the two most important line 1-2 and 1-3 are chosen. Lines 1-2 and 1-3 are not only connected with large generators but also have large line ratings, and thus the hardening

cost is high. Due to the hardening of line 1-3, it survives from seismic attack by protecting 2980MWh electricity load and 10Sm^3 gas load from shedding. When the budget increases above 2, the investment cost and load shedding change slowly. Fig. 4-6 shows the load shedding curve for both electricity and gas with respect to different investment cost. When the investment cost increases, both electricity and gas load shedding decreases. The additional investment cost increasing from 50×10^3\$ to 116×10^3\$ helps to prevent load shedding greatly for both electricity and gas network. When the investment cost is above 116×10^3\$, the impact on load shedding is less effective.

4.7.4 Comparison with Robust Optimization

RO as a benchmark method is compared with the proposed DRO method in terms of mathematical performance in cases 1, 2 and 3. From TABLE 4-6, it can be observed that RO yields higher costs in all the three cases. Overall, the total cost and operation cost of DRO are 13% and 18% less than those of RO respectively. The reason is that RO always considers line damages that cause the most severe load shedding. Therefore, in the first stage, RO makes decisions on hardening investment to protect the system before the potential worst damage. In the second stage, under the worst seismic attack, load shedding is made while the whole system flow balance is ensured.

4.7.5 Discussion on Numerical Results

Three cases are extensively investigated and the resulting difference shows that case 2, i.e., the two-stage model including resilience enhancement planning and emergency response for IES, outperforms cases 1 and 3. Compared with case 1 which only contains emergency response to maintain system power balance, case 2 provides a more secure and reliable operation scheme with 54% less load shedding cost. In comparison with case 3 which is implemented on the electricity system without gas system integration, case 2 produces better solution with less load shedding and investment cost. Since the interdependency between electricity and gas systems enables coordinated energy flow to maintain both power and gas balance, it is effective to reduce load shedding and ensure the security of IES. The benefits of using the newly developed DRO over RO for all three cases are also analyzed, which results in reduced expected operation cost and total cost. The reason is that DRO captures the uncertainty of seismic attacks through partial distribution information of uncertainties via ambiguity sets, i.e., moment

information. It considers more specific uncertainty information than RO and accordingly produces less-conservative results.

The extensive case study and analysis illustrate the advantages of DR-SIP, which are:
1) DR-SIP is a hybrid optimization model containing both planning and operation schemes. It not only provides an optimal hardening plan to enhance resilience against seismic attacks but takes actions to maintain supply and demand balance via load shedding, ensuring the security for IES in two stages.
2) The impact of seismic attacks on IES is assessed by considering historical data of seismic events in a probabilistic manner. Thus, the impact of seismic attacks can be easily included in the optimization model for resilience enhancement.
3) The developed data-driven DRO method is less conservative than RO because the statistical information of the uncertainty of seismic attacks is utilized.
4) This paper demonstrates that the integrated planning model can further improve the resilience of electricity systems, following the trend multi-vector energy system integration.

4.8 Chapter Summary

In this paper, a two-stage DRO method is developed to enhance the resilience of an IES under seismic attacks with combined planning and operation strategies. The proposed method provides optimal hardening plans for specific power lines and gas pipelines under different seismic intensity levels and investment budgets. Through extensive case study demonstrations, the key findings are as follows: i) In the first stage, DR-SIP effectively determines the most vital lines to harden. In the second stage, DR-SIP optimally shed loads in order to keep system balance and minimize the system operation cost; ii) With RO that considers the most extreme event and serious damage, the proposed DRO provides less conservative results for both planning and operation stages with 13% less cost; iii) Investment plan with higher budget is more likely to yield a reliable IES with high resilient performance; iv) The optimal hardening plan is effective for protecting transmission lines and loads and IES is more resilient than electricity network against seismic attacks. This method can help system operators to make economical hardening and operation strategies to improve the resilience of integrated energy system under seismic attacks.

Chapter 5

Two-Stage Coordinated Risk Mitigation Strategy for Integrated Electricity and Gas Systems under Malicious False Data Injections

This chapter proposes to apply two-stage distributionally robust optimization to analyse and resolve the integrated electricity and gas system (IEGS) optimisation under false data injection attacks. This work provides system operators with a powerful model to operate the IEGS with enhanced cyber security and high penetrated renewable energy.

Statement of Authorship

This declaration concerns the article entitled:			
Coordinated Risk Mitigation Strategy For Integrated Energy Systems Under Cyber-Attacks			
Publication status: Published			
Publication details (reference)	P. Zhao, C. Gu and D. Huo, "Coordinated Risk Mitigation Strategy For Integrated Energy Systems Under Cyber-Attacks," in ***IEEE Transactions on Power Systems***, vol. 35, no. 5, pp. 4014-4025, Sept. 2020, doi: 10.1109/TPWRS.2020.2986455.		
Candidate's contribution to the paper	The candidate and the second author jointly proposed the idea of the paper, and they designed the methodology. The candidate executed all the coding to derive the experimental results. Other authors helped the candidate with the design of case studies, format of the paper, and improvement of academic writing. The percentage of the candidate did compared with the whole work is indicated as follows: Formulation of ideas: 70% Design of methodology: 80% Experimental work: 90% Presentation of data in journal format: 80%		
Statement from candidate	This paper reports on original research I conducted during the period of my Higher Degree by Research candidature.		
Signed	Pengfei Zhao	Date	01/06/2020

5.1 Abstract

The dramatic increase of cyber-attacks on energy systems can cause huge losses, which has drawn extensive attention due to the fast integration of information communication technologies (ICTs). This issue is becoming worse with the integration of electricity and gas systems (IEGS), facilitated by gas generation and new coupling technologies.

This paper investigates the risk and mitigation strategies for IEGS under false data injection attacks (FDIA) in a hierarchical two-stage framework. The FDIA on both electricity and gas systems are modelled through injecting falsified data by adversaries. To mitigate the adverse impacts, a novel two-stage distributionally robust optimization (DRO) is proposed: i) day-ahead operation to determine initial operation scheme and ii) real-time corrective operation with the realization of FDIA and renewable generation uncertainties. A semidefinite programming is formulated for the original problem and it is then solved by a convex optimization-based algorithm. A typical IEGS is used for case demonstration, which shows that the proposed model is effective in mitigating the risks caused by potential FDIA and renewable uncertainties, by optimal coordinating energy infrastructures and load shedding. This work provides system operators with a powerful model to operate the IEGS with enhanced cyber security and high penetrated renewable energy. It can be easily extended to mitigate other natural and malicious attacks for IEGS.

5.2 Nomenclature

A. Indices and sets

t, T	Index and set for time periods.
b , B	Index and set for electricity buses.
i_e, I_e	Index and set for electricity generators.
i_g, I_g	Index and set for gas wells.
GT	Index for gas turbine.
j, J	Index and set for renewable generators.
l_e, L_e	Index and set for power lines.
l_g, L_g	Index and set for gas pipelines.
k_e, K_e	Index and set for electric loads.
k_g, K_g	Index and set for gas loads.

B. Parameters

AIL	Attack injection level for FDIA.

$\lambda_{i_e}^a, \lambda_{i_e}^b, \lambda_{i_e}^c$	Cost coefficients for of electricity generator i_e.
λ_{i_g}	Cost coefficient for gas well i_g.
$\lambda_{i_e}^+, \lambda_{i_e}^-$	Cost coefficient for up and down reserve of electricity generator i_e.
$\lambda_{i_e}^{re}, \lambda_j^{re}$	Regulation cost coefficient for electricity generator i_e and renewable generator *j*.
$\lambda_{k_e}^{ls}, \lambda_{k_g}^{ls}$	Penalty cost coefficient for electricity and gas load shedding.
$\omega_j^s(t)$	Forecasted output of renewable generator *j* at time t.
$R_{i_e}^+, R_{i_e}^-$	Maximum up and down reserve capacity of electricity generator i_e at time t.
R_{GT}^+, R_{GT}^-	Maximum up and down reserve capacity of gas turbine GT at time t.
$P_{i_e,max}, P_{i_e,min}$	Maximum and minimum output of electricity generator i_e.
$P_{i_g,max}, P_{i_g,min}$	Maximum and minimum output of gas well i_g.
$P_{GT,max}, P_{GT,min}$	Maximum and minimum output of gas turbine GT.
x_{l_e}	Resistance of power line l_e.
$f_{l_e,max}$	Maximum power flow of line l_e.
$f_{l_g,max}$	Maximum gas flow of line l_g.
$\omega_{j,t}^s$	Forecasted renewable generation at time t.
$Pr_{l_g,max}$, $Pr_{l_g,min}$	Maximum and minimum gas pressure of gas pipeline l_g.
γ_{l_g}	Coefficient for Weymouth equation.
D_{l_g}, L_{l_g}	Diameter and length of pipeline l_g.
F_{l_g}	Pipeline friction coefficient.
R	Specific gas constant.
Z	Compression factor of pipeline l_g.
ρ_{l_g}	Gas density.
$Temp$	Temperature.
$P_{k_e,t}, P_{k_g,t}$	Electricity and gas load at time t.
$P_{k_e,max}^{ls}, P_{k_g,max}^{ls}$	Maximum electricity and gas load shedding at time t.

$\eta_{i_e,t}, \eta_{GT,t}$	Participation factor for reserves of electricity generator and gas turbine at time t.

C. Variables and functions

$P^s_{i_e,t}$,$P^{re}_{i_e,t}$	Scheduled and regulated output of electricity generator i_e at time t.
$P^s_{i_g,t}$,$P^{re}_{i_g,t}$	Scheduled and regulated output of gas well i_g at time t.
$P^s_{GT,t}, P^{re}_{GT,t}$	Scheduled and regulated output of gas turbine GT at time t.
$r^+_{i_e,t}, r^-_{i_e,t}$	Up and down reserve of electricity generator i_e at time t.
$r^+_{GT,t}, r^-_{GT,t}$	Up and down reserve of gas turbine GT at time t.
$f^s_{l_e,t}, f^{re}_{l_e,t}$	Scheduled and regulated power flow.
$f^s_{l_g,t}, f^{re}_{l_g,t}$	Scheduled and regulated gas flow.
$f^{ini}_{l_g,t}, f^{ter}_{l_g,t}$	Gas flow from initial node and to terminal node of pipeline l_g at time t.
$Pr^s_{l_g,t}, Pr^{re}_{l_g,t}$	Scheduled and regulated gas pressure of gas pipeline l_g at time t.
$Pr^{s,ini}_{l_g,t}$,$Pr^{s,ter}_{l_g,t}$	Scheduled gas pressure of initial and terminal nodes of pipeline l_g at time t.
$Pr^{re,ini}_{l_g,t}$,$Pr^{re,ter}_{l_g,t}$	Regulated gas pressure of initial and terminal nodes of pipeline l_g at time t.
$P^{ls}_{k_e,t}$	Electricity load shedding at time t.
$P^{ls}_{k_g,t}$	Gas load shedding at time t.
x, y	Vectors of first and second stage variables.
$Pf(\,)$	Probability function.
$E_P[\,]$	Expectation over distribution.
$\langle\,\rangle$	Trace of matrix.
ψ_0,ψ_j, Ψ_{jk}, τ	Dual variables.

D. Uncertainty

$\xi_{j,t}$	Real-time renewable power output of j at time t.
$\Delta P_{k_e,t}, \Delta P_{k_g,t}, \rho^F_{l_g}$	FDIA on electricity load, gas load and gas density at time t.
D	Ambiguity set for FDIA and renewable uncertainty.

μ, Σ	Mean vector and covariance matrix for FDIA and renewable uncertainty.
Θ	Second moment matrix.
VS	Polyhedral set of extreme points.

5.3 Introduction

Power systems have evolved to be more intelligent, efficient and reliable with the increasing dependence on data communication infrastructures [87]. The information and communication technology (ICT) supports bidirectional information flows and thus enhances the optimal control of the physical power system with better observability and controllability. However, high integration and modernization of ICT can naturally raise threats to power system security [88]. The adversary can launch false data injection attacks (FDIA) to tamper critical data and inject falsified data, which brings serious challenges to state estimators, indirectly affecting system operation and control. In 2015, three Ukrainian regional power distribution companies were attacked by FDIA which caused power outages for 225,000 customers [89].

Existing research of FDIA most focuses on investigating i) maximally launching FDIA to cause damages, ii) detection algorithm against FDIA and iii) mitigation and protection schemes against FDIA. As for attack modelling and detection, paper [90] models how an adversary can trigger sequential outages on targeted branches by identifying critical branches. A stochastic model is proposed to design FDIA that affects electricity market by adopting imperfect grid information [91]. Paper [92] proposes an FDIA that can be launched through the approximation on system states based on injection measurements. An online anomaly detection algorithm is used to detect FDIA based on load forecasting and generation scheduling [93], where the minimum attack magnitudes and detection thresholds are determined. A detection and isolation scheme is proposed in [94] by using interval observer based on the physical dynamics of grids. State estimation is of significance in FDIA detection. However, malicious FDIA can be masked and hidden through judiciously designing residue of bad data detection [95, 96]. Therefore, mitigation strategy is the final barrier for protecting power systems provided that detection is failed. A corrective scheme is proposed to address overloading and uneconomic dispatch in [97] against the worst-case FDIA. Paper [98] proposes a unit commitment model by using a trilevel optimization model, which is converted into a

bilevel mixed integer programming problem.

The increasing demand growth of both power and gas systems, low price of natural gas resources, and conversion technologies between the two systems, e.g., gas-fired units and power-to-gas facilities, have promoted the interdependency between power and gas systems. Consequently, modelling and optimizing the two independent systems as an entity can facilitate the economy and security for both systems. Integrated electricity and gas systems (IEGS) realizes the coordination between energy infrastructures in both power and gas systems.

The electricity and natural gas systems are increasingly independent, interconnected by many coupling technologies to form IEGS. Conversion technologies between the two systems include gas-fired units and power-to-gas facilities. Combined heat and power (CHP) enables the conversion of gas to both heat and electricity [99, 100]. Power-to-gas (P2G) facilities can convert excessive renewable energy to synthetic natural gas [21, 29]. The conversion from gas to power is mainly realized by utilizing gas turbines [101, 102]. In some compressor stations of natural gas systems, electricity is used to drive compressors. The interdependency produces many benefits, including enhanced security of supply, more absorption of renewable energy, but there are also many adverse impacts. Cascading failures in one system can propagate to the other and the cyber- attacks on one system can affect the security of the other.

Existing IEGS literatures on making use of its unique interdependency generally concentrates on i) operation under normal conditions, ii) security-based operation under reliability issues and iii) resilience enhancement and operation strategies under natural disasters. Paper [24] proposes an optimal operation scheme for IEGS considering electricity demand response and the impact on the entire system is profound due to the strong interdependency of power and gas systems. A-low carbon IEGS community with heat delivery system is proposed in [103], where the uncertainties of renewable generation and demand are handled by stochastic optimization (SO). Paper [104] models a security-constrained unit commitment against N - k outages by using robust optimization (RO). Nonlinear gas flow is relaxed into a second-order cone problem for convexity. To enhance the resilience of IEGS, a robust network hardening strategy is proposed in [76], considering the uncertainties of natural disasters. Paper [105] proposes a minimax-regret robust unit commitment model for enhancing the resilience of IEGS against the extreme weather obtained by spatial dynamic method.

Leveraging between RO and SO, distributionally robust optimization (DRO) is

widely applied in power systems to handle uncertainties [56, 57, 64, 106, 107]. SO either assumes specific knowledge of probability distributions or requires a large number of uncertainty samples, which is not always practical and can cause high computational burden. RO accommodates uncertainties in predefined uncertainty sets and considers the worst-case scenario, which could have extremely low probability and thus produces over-conservative results. DRO, taking the advantage of distributional information, e.g., moment information, deals with uncertainties within a feasible set, called ambiguity set. Therefore, compared with RO, DRO determines expected results over all possible distributions, which are less-conservative. Compared with SO, DRO avoids intensive computation, thus improving calculation efficiency. Paper [56] applies DRO to a risk-based optimal gas-power flow. An optimal scheduling of IEGS considering electricity and gas load uncertainties is proposed in [57].

Due to the strong interdependency between electricity and gas systems in IEGS, the FDIA on either electricity or gas system can propagate to each other. The adverse impact can be exaggerated when there is large volume of uncertain renewables in the electricity system. But limited effort is dedicated to studying the impact of FDIA on IEGS. This paper proposes a two-stage risk mitigation strategy to address the uneconomic operation of IEGS under FDIA considering renewable generation uncertainties. FDIA is assumed to attack both electricity and gas meter readings, including i) load measurement of electricity and gas systems and ii) gas density measurement. In the first stage, the day-ahead optimization determines an optimal IEGS scheduling scheme based on forecasted renewable generation without considering potential FDIA. In the second stage, both FDIA and renewable uncertainties are revealed, a real-time corrective optimization is built to minimize the attack impacts through load shedding and adjusting generation output. The original problem is converted into equivalent semidefinite programming (SDP) and a constraint generation algorithm (CGA) is adopted to solve the SDP problem. For conciseness and simplicity, the proposed distributionally robust FDIA mitigation scheme is represented by DR-FMS.

The major contribution of this paper is as follows:

1) It models FDIA in an IEGS for the first time, particularly on natural gas load and density measurement, where existing research only focuses on FDIA on electricity systems.

2) Uncertainties of renewable resources are considered in the proposed model as they can worsen system operation conditions during FDIA, compared to existing FDIA papers that ignore the impact of renewable uncertainties.

3) Compared to SO and RO for modelling FDIA, the ambiguous distribution of DRO developed in this paper, which is less data-dependent and conservative, can better characterize uncertain variables.

4) A two-stage FDIA mitigation scheme is proposed for the first time to conduct the day-ahead and real-time operation, which is more powerful and convenient to be used by system operators to ensure the efficiency and security of the IEGS.

The rest of this paper is organized as follows. Section 5.4 models FDIA for both electricity and gas sides. Section 5.5 presents problem formulation of the DR-FMS. The DRO methodology regarding and associated reformulations are given in Section 2.1.2. Section 5.6 demonstrates case studies and performance of the DR-FMS. Finally, the conclusion is given in Section 5.7.

5.4 Attack Modelling

This section presents the attack modelling for electricity and gas system. State estimation is a powerful tool to detect FDIA by processing raw data measurements, but a successful FDIA can be undetectable by adversary's stealthy design.

5.4.1 Attacks on Electricity System

The nonlinear relationship between state variable x and measurement z is given in (5-1), where $h(x)$ denotes the nonlinear vector function of x and e is the error measurement. Based on DC state estimation, equation (5-1) can be transformed into (5-2), where H represents the Jacobian matrix.

$$z = h(x) + e \tag{5-1}$$

$$z = Hx + e \tag{5-2}$$

After the realization of FDIA, the measurement vector z becomes $z_{bad} = z + a$, and the estimated state vector can be represented as $\hat{x}_{bad} = \hat{x} + c$ where a is attack vector

and c is the resulted deviation vector of state variable after FDIA. Accordingly, to determine the estimated state variable, $\hat{x}_{bad}$ can be formulated as:

$$\hat{x}_{bad} = (H'WH)^{-1}H'Wz_{bad} \tag{5-3}$$

The largest normalized residual (LNR) can be used to detect and identify measurement errors by (5-4). If the residual is less than a threshold ε, then the state estimate is valid without FDIA.

$$LNR = \|z - H\hat{x}\| \leq \varepsilon \tag{5-4}$$

Then, equation (5-5) representing LNR is given based on (5-3) and (5-4). Finally, equation (5-6) is obtained.

$$LNR = \|z + a - H((H'WH)^{-1}H'Wz_{bad})\| \tag{5-5}$$

$$LNR = \|z - H\hat{x} + (a - Hc)\| \tag{5-6}$$

If a is the linear combination of H and c, i.e., $a = Hc$, then $LNR = \|z - H\hat{x}\|$ has no change of residual. Therefore, a successful FDIA is launched which can evade detection. As a special case of FDIA, load measurement can be attacked according to [95, 96] by enforcing the sum of load attack vector to be zero in (5-7). For simplicity, the FDIA on electricity load is represented by EL-FDIA. Equation (5-8) constraints the attack deviation by attack injection level (AIL).

$$\sum \Delta P_{k_e,t} = 0 \tag{5-7}$$

$$-AIL_{k_e}P_{k_e,t} \leq \Delta P_{k_e,t} \leq AIL_{k_e}P_{k_e,t} \tag{5-8}$$

5.4.2 Attack on Gas System

The FDIA on a gas system is considered on both gas load and density measurement. Similar to FDIA on electricity load measurement, the FDIA on gas load measurement and density are given in (5-9) and (5-10), namely GL-FDIA and GD-FDIA. The changed gas density measurement results in a change of Weymouth coefficient γ_{l_g}. Accordingly, the initial coefficient in (5-11) is changed to (5-12) under FDIA.

$$0 \leq \Delta P_{k_g,t} \leq AIL_{k_g}P_{k_g,t} \tag{5-9}$$

$$\rho_{l_g} \leq \rho_{l_g}^F \leq (1 + \beta_d)\rho_{l_g} \tag{5-10}$$

TABLE 5-1 TWO-STAGE MITIGATION FRAMEWORK

	Decision variables	Objective	Uncertainty treatment
Stage I	$P^{s}_{i_e,t}, P^{s}_{i_g,t}, P^{s}_{GT,t}, r^{+}_{i_e,t}, r^{-}_{i_e,t}, r^{+}_{GT,t}, r^{-}_{GT,t}, \theta^{s,ini}_{l_e,t}, \theta^{s,ter}_{l_e,t}, f^{s}_{l_e,t}, Pr^{s^2}_{l_g,t}, f^{s}_{l_g,t}$	Generation and reserve cost for electricity generators and gas turbine	Renewable generation forecast
Stage II	$P^{re}_{i_e,t}, P^{re}_{i_g,t}, P^{re}_{GT,t}, P^{ls}_{k_e,t}, P^{ls}_{k_g,t}, \theta^{re,ini}_{l_e,t}, \theta^{re,ter}_{l_e,t}, f^{re}_{l_e,t}, Pr^{re^2}_{l_g,t}, f^{re}_{l_g,t},$	Penalty cost for deviation of renewable, electricity and gas wells Load shedding cost	Uncertain renewable generation, FDIA on electricity load, gas load and gas density based on moment information

$$\gamma_{l_g} = \left(\frac{\pi}{4}\right)^2 \frac{\alpha^2 D_{l_g}^5}{L_{l_g} F_{l_g} RZ \rho_{l_g}{}^2 Temp} \tag{5-11}$$

$$\gamma_{l_g}^{F} = \left(\frac{\pi}{4}\right)^2 \frac{\alpha^2 D_{l_g}^5}{L_{l_g} F_{l_g} RZ \rho_{l_g}^{F}{}^2 Temp} \tag{5-12}$$

5.5 Two-Stage Risk Mitigation Scheme

The risk mitigation for IEGS under potential FDIA consists of: i) day-ahead operation without considering FDIA or renewable uncertainties and ii) real-time operation actions for a corrective mitigation scheme under potential FDIA with the realization of renewable uncertainties. The objective functions and associated constraints are presented in this section.

5.5.1 DR-FMS Objective Function

A summary of decision variables, objective functions and uncertainty modelled in the two stages is presented in TABLE 5-1. Equation (5-13) presents the day-ahead operation objective function in the first stage. The first four terms represent the generation cost of electricity and gas respectively. Reserve costs of electricity generators are shown in the rest. It is noted that the reserve capacity is prepared for FDIA and uncertainties from renewable resources.

$$\Gamma_1 = \min \sum_{i_e \in I_e, i_g \in I_g, t \in T} \lambda^{a}_{i_e} P^{s}_{i_e,t}{}^2 + \lambda^{b}_{i_e} P^{s}_{i_e,t} + \lambda^{c}_{i_e} + \lambda_{i_g} P^{s}_{i_g,t} + \lambda^{+}_{i_e} r^{+}_{i_e,t} + \lambda^{-}_{i_e} r^{-}_{i_e,t} \tag{5-13}$$

The real-time objective function in the second stage is given in (5-14), which mitigates the impact against the presence of FDIA and renewable uncertainty. The first three terms represent the penalty cost for renewable generators, electricity generators and gas wells when regulated generation deviates from scheduled generation. The final two terms represent electricity and gas load shedding cost.

$$\Gamma_2 = \min \sum_{i_e \in I_e, i_g \in I_g, t \in T, k_e \in K_e, k_g \in K_g} +\lambda_j^{re}\left|\omega_{j,t}^s - \xi_{j,t}\right| + \lambda_{i_e}^{re}\left|P_{i_e,t}^s - P_{i_e,t}^{re}\right| + \lambda_{i_g}^{re}\left|P_{i_g,t}^s - P_{i_g,t}^{re}\right| + \lambda_{k_e}^{ls} P_{k_e,t}^{ls} + \lambda_{k_g}^{ls} P_{k_g,t}^{ls} \quad (5\text{-}14)$$

5.5.2 Proposed Coordinated Modelling of IEGS

The IEGS is a tight coupling entity due to the strong interdependency between electricity and gas systems. Accordingly, the two systems should be modelled together by one decision maker. The modelling of IEGS in the existing literatures can be generally categorized into three types: i) Modelling from the perspective of electricity system operators, which overlooks the operational and security constraints of gas system [108, 109]. This ignorance will cause the physical gas flow violation due to the renewable power fluctuation and load variability; ii) Sequential optimization for IEGS [110, 111], which firstly solves the power system model for determining the optimal schedule for generators while neglects the operational constraints of gas system. Based on the obtained solution from power system, the gas system model can be solved and iii) Co-optimization for IEGS which optimizes the comprehensive objective for both electricity and gas systems simultaneously. Consequently, the optimal solution for the entire IEGS can be obtained.

This paper provides a simultaneous coordinated model for the electricity and gas systems. Due to the different characteristics of electricity and gas systems, the operational constraints of two systems are nonrelevant. However, the two systems are solved interdependently with the gas turbine interconnected between the two systems. The gas flow through the gas turbine can be used to generate power flow, which is considered as the supplement for electricity system.

5.5.3 Day-ahead Operation

The day-ahead operation scheme is implemented based on renewable generation forecast without considering FDIA risks, whose constraints are shown in (5-15)-(5-28). Constraint (5-15) and (5-16) limit the reserve capacity for electricity generators and gas turbine. The scheduled output of electricity generators and gas turbine are enforced within limits in (5-17) and (5-18). The linearized DC power flow is given in (5-19) and (5-20). Constraint (5-21) ensures the power balance. Gas well output is limited in (5-22). Gas pressure is limited in (5-23). Constraint (5-24) means the pressure at the initial node is larger than the terminal node since the proposed gas system has a radial

topology. Weymouth gas equation for describing gas flow is shown in (5-25) and (5-26), where the coefficient is defined in (5-11). Gas turbine connects two interdependent systems as a coupled infrastructure. Constraint (5-27) presents the transformation from gas flow injection to power generation. The gas balancing condition is given in (5-28).

$$0 \le r^{+}_{\{\cdot\},t} \le R^{+}_{\{\cdot\}}, \{\cdot\} = i_e, GT \tag{5-15}$$

$$0 \le r^{-}_{\{\cdot\},t} \le R^{-}_{\{\cdot\}}, \{\cdot\} = i_e, GT \tag{5-16}$$

$$P^{s}_{\{\cdot\},t} + r^{+}_{\{\cdot\},t} \le P_{\{\cdot\},max}, \{\cdot\} = i_e, GT \tag{5-17}$$

$$P_{\{\cdot\},min} \le P^{s}_{\{\cdot\},t} - r^{-}_{\{\cdot\},t}, \{\cdot\} = i_e, GT \tag{5-18}$$

$$x_l f^{s}_{l_e,t} = \left(\theta^{s,ini}_{l_e,t} - \theta^{s,ter}_{l_e,t}\right) \tag{5-19}$$

$$-f^{s}_{l_e,max} \le f^{s}_{l_e,t} \le f^{s}_{l_e,max} \tag{5-20}$$

$$\sum_{i_e \in I_e} P^{s}_{i_e,t} + P^{s}_{GT,t} + \sum_{j \in J} \omega^{s}_{j,t} + \sum_{l_e \in L_e} f^{s,ini}_{l_e,t} - \sum_{l_e \in L_e} f^{s,ter}_{l_e,t} = \sum_{k_e \in K_e} P_{k_e,t} \tag{5-21}$$

$$P_{i_g,min} \le P^{s}_{i_g,t} \le P_{i_g,max} \tag{5-22}$$

$$Pr^{2}_{l_g,min} \le Pr^{s^2}_{l_g,t} \le Pr^{2}_{l_g,max} \tag{5-23}$$

$$Pr^{s,ini}_{l_g,t} \ge Pr^{s,ter}_{l_g,t} \tag{5-24}$$

$$f^{s}_{l_g,t}{}^{2} = \gamma_{l_g}\left(Pr^{s,ini^2}_{l_g,t} - Pr^{s,ter^2}_{l_g,t}\right) \tag{5-25}$$

$$0 \le f^{s}_{l_g,t} \le f^{s}_{l_g,max} \tag{5-26}$$

$$P^{s}_{GT,t} = c_{GT} f^{s}_{l_g,GT} \tag{5-27}$$

$$\sum_{i_g \in I_g} P^{s}_{i_g,t} + \sum_{l_g \in L_g} f^{s,ini}_{l_g,t} - \sum_{l_g \in L_g} f^{s,ter}_{l_g,t} = \sum_{k_g \in K_g} P_{k_g,t} \tag{5-28}$$

5.5.4 Real-time Risk Mitigation

Considering potential FDIA and uncertainties of renewable resources, real-time risk mitigation is presented in the second stage to mitigate uneconomic dispatch. The approach is distributionally robust against FDIA and renewable uncertainty. The regulated generator and gas turbine output are shown in (5-29). Constraint (5-30) represents the electricity and gas load shedding limits. The limits considered in the

model is based on the existing research [112]. The regulated power flow is constrained in (5-31) and (5-32). Constraint (5-33) presents the limits for gas wells. The regulated gas pressure and flow are limited in (5-34)-(5-37). Based on (5-12), the new Weymouth coefficient $\gamma_{l_g}^{F}$ influenced by the attacked gas density is applied. Constraint (5-38)-(5-40) show that the power imbalance caused by renewable uncertainties should be offset by adjusting the reserves of generators and gas turbine. Specifically, constraint (5-38) ensures the deviation of renewable generation is within the range of up and down reserve limits. In (5-39) and (5-40), the adjustment factor $\eta_{i_e,t}$ and $\eta_{i_g,t}$ are the regulation commitment from generators and gas turbine to mitigate renewable uncertainties. Constraint (5-41) presents the regulated power generation of gas turbine. Constraint (5-42) and (5-43) ensure power and gas balance in the second stage.

$$P_{\{\cdot\},t}^{re} - r_{\{\cdot\},t}^{-} \le P_{\{\cdot\},t}^{re} \le P_{\{\cdot\},t}^{re} + r_{\{\cdot\},t}^{+}, \{\cdot\} = i_e, GT \tag{5-29}$$

$$0 \le P_{\{\cdot\},t}^{ls} \le P_{\{\cdot\},max}^{ls}, \{\cdot\} = k_e, k_g \tag{5-30}$$

$$x_l f_{l_e,t}^{re} = \left(\theta_{l_e,t}^{re,ini} - \theta_{l_e,t}^{re,ter}\right) \tag{5-31}$$

$$-f_{l_e,max}^{re} \le f_{l_e,t}^{re} \le f_{l_e,max}^{re} \tag{5-32}$$

$$P_{i_g,min} \le P_{i_g,t}^{re} \le P_{i_g,max} \tag{5-33}$$

$$Pr_{l_g,min}^{2} \le Pr_{l_g,t}^{re^2} \le Pr_{l_g,max}^{2} \tag{5-34}$$

$$Pr_{l_g,t}^{re,ini} \ge Pr_{l_g,t}^{re,ter} \tag{5-35}$$

$$f_{l_g,t}^{re\ 2} = \gamma_{l_g}^{F}\left(Pr_{l_g,t}^{re,ini^2} - Pr_{l_g,t}^{re,ter^2}\right) \tag{5-36}$$

$$0 \le f_{l_g,t}^{re} \le f_{l_g,max} \tag{5-37}$$

$$r_{\{\cdot\},t}^{-} \le \eta_{\{\cdot\},t} \sum_{j\in J}\left(\omega_{j,t}^{s} - \xi_{j,t}\right) \le r_{\{\cdot\},t}^{+}, \{\cdot\} = i_e, GT \tag{5-38}$$

$$0 \le \eta_{\{\cdot\},t} \le 1, \{\cdot\} = i_e, GT \tag{5-39}$$

$$\sum_{i_e\in I_e} \eta_{i_e,t} + \sum_{i_g\in I_g} \eta_{i_g,t}^{GT} = 1 \tag{5-40}$$

$$P_{GT,t}^{re} = c_{GT} f_{l_g,GT}^{re} \tag{5-41}$$

$$\sum_{i_e \in I_e} P_{i_e,t}^{re} + \sum_{j \in J} \xi_{j,t} + P_{GT,t}^{re} = \sum_{k_e \in K_e} P_{k_e,t} + \Delta P_{k_e,t} - P_{k_e,t}^{ls} \tag{5-42}$$

$$\sum_{i_g \in I_g} P_{i_g,t}^{re} + \sum_{l_g \in L_g} f_{l_g,t}^{re,ini} - \sum_{l_g \in L_g} f_{l_g,t}^{re,ter} = \sum_{k_g \in K_g} P_{k_g,t} + \Delta P_{k_g,t} - P_{k_g,t}^{ls} \tag{5-43}$$

Constraint (5-25) contains one nonlinear term, i.e., '$f_{l_g,t}^{s\,2}$' and constraint (5-36) contains two nonlinear terms, i.e., '$f_{l_g,t}^{re2}$' and '$\gamma_{l_g}^{F}\left(Pr_{l_g,t}^{ini^2} - Pr_{l_g,t}^{ter^2}\right)$'. They need to be linearized for obtaining convex functions and guaranteeing global optimal solutions. A sufficiently large constant M_{l_g} can be used to linearize '$\gamma_{l_g}^{F}\left(Pr_{l_g,t}^{ini^2} - Pr_{l_g,t}^{ter^2}\right)$', shown in (5-44) and (5-45). The bilinear term '$f_{l_g,t}^{s\,2}$' can be linearized by piecewise linear approximation by separating nonlinear function into pieces. Readers are referred to [23] for details. It should be noted that '$Pr_{l_g,t}^{ini^2}$' does not require linearization since it is regarded as squared form throughout the paper.

$$f_{l_g,t}^{re2} \le \left(Pr_{l_g,t}^{re,ini^2} - Pr_{l_g,t}^{re,ter^2}\right) + \left(1 - \gamma_{l_g}^{F}\right) M_{l_g} \tag{5-44}$$

$$f_{l_g,t}^{re2} \ge \left(Pr_{l_g,t}^{re,ini^2} - Pr_{l_g,t}^{re,ter^2}\right) + \left(1 - \gamma_{l_g}^{F}\right) M_{l_g} \tag{5-45}$$

5.6 Case Studies

A combined IEEE 30-bus electricity system and a 6-node gas system is used to test the effectiveness of the DR-FMS through the extensive case studies [57]. In the case studies, three types of FDIA are considered, namely EL-FDIA, GL-FDIA and GD-FDIA, which represent FDIA on electricity load, gas load and gas density, respectively. For EL-FDIA, the total load is unchanged, which is the fundamental condition of FDIA

TABLE 5-2 PARAMETERS OF GAS WELLS

Node No.	$P_{i_g,max}$ (kcf/h)	$P_{i_g,min}$ (kcf/h)	λ_{i_g}
4	35	10	2.2
6	70	20	2

TABLE 5-3 GENERATOR PARAMETERS

Bus No.	$P_{i_e,min}$ (MW)	$P_{i_e,max}$ (MW)	$R^+_{i_e}$, $R^-_{i_e}$ (MW)	a_{i_e}	b_{i_e}	c_{i_e}
1	50	200	20	0.004	2	6
2	20	80	16	0.002	2	6
5	15	50	10	0.006	1	8
8	10	35	7	0.008	3	10
11	10	30	10	0.025	3	18
13	12	40	16	0.025	3	18

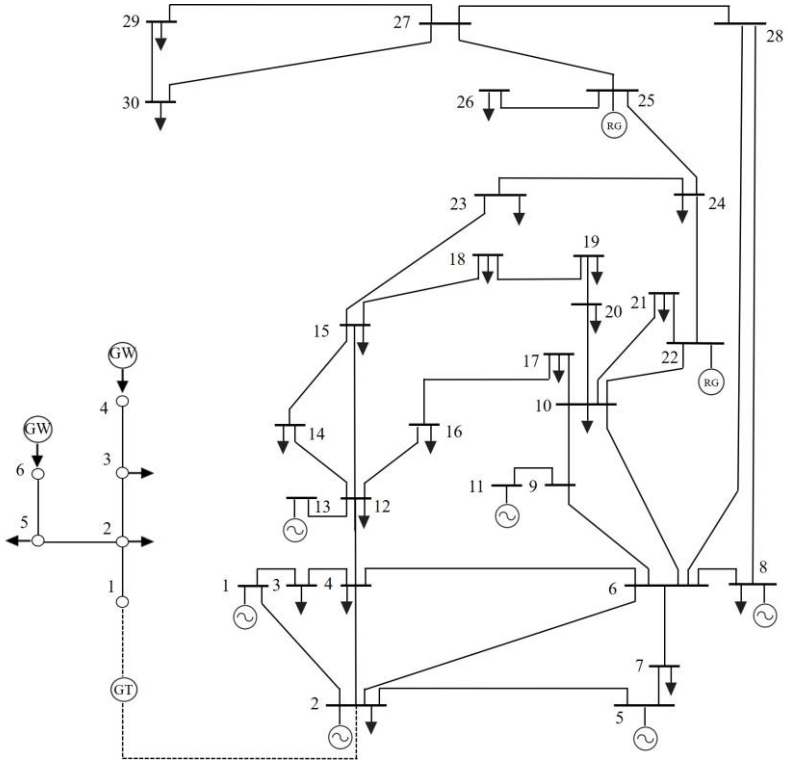

Fig. 5-1. Modified IEEE 30-bus system.

for evading the detection. The modelling of EL-FDIA can be also found in [95, 97, 113].

The following 10 cases are considered:

Case 1: Single-stage deterministic optimization for IEGS without considering FDIA or renewable uncertainty.

Case 2: RO based FMS with three types of FDIA (*AIL* =5%).

Case 3: Case 2 considering renewable uncertainty (*AIL* =5%).

Case 4: Two-stage DR-FMS considering FDIA on electricity load (*AIL* =5%).

Case 5: Case 4 considering FDIA on both gas and electricity load (*AIL* =5%).

Case 6: Case 5 considering FDIA on gas density (*AIL* =5%).

Case 7: Case 6 considering renewable uncertainty (*AIL* =5%).

Case 8-10: Case 7 with *AIL* =10%, 15% and 20%.

In case 3 and 7, the addition of renewable uncertainty is considered and the *AIL* is still 5% as case 2 and 4. The proposed test network is shown in Fig. 5-1, which contains 30 buses, 6 electricity generators, 2 renewable generators, 2 gas wells, 21 electricity loads and 3 gas loads. The renewable generators are connected to bus 22 and 25 with 60MW for each output. Parameters of electricity generators, gas wells are given in TABLEs 5-2 and 5-3, which can be found in [66].

The deterministic method for case 1 is a deterministic global optimization algorithm for solving linear programming. The reasons for not using metaheuristic optimization methods are: i) The deterministic linear programming problem solved by deterministic global optimization and metaheuristic optimization methods have similar results [114-116]; ii) The focus of this paper is to address FDIA and design mitigation schemes. The deterministic optimization method in case 1 is only used for comparison; iii) In practice, system operators implement economic dispatch after the data-filtering by state estimators, which requires high computational efficiency;; and iv) Metaheuristic methods, such as genetic algorithm and particle swarm optimization, easily converge prematurely and could be trapped into a local minimum, particularly with complex problems [117].

It should be noted that the DR-FMS considers the worst-case uncertainty distribution for both FDIA and renewable energy from all candidate distributions. Based on the partial distributional information, i.e., mean value vector and covariance matrix, DR-FMS can test all possible distributions modelled by moment information. Accordingly, this worst-distribution oriented mitigation scheme is a data-driven approach and actually tests a variety of scenarios.

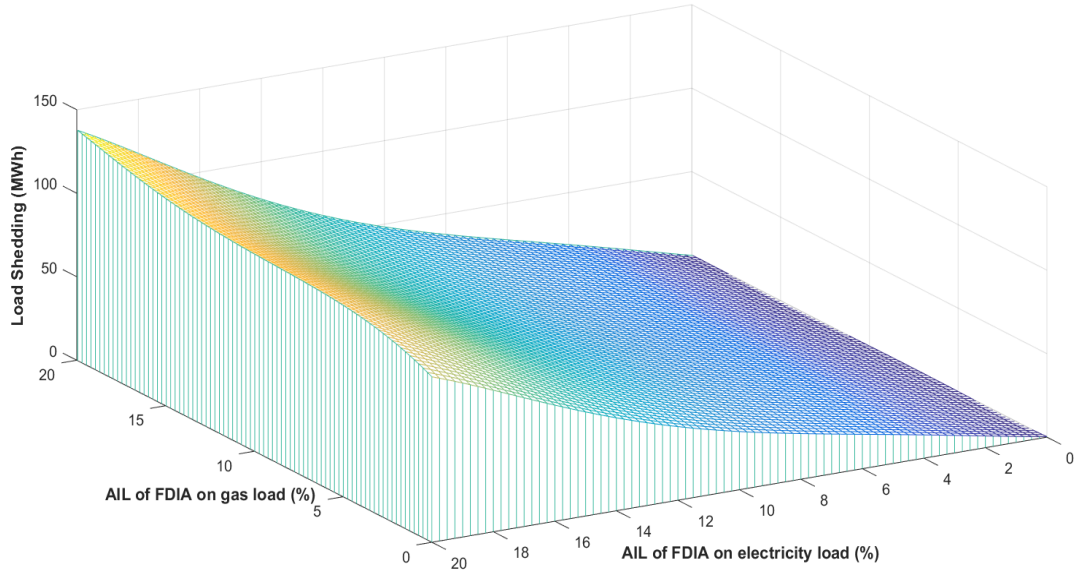

Fig. 5-2. Electricity load shedding under EL-FDIA and GD-FDIA.

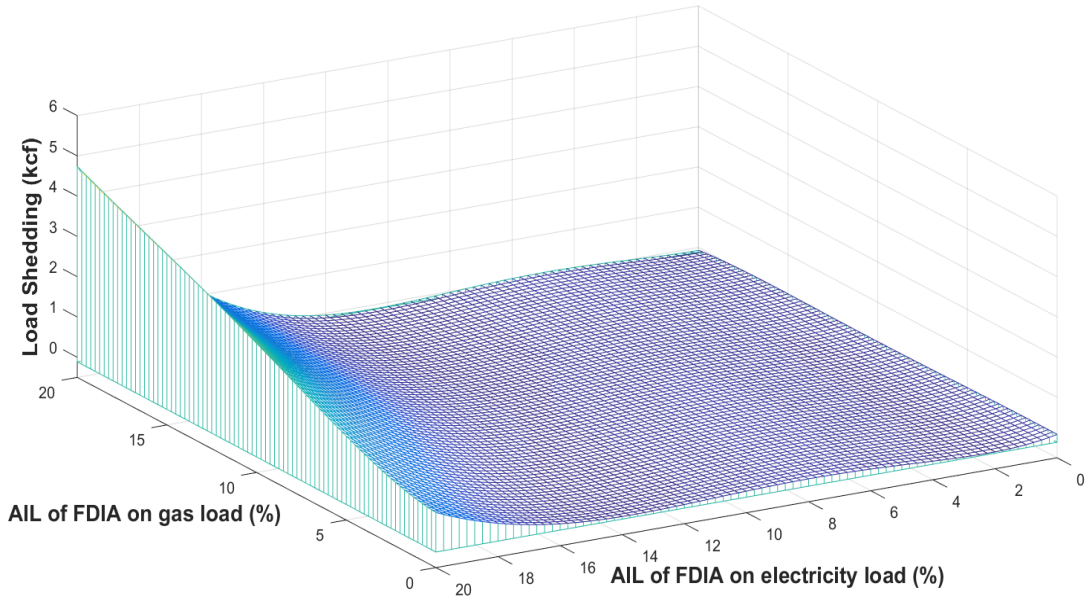

Fig. 5-3. Gas load shedding under EL-FDIA and GL-FDIA.

5.6.1 Studies on Economic Performance

Firstly, the economic performance for all 10 cases under different combinations of uncertainties is shown in TABLE 5-4. Case 10 has the highest total cost, i.e., \$132000, which is 21% higher than that of case 1, since EL-FDIA and GD-FDIA are comprehensively considered with the highest *AIL*. Case 1 has the lowest economic result since the deterministic model is applied. When considering the FDIA handled by RO in case 2 and DRO in case 6, the total cost increases by 11% and 10% respectively. In addition to the only consideration of FDIA by case 2, in case 3, when renewable

uncertainty is further considered, the expected total cost increases by 4%. The total economic cost of case 3 is $13080, higher than that in case 4. The main reasons are: i) case 3 considers all three types of FDIA while case 4 only considers EL-FDIA; ii) case 3 considers renewable uncertainty while case 4 does not, iii) case 3 is implemented under RO, which provides more conservative solutions even in the single-stage framework. For case 4, the second stage of DR-FMS considers corrective actions for the day-ahead operation, which accounts for a small portion of the total cost. The big portion of cost is from the first stage, because generation costs for electricity generators and gas wells are considered; and iv) the two-stage framework is a combination of stochastic programming, which derives more flexible second-stage decisions to adjust first-stage decisions and hedges against uncertain FDIA and renewable generation after their realization in the second stage [118, 119]. From case 4 to 10, two-stage DRO is applied, where different types of FDIA are considered in cases 4-7 and sensitivity analysis is studied for cases 7-10. Both the first-stage and second-stage expected costs are increasing for cases 4-7 from only considering EL-FDIA to considering all three types of FDIA with renewable uncertainties. It can be found that GL-FDIA has the largest impact on economic performance, i.e., the total cost of case 5 has 4.7% more cost than case 4. On the contrary, GD-FDIA has the least impact on economic performance with a 1.4% rise of total cost from case 5 to case 6. From case 7 to 10, 15% more *AIL* causes an increase of total cost from $124252 to $132000. It should be noted that although EL-FDIA does not increase the overall load increase since some loads are increasing while the rest are decreasing, FDIA aims at attacking critical loads for causing economic losses. Accordingly, under these three types of FDIA with high risks, DR-FMS is more suitable for risk assessment and mitigation considering the worst-distribution. This advantage with less-conservative solutions is reflected in the comparison between cases 2 and 6 as wells as cases 3 and 7, where cases 6 and 7 reduce $1215 and $1558 compared with cases 2 and 3, respectively.

TABLE 5-4 ECONOMIC PERFORMANCE FOR CASES 1-10

Economic result	Case 1	Case 2	Case 3	Case 4	Case 5	Case 6	Case 7	Case 8	Case 9	Case 10
First-stage cost ($)	108930	120955	125810	108835	113922	115465	119250	120880	122140	123480
Expected Second-stage cost ($)	0	0	0	3895	4132	4275	5292	7862	8043	8520
Total cost ($)	108930	120955	125810	112730	118054	119740	124252	128742	130183	132000

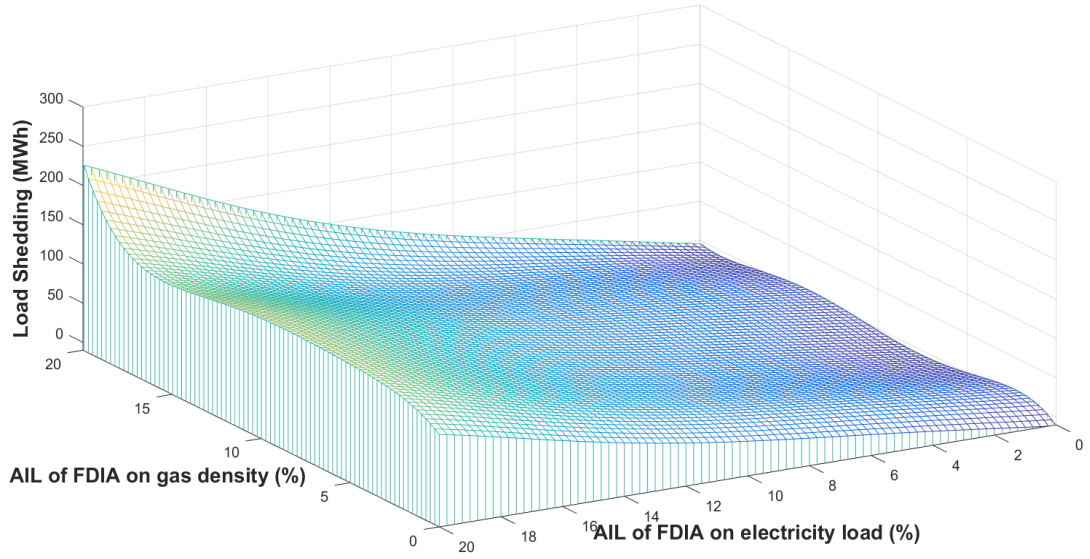

Fig. 5-4. Electricity load shedding under EL-FDIA and GD-FDIA.

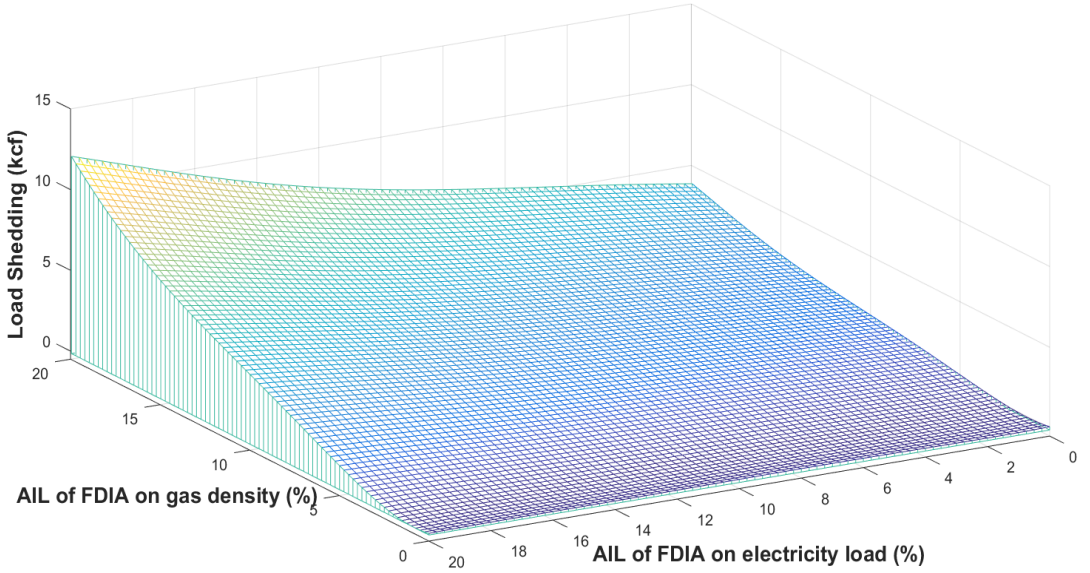

Fig. 5-5. Gas load shedding under EL-FDIA and GD-FDIA.

5.6.2 Studies on Load Shedding

To maintain the feasibility of optimization and system balance under FDIA and renewable uncertainty, it is necessary to implement load shedding. The electricity load shedding (ELS) and gas load shedding (GLS) for 24 hours under FDIA are given in Figs. 5-2 and 5-3. In Fig. 5-2, ELS is up to 140MWh when EL-FDIA and GL-FDIA are both 20%. ELS is not sensitive to increase when only increasing GL-FDIA level, but sensitive when increasing EL-FDIA. The reason is that the scale of electricity load is much larger than the gas load. Therefore, the GL-FDIA has a minor effect on ELS. In

TABLE 5-5 FCR FOR CASE 4-10

FCR	Line 1-2	Line 6-7	Line 27-28
Case 4	56%	56%	45%
Case 5	57%	69%	50%
Case 6	59%	78%	54%
Case 7	76%	87%	62%
Case 8	89%	93%	65%
Case 9	100%	95%	80%
Case 10	100%	96%	83%
FCR	Pipeline N4-N3	Pipeline N6-N5	Pipeline N1-2
Case 4	53%	63%	64%
Case 5	66%	65%	65%
Case 6	77%	66%	67%
Case 7	86%	66%	90%
Case 8	97%	68%	93%
Case 9	100%	68%	97%
Case 10	100%	69%	100%

Fig. 5-3, GLS reaches up to 4.7kcf when FDIA is at the maximum level. GLS increases smoothly when *AIL* of EL-FDIA is under 17% while increases significantly when it is over 17%.

The ELS and GLS under EL-FDIA and GD-FDIA are shown in Fig. 5-4 and Fig. 5-5. Compared with GL-FDIA in Fig. 5-2, 84 MWh more ELS is made when considering the GD-FDIA. Since the wrong gas density can directly influence the gas flow. When there is no EL-FDIA, ELS caused by GD-FDIA can still reach up to 3MWh. In Fig. 5-5, GLS reaches 13kcf at the maximum *AIL* compared with the 4.7kcf in Fig. 5-3, which again proves the significant impact of gas density on GLS. EL-FDIA and GL-FDIA show the similar impact on GLS, i.e., GLS increases by 10kcf when fixing GL-FDIA and increasing EL-FDIA while GLS increases by 13kcf when fixing EL-FDIA and only increasing GL-FDIA. Since as observed from Fig. 5-2, the scale magnitude of electricity load is much larger than gas load, which largely influences on both ELS and GLS.

As observed from Figs. 5-4 and 5-6, the impact of GL-FDIA and GD-FDIA on ELS is minor when EL-FDIA is 0%. It shows that when one type of FDIA is manipulated, the impact on ELS is minor. However, when multiple types of FDIA are conducted in,

TABLE 5-6 EL-FDIA ON GAS LOAD SHEDDING

AIL	0%	2%	4%	6%	8%	10%	12%	14%	16%	18%	20%
GLS (kcf)	1.46	1.67	1.88	2.09	2.30	2.53	2.84	3.19	3.62	4.08	4.54

TABLE 5-7 GL-FDIA ON ELECTRICITY LOAD SHEDDING

AIL	0%	2%	4%	6%	8%	10%	12%	14%	16%	18%	20%
ELS (MWh)	34.3	36.8	39.8	39.9	41.1	41.4	42.3	42.9	43.7	48.0	48.53

TABLE 5-8 GD-FDIA ON ELECTRICITY LOAD SHEDDING

AIL	0%	2%	4%	6%	8%	10%	12%	14%	16%	18%	20%
ELS (MWh)	34.5	48.7	48.7	48.7	48.7	48.7	48.7	48.7	50.0	78.0	111.7

the impact on ELS could be large. In Fig. 5-2, with the AIL increase of both GL-FDIA and EL-FDIA, the ELS is massive, which is 99MWh when the AIL of GL-FDIA is 0% and 139MWh when AIL of GL-FDIA is 20%. The EL-FDIA is fixed but there is a 40MWh increase of GLS. In Fig. 5-5, GLS under EL-FDIA and GD-FDIA is given. When GD-FDIA is 0%, EL-FDIA has a low impact on GLS even when the AIL is 20%. However, when AIL of GD-FDIA is at 20%, GLS ranges from 4.7kcf to 13kcf, and when AIL of GD-FDIA is at 20%, GLS ranges from 4.7kcf to 13kcf. This indicates that the security interdependency between electricity and gas systems is minor when attackers only conduct one type of FDIA, but when multiple types of FDIA is attacking the IEGS, it will lead to massive load shedding.

5.6.3 Studies on Flow-Capacity Ratio

To study the FDIA impact on power and gas flow, in TABLE 5-5, flow-capacity ratio (FCR) for three power lines and three gas pipelines at the peak load time period are studied, which is defined as the percentage of flow divided by the line capacity. The FCR of line N1-N2 and pipeline N4- N3 and N1-2 all reach 100% when maximum *AIL* is considered since these three lines play vital parts for interconnecting buses and transmitting flow. From cases 4 to 7, there is a general increase for FCR of power lines and gas pipelines since types of FDIA are gradually incorporated. From cases 7 to 10, the FCR still monotonically increases when *AIL* is increasing from 5% to 20%. It should be noted that line 1-2 and line 27-28 are more sensitive to increase of *AIL* with a 24% and 21% increase respectively. Compared to pipeline N4-N3 which is prone to

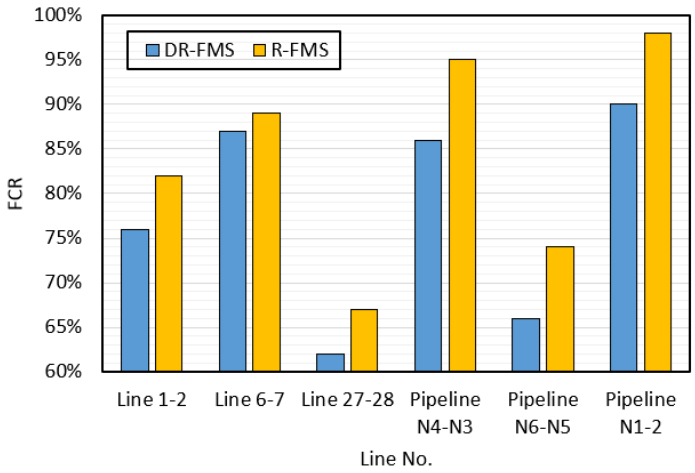

Fig. 5-6. FCR for power lines and gas pipelines at peak load period.

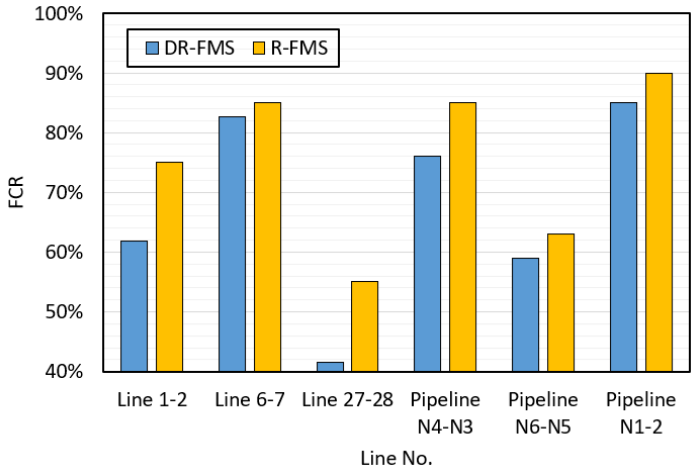

Fig. 5-7. FCR for power lines and gas pipelines at lowest load period.

overloading, the FCR of pipeline N6-N5 ranges only reaches 69%, indicating that gas flow is mainly sourced from the gas well connected to node 4.

5.6.4 Discussion on System Interdependency under FDIA

The interdependency between electricity and gas systems worsen the system security, i.e., the FDIA on electricity system has adverse impact on gas system and vice versa. TABLE 5-6, 5-7 and 5-8 present the impact of EL-FDIA on GLS, GL-FDIA on ELS and GD-FDIA on ELS, respectively. The EL-FDIA has minor impact on gas system compared with GL-FDIA on gas system and GL-FDIA or GD-FDIA have also minor impact on electricity system compared with EL-FDIA on electricity system. In order to observe a more obvious result, TABLE 5-6 is under the fixed 10% of GD-FDIA and TABLEs 5-7 and 5-8 are under the fixed 10% of EL-FDIA.

A smooth increase of GLS is shown in TABLE 5-6, i.e., the increase of GLS with the 20% increase of EL-FDIA is only 3kcf. The GLS accounts for 1% when EL-FDIA is at 20%. The potential reasons for this result are i) the electricity system is resilient enough based on multiple electricity generators and renewable generators which does not require massive supply from gas system and ii) the overall operation cost and load shedding of IEGS will increase significantly provided that gas system provides more supply to electricity system while implements more GLS. In TABLE 5-7, GL-FDIA causes 48.5MWh ELS when *AIL* is at 20%. The result is on the contrary of TABLE 5-6 since GL-FDIA causes gas wells supply more on gas system itself, which can be also viewed from Fig. 5-3. The increase of GL-FDIA does not result in significant increase of GLS, which indicates that there is far less gas to power flow. In TABLE 5-8, GD-FDIA shows a more severe impact on ELS. The ELS when GD-FDIA is 0% is only 34.5MWh while it increases dramatically and reaches 111.7 when GD-FDIA is 20%. The reason is that GD-FDIA directly increases the gas density, which accordingly limits the gas flow and the gas turbine production is restricted.

5.6.5 Comparison with RO Based Mitigation Scheme

State estimation calculates the states of all buses and filters raw measurements based on the data from the SCADA system. Then reliable measurement will be provided to system operators to conduct system operation, e.g., economic dispatch, optimal power flow and contingency analysis, etc. In practice, there are three possible scenarios under FDIA: i) FDIA is detected by state estimator, thus launched unsuccessfully; ii) FDIA is launched successfully and the system operator takes immediate corrective measures according to the falsified measurements; iii) FDIA is launched successfully but the risk mitigation scheme proposed in this paper can be deployed.

The first scenario can be handled by deterministic optimization shown in case 1 based on the ‘clean’ load measurement with false data filtered out. The second scenario needs to be modelled with the expectation of optimization solutions. The realization for the second scenario requires huge computational burden since the computational dimension is large, i.e., i) EL-FDIA can be manipulated on 20 electricity loads, ii) GL-FDIA can be manipulated on 3 gas loads, iii) GD-FDIA can be manipulated on 4 gas pipelines and iv) this mitigation scheme considers 24 time periods. For the sake of computational efficiency, the mitigation scheme based on scenario approach is ignored in this study. The third scenario is computational efficient and can be modelled by either DR-FMS

or robust optimization based FDIA mitigation scheme (R-FMS). Furthermore, the real-time mitigation can be implemented prior to the real attacks by considering reasonable and relatively reliable attack scenarios. Note that the FDIA includes EL-FDIA, GL-FDIA and GD-FDIA. DR-FMS which mimics moderate-conservative FDIA scenarios is compared with R-FMS representing the worst-case FDIA scenario on the system.

The comparison made between DR-FMS and R-FMS is in Figs. 5-8 and 5-9. In general, the (flow-capacity ratio) FCR from R-FMS is higher than that from DR-FMS for all power lines and gas pipelines. In Fig. 5-6, the FCR in pipeline N1-2 has the highest level. The FCR solved by DR-FMS is 90% and 98% by R-FMS. Pipeline N4-N3 has the second-highest FCR and the difference between DR-FMS and R-FMS is 9%. Fig. 5-7 depicts the FCR at the lowest load period, which shows lower FCR for all power lines and gas pipelines. The largest FCR difference from DR-FMS and R-FMS is for line 27-28, which is 13%. For line 6-7, the FCR difference modelled by two schemes is the lowest for both peak and lowest load period. To summarize, DR-FMS not only provide more economic operation scheme but yields lower FCR since the FDIA is considered in a moderate robust manner.

5.7 Chapter Summary

A risk mitigation scheme for IEGS against FDIA is proposed in this paper with a two-stage DRO model. The hierarchical two-stage framework is able to determine both day-ahead and real-time system optimal operation schemes considering the impact of FDIA and renewable uncertainties on electricity load, gas load and gas density. A tractable SDP formulation is built for the original DR-FMS, which is solved by CGA in an iterative manner. Through the extensive case studies, the key findings are listed below:

- Considering all three types of FDIA, i.e., EL-FDIA, GL-FDIA and GD-FDIA, leads to higher economic results and more load shedding than considering two types or one type of FDIA.
- Load shedding is more sensitive to EL-FDIA than GD-FDIA or GL-FDIA.
- DRO provides less-conservative results than RO in terms of economic performance and load shedding.
- Renewable generation uncertainty is necessary to consider, which leads to 3.7% more operation cost.

The proposed DR-FMS ensures the economic performance of IEGS by providing a two-stage risk mitigation scheme via implementing efficient load shedding under FDIA and renewable uncertainty. The beneficiaries of this work inlcude: network operators can have powerful operation models, end customers will enjoy better supply security, and renewable can penetrate to the maximum level without much curtailment.

Chapter 6

Voltage Management in Integrated Energy Systems Considering Interdependency and Renewable Uncertainty

This chapter investigates the volt-VAR optimization within the integrated electricity and gas systems. The optimal voltage management is achieved through efficiently coordinating the operation of on-load tap changers, photovoltaic systems, and shunt capacitor banks

Statement of Authorship

This declaration concerns the article entitled:			
Voltage Management in Integrated Energy Systems Considering Interdependency and Renewable Uncertainty			
Publication status: Accepted			
Publication details (reference)	P. Zhao, C. Gu, Y. Xiang, X. Zhang, Y. Shen and S. Li, "Reactive Power Optimization in Integrated Electricity and Gas Systems," in ***IEEE Systems Journal***, doi: 10.1109/JSYST.2020.2992583.		
Candidate's contribution to the paper	The candidate and the second author jointly proposed the idea of the paper, and they designed the methodology. The candidate designed the case studies, and executed most of the coding to derive the experimental results. The third author helped the candidate with the format of the paper, and improvement of academic writing. The percentage of the candidate did compared with the whole work is indicated as follows: Formulation of ideas: 70% Design of methodology: 80% Experimental work: 90% Presentation of data in journal format: 70%		
Statement from candidate	This paper reports on original research I conducted during the period of my Higher Degree by Research candidature.		
Signed	Pengfei Zhao	Date	03/04/2020

6.1 Abstract

Volt/VAR optimization (VVO) is one important operation in distribution systems to maintain acceptable voltage profiles. However, the high penetration of renewable generation poses severe challenges to VVO, leading to voltage deviation and fluctuation. This is further complicated by the growing coupling between electricity and natural gas systems. To resolve unacceptable voltage deviation under energy system interdependency, this paper proposes a co-optimization of VVO for an integrated electricity and gas system (IEGS) with uncertain renewable generation. A two-stage data-driven distributionally robust optimization (DRO) is developed to model the coordinated optimization problem, which determines two-stage VVO and operation schemes with dispatch and corrective adjustment through active power regulation and reactive power support in both day-ahead and real-time stage. A semidefinite programming is reformulated to ensure the tractability and the proposed problem is solved by a constraint generation framework. Simulation studies are conducted on a 33-bus-6-node and a 69-bus-20-node IEGS. Case studies demonstrate that the interdependency between electricity and gas systems reduces 4.7% of operation cost and a significant rise in the voltage profile.

6.2 Nomenclature

Indices and sets

t, T	Index and set for time periods.
b , B	Index and set for electricity buses.
i_e, I_e	Index and set for traditional distributed generators (DG).
i_g, I_g	Index and set for natural gas sources.
gt,GT	Index and set for gas turbines.
j, J	Index and set for renewable power generators.
l_e, L_e	Index and set for power lines.
l_g, L_g	Index and set for gas pipelines.
k_e, K_e	Index and set for electric loads.
k_g, K_g	Index and set for gas loads.

Parameters

w_1^V, w_1^E	Weighting coefficients for voltage regulation and economic dispatch oriented sub-objectives in the first stage.
w_2^V, w_2^E	Weighting coefficients for voltage regulation and economic dispatch oriented sub-objectives in the second stage.
π_v	the penalty cost coefficient for penalizing the voltage deviation.
V_b^{ref}	Nominal voltage magnitude.
$\lambda_{sub}^a, \lambda_{sub}^r$	Unit cost for active and reactive power supplied from upper market.
$\lambda_{i_e}^a, \lambda_{i_e}^b, \lambda_{i_e}^c$	Cost coefficients for generation of traditional DG i_e.
λ_{i_g}	Cost coefficient for generation of natural gas source i_g.
$\lambda_{i_e}^+$, $\lambda_{i_e}^-$	Cost coefficient for up and down reserve of traditional DG i_e.
$\lambda_{i_e}^{re}, \lambda_j^{re}$	Regulation cost coefficient for traditional DG i_e and renewable power generator j.
$\lambda_{k_e}^{ls}$, $\lambda_{k_g}^{ls}$	Penalty cost coefficient for electricity and gas load shedding.
$P_{sub,max}$	Maximum active power transfer of substation.
$R_{i_e}^+$, $R_{i_e}^-$	Maximum up and down reserve capacity of traditional DG i_e at time *t*.
R_{gt}^+, R_{gt}^-	Maximum up and down reserve capacity of gas turbine *gt* at time t.
$P_{i_e,max}$, $P_{i_e,min}$	Maximum and minimum output of tradiational DG i_e.
$P_{i_g,max}$, $P_{i_g,min}$	Maximum and minimum output of natural gas source i_g.
$P_{gt,max}$, $P_{gt,min}$	Maximum and minimum output of gas turbine *gt*.
$V_{b,max}, V_{b,min}$	Maximum and minimum voltage limit.
δ^{OLTC}	Size of change for each step in OLTC tap position.
nTP_{max}^{OLTC}	Maximum allowed number of switching operations of OLTC.
$\omega_{j,t}^{P,s}$	Forecasted active power output of renewable power generator *j* at time *t*.

u_{PV}	Associated coefficient for connecting active and reactive PV power.
$PF_{pv,min}$	Minimum power factor of PV system *pv*.
Q_{cb}^{cap}	Reactive power capability for capacitor bank *cb*.
V_0	Reference voltage magnitude.
$f_{l_e,max}^{a,}$, $f_{l_e,max}^{r,}$	Maximum active and reactive power flow of line l_e.
$P_{k_e,t}$, $Q_{k_e,t}$, $P_{k_g,t}$	Active and reactive electricity load and gas load at time *t*.
$Pr_{l_g,max}$, $Pr_{l_g,min}$	Maximum and minimum gas pressure of gas pipeline l_g.
γ_{l_g}	Coefficient for Weymouth equation.
$f_{l_g,max}$	Maximum gas flow of pipeline l_g.
$P_{k_e,max}^{ls}$, $P_{k_g,max}^{ls}$	Maximum electricity and gas load shedding at time *t*.
$\eta_{i_e,t}$, $\eta_{gt,t}$	Participation factor for reserves of traditional DG i_e and gas turbine *gt* at time *t*.

Variables and functions

$P_{sub,t}^{s}$,$Q_{sub,t}^{s}$	Scheduled active and reactive power supply from upper market.
$P_{sub,t}^{re}$,$Q_{sub,t}^{re}$	Regulated active and reactive power supply from upper market.
$P_{i_e,t}^{s}$,$P_{i_e,t}^{re}$	Scheduled and regulated output of traditional DG i_e at time *t*.
$P_{i_g,t}^{s}$,$P_{i_g,t}^{re}$	Scheduled and regulated output of natural gas source i_g at time *t*.
$r_{i_e,t}^{+}$, $r_{i_e,t}^{-}$	Up and down reserve of traditional DG i_e at time *t*.
$r_{gt,t}^{+}$, $r_{gt,t}^{-}$	Up and down reserve of gas turbine *gt* at time t.
$V_{b,t}^{s}$, $V_{b,t}^{re}$	Scheduled and regulated voltage of bus b at time *t*.
$V_{sub,t}^{s}$, $V_{sub,t}^{re}$	Scheduled and regulated voltage of substation at time *t*.
$TP_t^{s,OLTC}$, $TP_t^{re,OLTC}$	Scheduled and regulated tap position of OLTC at time *t*.
$\omega_{j,t}^{Q,s}$, $\omega_{j,t}^{Q,re}$	Scheduled and regulated reactive power output of renewable power generator *j* at time *t*.
$u_{cb,t}^{s}$, $u_{cb,t}^{re}$	Scheduled and regulated switch status for capacitor bank *cb* at time *t*.

$Q_{cb,t}^{s}$, $Q_{cb,t}^{re}$	Scheduled and regulated reactive power output for capacitor bank *cb* at time *t*.
$V_{b,t}^{s,ini}$, $V_{b,t}^{s,ter}$	Scheduled voltage magnitude for initial and terminal nodes.
$V_{b,t}^{re,ini}$, $V_{b,t}^{re,ter}$	Regulated voltage magnitude for initial and terminal nodes.
$f_{l_e,t}^{a,s}$, $f_{l_e,t}^{r,s}$	Scheduled active and reactive power flow at time *t*.
$f_{l_e,t}^{a,re}$, $f_{l_e,t}^{r,re}$	Regulated active and reactive power flow at time *t*.
$f_{l_g,t}^{ini}$, $f_{l_g,t}^{ter}$	Gas flow from initial node and to terminal node of pipeline l_g at time *t*.
$Pr_{l_g,t}^{s}$, $Pr_{l_g,t}^{re}$	Scheduled and regulated gas pressure of gas pipeline l_g at time *t*.
$Pr_{l_g,t}^{s,ini}$,$Pr_{l_g,t}^{s,ter}$	Scheduled gas pressure of initial and terminal nodes of pipeline l_g at time *t*.
$Pr_{l_g,t}^{re,ini}$,$Pr_{l_g,t}^{re,ter}$	Regulated gas pressure of initial and terminal nodes of pipeline l_g at time *t*.
$P_{k_e,t}^{ls}$, $P_{k_g,t}^{ls}$	Electricity and gas load shedding at time *t*.
x, *y*	Vectors of first and second stage variables.
Uncertainty	
$\xi_{j,t}$	Uncertainty of renewable power forecast of *j* at time *t*.
$D_{\xi_{j,t}}$	Ambiguity set for renewable power uncertainty.
$\mu_{\xi_{j,t}}, \Sigma_{\xi_{j,t}}$	Mean vector and covariance matrix for renewable forecast uncertainty.
Θ	Second moment matrix.
VS	Polyhedral set of extreme points.

6.3 Introduction

Volt-VAR optimization (VVO) is one primary function in the distribution management system to maintain voltage in an acceptable range by optimally coordinating equipment, e.g., capacitor banks, on-load tap changers (OLTC) and voltage regulators [120-130]. Paper [121] proposes a deterministic VVO as mixed-integer quadratic programming to control voltage and VAR devices for day-ahead operation. Considerable loss reduction and total demand reduction are achieved through

the proposed VVO. To achieve energy savings and peak demand reduction through voltage reduction, a multi-objective VVO is proposed in [122] using a nondominated sorting genetic algorithm. Paper [123] proposes a three-phase distribution system considering unbalancing with battery storage providing reactive power. Both power loss and energy purchase cost are minimized. In [124], to extend the life of distribution system transformers, a detailed model of life loss is proposed to estimate the ageing reduction of transformers under VVO.

The penetration of renewable energy has dramatically increased over the past decade. However, due to its variable and intermittent nature, it poses operational and security challenges to VVO by affecting normal operations of OLTCs and capacity banks [127, 131, 132]. Existing literature has considered renewable power uncertainties in designing economic and reliable periodical equipment scheduling plans. A two-stage chance-constrained VVO is employed to handle the uncertainties of distributed generation and load demand [127]. Paper [131] proposes a chance-constrained optimization to model the randomness of renewable energy and minimize feeder power losses while avoiding voltage violations, solved by a gradient descent based algorithm. A hierarchical robust optimization (RO) is adopted for coordinating reactive compensators to guarantee voltage magnitudes [132]. This reactive power optimization is formulated to a mixed-integer convex-based programming based on the conic relaxation of the branch flow. And a modified column-and-constraint generation algorithm based on the second-order cone programming is employed to solve the problem.

The interdependency of multi-energy systems, electricity, natural gas, and heating/cooling, is also becoming markedly common, which has many implications for VVO. Research on integrated electricity and gas systems (IEGS) is widely investigated in traditional problems, e.g., modelling, operation and planning [133-135]. However, high renewable integration brings security and operational challenges to managing IEGS, particularly to system voltage, due to intermittency and fluctuation, [104, 110, 135]. To hedge against renewable power uncertainty in IEGS, deterministic optimization, two-stage and multi-stage stochastic optimization (SO) have been widely used [110]. For example, paper [104] proposes a robust security-constrained unit commitment in IEGS considering distributed natural gas storage to enhance operational reliability.

Overall, RO and SO are the two main approaches to handle uncertainties from growing renewable energy resources for both VVO and IEGS operation problems. As for SO, it either assumes an explicit distribution for random variable or requires a large number of data samples. It is prone to causing errors when the historical data is not adequately sufficient to represent true distributions and inevitably leads to high computational burden if a large number of data samples are used. As for RO, it does not require an exact probability distribution but constrains uncertain variables in a predefined uncertainty set. RO considers the worst-case scenario against all realizations characterized by uncertainty sets, which could have extremely low probability and thus produces over-conservative results. In practice, it is rare that the uncertainty realization appears on the bounds of uncertainty set. The interval-based RO strictly ensures that the optimization is feasible even considering the worst-case solution. The uncertainty is treated as variables bounded within the predetermined set without the association with any probability distribution.

Therefore, it is of necessity to handle the uncertainty through a relative less conservative optimization technique without requiring large datasets. As a promising optimization method to handle uncertainties, distributionally robust optimization (DRO) inherits the advantages of both RO and SO, overcoming the explicit assumptions on probability distributions of SO and over-conservatism of RO [65, 136-138]. For DRO, the ambiguity set is constructed by statistical information, such as moment, to restricting possible distributions. Based on more valuable distribution information, research finds that the best estimate of the distribution can be obtained through the statistical fitting. Accordingly, statistical distance information can be added in the ambiguity set and thus the size of the ambiguity set can be controlled. In addition, compared with RO, DRO determines expected results over all possible distributions, which are less-conservative.

Paper [78] proposes a risk-based optimal gas power flow by using DRO. It considers the zonal linepack and linepack reserve to distinguish fuel suppliers and ensure the security of gas systems. A security-constrained two-stage ED with renewable power uncertainty modelled by DRO is designed in [64]. The segregated linear decision rule is used to affinely approximate the decision variables after the first time period which reduces the computational burden. Paper [57] investigates a DRO for IEGS considering the uncertainties of electricity and gas loads. Price-Based demand response is

considered to improve energy efficiency and economic benefits. DRO can provide a less conservative solution for VVO problem when capturing renewable uncertainties and thus mitigate the impact on voltage deviations caused by renewable uncertainties. In addition, the two-stage framework contains both day-ahead and real-time framework, which provides flexible measures for system operators with adjustment capability.

This paper proposes a novel coordinated two-stage multi-objective optimization for voltage control in economic dispatch (ED), considering uncertain renewable generation and multi-vector energy system integration. The two-stage voltage constrained optimization is referred to as TS-VCO for simplicity. The optimal voltage is achieved through efficiently coordinating the operation of OLTCs, photovoltaic (PV) systems, and shunt capacitor banks. In the first stage, based on historical PV output, an initial day-ahead operation plan for traditional DGs, natural gas sources, OLTCs and capacitor banks is produced to maintain voltage and minimize daily operation cost. In the second stage, after the realization of uncertain PV output, the recourse action is developed to control voltage controlling those devices, meanwhile minimizing system operation cost in real time. The original TS-VCO is transformed into a conic tractable form with the dual formulation and solved by constraint generation algorithm (CGA). Case studies demonstrate that voltage control devices and dispatchable generators can be optimally controlled and coordinated to realise the designed objectives.

The main contributions of this paper are as follows:

1) To the best of authors' knowledge, none existing work has investigated VVO in an IEGS, where this paper is the first such effort to fill the research gap. The strong coupling of power and gas infrastructure and tight interdependency between two systems are considered.
2) It develops a multi-objective coordinated optimization for maintaining acceptable voltage while considering system operation cost of IEGS, which ensures system security and economic performance.
3) The two-stage DRO approach is first applied in VVO, which provides less-conservative results using RO and requires fewer data samples. It can handle renewable uncertainties effectively, providing flexible measures for IEGS operators.

The rest of this paper is organized as follows. Section 6.4 presents objective function and system constraints of TS-VCO. The DRO method and associated reformulations are presented in section 2.1.2. Section 6.5 demonstrates case studies and the

performance of the TS-VCO. Section 6.6 concludes this paper.

6.4 Problem formulation

The proposed TS-VCO contains i) day-ahead co-optimization that restricts voltages for all buses while scheduling traditional DGs and natural gas sources, and ii) real-time recourse action that regulates voltage and redispatches generators considering PV output uncertainty. When implementing economic operation in distribution systems, the voltage profile of each bus can also be improved by optimally coordinating voltage regulating equipment [139-142]. In this paper, maintaining the voltage deviation within an acceptable range is considered as voltage profile improvement.

6.4.1 TS-VCO Objective Function

The first-stage problem in (6-1) is to simultaneously minimize i) the voltage deviation for all buses, Γ_1^V in (6-2) and ii) the cost of generation and reserve capacity, Γ_1^E in (6-3), respectively. Γ_1^V represents the total voltage deviation for all buses in the entire time horizon. Γ_1^E includes i) generation cost of traditional DGs and natural gas sources and ii) reserve cost of traditional DGs. The generation cost function of traditional DGs is quadratic with coefficients a_i, b_i and c_i. The weighting coefficients w_1^V and w_1^E represent the priorities that TS-VCO have on Γ_1^V and Γ_1^E, respectively. It should be noted that the penalty cost coefficient π_v is applied for penalizing the voltage deviation on each bus. The penalty cost coefficient enables to transform voltage deviation to monetary lost which can be combined with operation cost.

$$\Gamma_1 = \min w_1^V \pi_v \Gamma_1^V + w_1^E \Gamma_1^E \tag{6-1}$$

$$\Gamma_1^V = \min \sum_{b\in B, t\in T} \left| V_{b,t}^s - V_b^{ref} \right| \tag{6-2}$$

$$\begin{aligned} \Gamma_1^E = \min \sum_{i_e\in I_e, i_g\in I_g, t\in T} & \lambda_{sub}^a P_{sub,t}^s + \lambda_{sub}^r Q_{sub,t}^s + \lambda_{i_e}^a {P_{i_e,t}^s}^2 + \lambda_{i_e}^b P_{i_e,t}^s \\ & + \lambda_{i_e}^c + \lambda_{i_g} P_{i_g,t}^s + \lambda_{i_e}^+ r_{i_e,t}^+ + \lambda_{i_e}^- r_{i_e,t}^- \end{aligned} \tag{6-3}$$

Similar to (6-1)-(6-3), (6-4)-(6-6) are the second-stage overall objective and sub-objectives. The second-stage optimization considers load shedding to keep the system balance under fluctuation caused by renewable uncertainties. It should be noted that Γ_2^E contains i) the penalty cost for PV curtailment, ii) regulated generation cost of traditional DGs and natural gas sources and iii) electricity and gas load shedding cost.

$$\Gamma_2 = \min w_2^V \pi_v \Gamma_2^V + (1 - w_2^V)\Gamma_2^E \tag{6-4}$$

$$\Gamma_2^V = \min \sum_{b\in B, t\in T} \left|V_{b,t}^{re} - V_b^{ref}\right| \tag{6-5}$$

$$\begin{aligned}\Gamma_2^E = \min \sum_{i_e\in I_e, i_g\in I_g, t\in T, k_e\in K_e, k_g\in K_g} & \lambda_{sub}^a P_{sub,t}^{re} + \lambda_{sub}^r Q_{sub,t}^{re} \\ & + \lambda_j^{re}\left|\omega_{j,t}^s - \xi_{j,t}\right| + \lambda_{i_e}^{re}\left|P_{i_e,t}^s - P_{i_e,t}^{re}\right| + \lambda_{i_e}^{re}\left|P_{i_g,t}^s - P_{i_g,t}^{re}\right| \\ & + \lambda_{k_e}^{ls} P_{k_e,t}^{ls} + \lambda_{k_g}^{ls} P_{k_g,t}^{ls}\end{aligned} \tag{6-6}$$

6.4.2 Day-ahead VVO

In the first stage, the day-ahead optimization is based on the forecasted renewable output before its uncertainty realised. Equations (6-7)-(6-29) represent the first-stage constraints. The active and reactive power for substation injected from the upper level is limited in (6-7) and (6-8). The up and down reserve capacity for traditional DGs and gas turbines is constrained in (6-9) and (6-10). In the distribution network, the proposed day-ahead reserve capacity is for compromising the real-time renewable power uncertainties. Constraints (6-11)-(6-12) ensure the generation of traditional DGs and gas turbines within the predefined limits considering reserve capacity. The voltage magnitude for all buses is regulated in (6-13) by setting minimum and maximum limits. In (6-14), the substation voltage can be determined by OLTC tap position and the step size of each tap position. Constraint (6-15) regulates the total operation number of OLTC tap since too many operations will accelerate the wear process of the transformer [128, 143, 144]. In (6-16), the reactive power of PV is described by the forecasted active PV power output and the power factor as defined in (6-17). The reactive power from capacity banks is given in (6-18). The linearized DistFlow for distribution systems is presented in (6-19) and (6-20). The power balance constraints for active and reactive power are in (6-21) and (6-22). The output of natural gas sources is constrained in (6-23). Equations (6-24) and (6-25) are the constraints on gas pressure, where, in distribution systems, the pressure of initial nodes is always higher than terminal nodes. In (6-26), Weymouth equation is used to characterize the relationship between gas flow and pressure. The gas flow is constrained in (6-27). The relationship between the gas turbine output and injected gas flow is given in (6-28). And equation (6-29) models nodal gas balancing.

$$0 \le P_{sub,t}^{s} \le P_{sub,max} \tag{6-7}$$

$$0 \le Q_{sub,t}^{s} \le Q_{sub,max} \tag{6-8}$$

$$0 \le r_{\{\cdot\},t}^{+} \le R_{\{\cdot\}}^{+}, \{\cdot\} = i_e, gt \tag{6-9}$$

$$0 \le r_{\{\cdot\},t}^{-} \le R_{\{\cdot\}}^{-}, \{\cdot\} = i_e, gt \tag{6-10}$$

$$P_{\{\cdot\},t}^{s} + r_{\{\cdot\},t}^{+} \le P_{\{\cdot\},max}, \{\cdot\} = i_e, gt \tag{6-11}$$

$$P_{\{\cdot\},min} \le P_{\{\cdot\},t}^{s} - r_{\{\cdot\},t}^{-}, \{\cdot\} = i_e, gt \tag{6-12}$$

$$V_{b,min} \le V_{b,t}^{s} \le V_{b,max} \tag{6-13}$$

$$V_{sub,t}^{s} = V_{sub}^{ref} + \delta^{OLTC} TP_t^{s,OLTC} \tag{6-14}$$

$$\sum_{t \in T} \left| TP_t^{s,OLTC} - TP_{t-1,}^{s,OLTC} \right| \le nTP_{max}^{OLTC} \tag{6-15}$$

$$0 \le \omega_{j,t}^{Q,s} \le u_{PV} \omega_{j,t}^{P,s} \tag{6-16}$$

$$u_{PV} = \sqrt{\frac{1 - PF_{PV,min}{}^{2}}{PF_{PV,min}{}^{2}}} \tag{6-17}$$

$$Q_{cb,t}^{s} = u_{cb,t}^{s} Q_{cb}^{cap} \tag{6-18}$$

$$V_{b,t}^{s,ini} - V_{b,t}^{s,ter} = \left(f_{l_e,t}^{a,s} r_{l_e} + f_{l_e,t}^{r,s} x_{l_e} \right) / V_0 \tag{6-19}$$

$$0 \le f_{l_e,t}^{\{\cdot\},s} \le f_{l_e,max}^{\{\cdot\},s}, \{\cdot\} = a, r \tag{6-20}$$

$$\sum_{i_e \in I_e} P_{i_e,t}^{s} + \sum_{j \in J} \omega_{j,t}^{P,s} + \sum_{l_e \in L_e} f_{l_e,t}^{a,s,ini} - \sum_{l_e \in L_e} f_{l_e,t}^{a,s,ter} + \sum_{gt \in GT} P_{gt,t}^{s} = \sum_{k_e \in K_e} P_{k_e,t} \tag{6-21}$$

$$\sum_{i_e \in I_e} Q_{i_e,t}^{s} + \sum_{j \in J} \omega_{j,t}^{Q,s} + \sum_{cb \in CB} Q_{cb,t}^{s} + \sum_{l_e \in L_e} f_{l_e,t}^{r,s,ini} - \sum_{l_e \in L_e} f_{l_e,t}^{r,s,ter} = \sum_{k_e \in K_e} Q_{k_e,t} \tag{6-22}$$

$$P_{i_g,min} \le P_{i_g,t}^{s} \le P_{i_g,max} \tag{6-23}$$

$$Pr_{l_g,min}^2 \le Pr_{l_g,t}^{s^2} \le Pr_{l_g,max}^2 \tag{6-24}$$

$$Pr_{l_g,t}^{s,ini} \ge Pr_{l_g,t}^{s,ter} \tag{6-25}$$

$$f_{l_g,t}^{s\ 2} = \gamma_{l_g}\left(Pr_{l_g,t}^{s,ini^2} - Pr_{l_g,t}^{s,ter^2}\right) \tag{6-26}$$

$$0 \le f_{l_g,t}^{s} \le f_{l_g,max} \tag{6-27}$$

$$P_{gt,t}^{s} = c_{gt} f_{l_g,gt}^{s} \tag{6-28}$$

$$\sum_{i_g \in I_g} P_{i_g,t}^{s} + \sum_{l_g \in L_g} f_{l_g,t}^{s,ini} - \sum_{l_g \in L_g} f_{l_g,t}^{s,ter} = \sum_{k_g \in K_g} P_{k_g,t} + \sum_{gt \in GT} P_{gt,t}^{s} \tag{6-29}$$

6.4.3 Real-time VVO

The real-time corrective dispatch is in the second stage considering renewable power uncertainty, which regulates voltage and generation output of traditional DGs and natural gas sources. Equations (6-30) and (6-31) limit the power transfer of substations. The regulated output of traditional DGs and gas turbines is given in (6-32). Electricity and gas load shedding constraint is in (6-33). Equation (6-34) is the constraint for voltages for all buses. The substation voltage is defined in (6-35). In (6-36), the regulated total operation number of OLTC tap is constrained. The reactive power of PV generators and capacity banks are ensured in (6-37) and (6-38). DistFlow is applied again in the second stage describing power flow in (6-39) and (6-40). The active and reactive power balance constraints are in (6-41) and (6-42), respectively. The regulated output of natural gas sources is given in (6-43). For modelling gas flow, the Weymouth equation is presented from (6-44)-(6-47) with gas pressure constrained. Constraint (6-48) describes the relationship between the gas flow injection and gas turbine output. The aim of the regulation of traditional DGs and natural gas sources is to mitigate adverse effects from renewable output deviation, which is achieved by adjusting reserves for power capacity from (6-49) to (6-51). In (6-49), renewable output deviation should be within the up and down reserve limits. To address renewable power uncertainty, the participation factors $\eta_{i_{e,t}}$ and $\eta_{i_{g,t}}$ are defined in (6-50) and (6-51) to represent the regulation commitment by traditional DGs and natural gas sources. Finally, (6-52) presents the balancing condition of the gas system.

$$0 \le P_{sub,t}^{re} \le P_{sub,max} \tag{6-30}$$

$$0 \le Q_{sub,t}^{re} \le Q_{sub,max} \tag{6-31}$$

$$P_{\{\cdot\},t}^{re} - r_{\{\cdot\},t}^{-} \le P_{\{\cdot\},t}^{re} \le P_{\{\cdot\},t}^{re} + r_{\{\cdot\},t}^{+}, \{\cdot\} = i_e, gt \tag{6-32}$$

$$0 \le P_{\{\cdot\},t}^{ls} \le P_{\{\cdot\},max}^{ls}, \{\cdot\} = k_e, k_g \tag{6-33}$$

$$V_{b,min} \le V_{b,t}^{re} \le V_{b,max} \tag{6-34}$$

$$V_{sub,t}^{re} = V_{sub}^{ref} + \delta^{OLTC} TP_t^{re,OLTC} \tag{6-35}$$

$$\sum_{t \in T} \left| TP_t^{re,OLTC} - TP_{t-1,}^{re,OLTC} \right| \le nTP_{max}^{OLTC} \tag{6-36}$$

$$0 \le \omega_{j,t}^{Q,re} \le u_{PV} \omega_{j,t}^{P,re} \tag{6-37}$$

$$Q_{cb,t}^{re} = u_{cb,t}^{re} Q_{cb,t}^{ref} \tag{6-38}$$

$$V_b^{re,ini} - V_b^{re,ter} = \left(f_{l_e,t}^{a,re} r_{l_e} + f_{l_e,t}^{r,re} x_{l_e} \right) / V_0 \tag{6-39}$$

$$0 \le f_{l_e,t}^{\{\cdot\},re} \le f_{l_e,max}^{\{\cdot\}}, \{\cdot\} = a, r \tag{6-40}$$

$$\sum_{i_e \in I_e} P_{i_e,t}^{re} + \sum_{j \in J} \xi_{j,t} + \sum_{gt \in GT} P_{gt,t}^{s} = \sum_{k_e \in K_e} P_{k_e,t} + \Delta P_{k_e,t} - P_{k_e,t}^{ls} \tag{6-41}$$

$$\sum_{i_e \in I_e} Q_{i_e,t}^{s} + \sum_{j \in J} \omega_{j,t}^{Q,s} + \sum_{cb \in CB} Q_{cb,t}^{s} + \sum_{l_e \in L_e} f_{l_e,t}^{r,s,ini} - \sum_{l_e \in L_e} f_{l_e,t}^{r,s,ter} = \sum_{k_e \in K_e} Q_{k_e,t} \tag{6-42}$$

$$P_{i_g,min} \le P_{i_g,t}^{re} \le P_{i_g,max} \tag{6-43}$$

$$Pr_{l_g,min}^{2} \le Pr_{l_g,t}^{re^2} \le Pr_{l_g,max}^{2} \tag{6-44}$$

$$Pr_{l_g,t}^{re,ini} \ge Pr_{l_g,t}^{re,ter} \tag{6-45}$$

$$f_{l_g,t}^{re} \left| f_{l_g,t}^{re} \right| = \gamma_{l_g} \left(Pr_{l_g,t}^{re,ini^2} - Pr_{l_g,t}^{re,ter^2} \right) \tag{6-46}$$

$$0 \le f_{l_g,t}^{re} \le f_{l_g,max} \tag{6-47}$$

$$P_{gt,t}^{re} = c_{gt} f_{l_g,gt}^{re} \tag{6-48}$$

$$r_{i_e,t}^{-} \le \eta_{i_e,t} \sum_{j \in J} \left(\omega_{j,t}^{s} - \xi_{j,t}\right) \le r_{i_e,t}^{+}, \{\cdot\} = i_e, gt \tag{6-49}$$

$$0 \le \eta_{\{\cdot\},t} \le 1, \{\cdot\} = i_e, gt \tag{6-50}$$

$$\sum_{i_e \in I_e} \eta_{i_e,t} + \sum_{gt \in GT} \eta_{i_g,t}^{gt} = 1 \tag{6-51}$$

$$\sum_{i_g \in I_g} P_{i_g,t}^{re} + \sum_{l_g \in L_g} f_{l_g,t}^{re,ini} - \sum_{l_g \in L_g} f_{l_g,t}^{re,ter} = \sum_{k_g \in K_g} P_{k_g,t} + \sum_{gt \in GT} P_{gt,t}^{re} - P_{k_g,t}^{ls} \tag{6-52}$$

6.5 Case Studies

As shown in Fig. 6-1, the proposed TS-VCO and CGA are firstly verified on a modified IEEE 33-bus system connected with a 6-node gas system in radial topology from [145] and [66]. A gas turbine connects the two separated systems, which generates electricity using natural gas. To testify the effectiveness of the TS-VCO in different conditions, comparison between 8 scenarios is considered and the details are given in

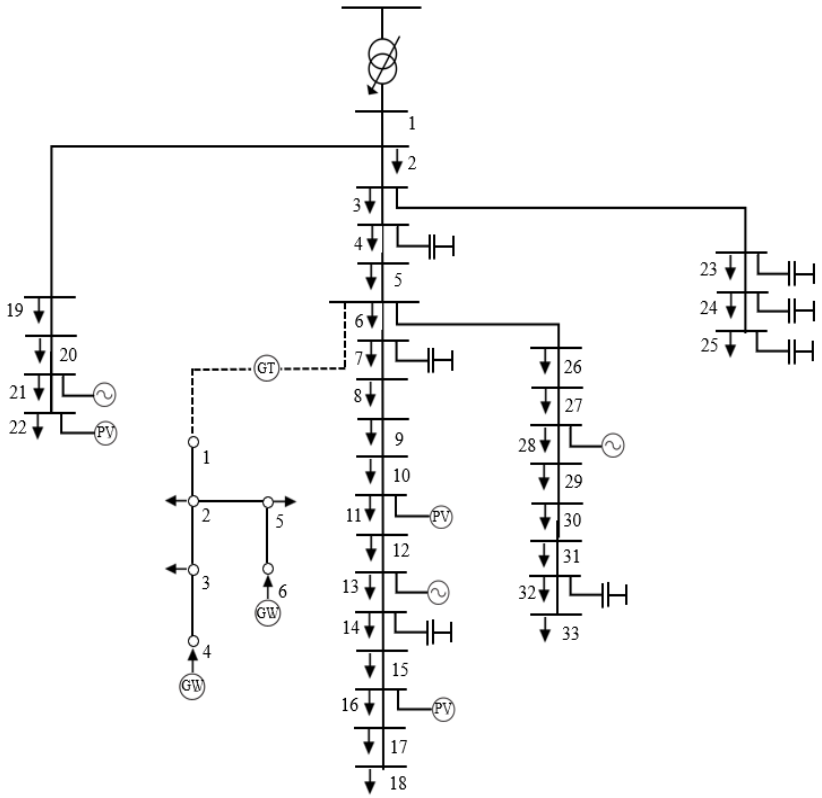

Fig. 6-1. A modified IEEE 33-bus system and a 6-node gas system.

TABLE 6-1 CASE ILLUSTRATION

Case No.	Weighting coefficients	Optimization method	PV system capacity (kVA)	Connected to gas system
1	$w^V = 0.5$	Deterministic	200	Yes
2	$w^V = 0.5$	Robust	200	Yes
3	$w^V = 0.5$	DRO	200	Yes
4	$w^V = 0.25$	DRO	200	Yes
5	$w^V = 0.75$	DRO	200	Yes
6	$w^V = 0.5$	DRO	400	Yes
7	$w^V = 0.5$	DRO	800	Yes
8	$w^V = 0.5$	DRO	200	No

TABLE 6-1. Cases 1-3 are used to compare mathematical performance of different optimization methods. Cases 3-5 compare the impact of varying optimization priorities on voltage deviation and economic performance. The impact of PV penetration and capacitor bank capacity are analysed in cases 3, 6 and 7. Case 8 studies the scenario without natural gas connection. In addition, a modified IEEE 69-bus system with a 20-node gas system is used for the test with 8 cases.

6.5.1 Studies on The 33-bus-6-node IEGS

In the electricity system shown in Fig. 6-1, it contains i) 3 traditional DGs connected with bus 13, 21 and 28, ii) 3 PV systems connected with bus 11, 16 and 22 with each capacity of 200kVA, and iii) 7 capacitor banks which have the same capacity of 30kVar. The substation transformer has 32 tap positions with a step size of 0.003 which ranges from -16 to 16. The maximum allowed operation number between two continuous-time slots for OLTC is set as 3. The voltage limit on each bus is set between 0.95 p.u. and 1.05 p.u.. The gas system has 6 nodes, containing 2 natural gas sources and 3 gas loads. The conversion factor 3.313 is used to convert \$/kcf to \$/MWh when simultaneously considering electricity and gas load shedding in IEGS. This paper uses 100\$/MWh and 120\$/kcf (400\$/MWh) as the shedding cost for electricity and gas load, respectively. The detailed parameters of natural gas sources and traditional DGs are given in TABLEs 6-2 and 6-3.

TABLE 6-2 PARAMETERS OF NATURAL GAS SOURCES

Node No.	$P_{i_g,min}$ (kcf/h)	$P_{i_g,max}$ (kcf/h)	λ_{i_g} ($/kcf)
4	1000	6000	2.2
6	1000	3000	2

TABLE 6-3 GENERATOR PARAMETERS

Bus No.	$P_{i_e,max}$ (MW)	$P_{i_e,min}$ (MW)	R_i^+, R_i^- (MW)	a_i ($/MW²)	b_i ($/MW)	c_i ($)
13	1.2	0.3	0.2	6000	7100	6200
21	1.2	0.3	0.2	4500	10500	4000
28	1.0	0.1	0.2	4500	10500	4000

A. Studies on Economic Performance

The economic performance for all cases is analysed first, presented in TABLE 6-4. The cost of the first and second stages are presented in TABLE 6-4. Case 5 has the highest total cost ($30111) while case 4 has the lowest cost ($25398) since the optimization priority of case 5 focuses on minimizing the voltage deviation while gives less focus on economic performance. Case 4 considers 75% of objective weighting on economic performance, which leads to $4713 less total cost than case 5. Cases 1-3 have the same optimization priority on sub-objectives and the same IEGS configuration. Case 1 provides a total cost of $27343, which is 5.8% and 2.8% less than case 2 and 3. The advantage of DRO is the less conservatism when modelling PV output uncertainty compared with RO, which is reflected in the 2.9% less cost of case 3 compared with case 2. Compared with case 3, the PV capacity is doubled and quadrupled in cases 6 and 7, which address the high generation of traditional DGs and natural gas sources. However, compared with case 3, case 6 and 7 cause higher second-stage cost due to the penalty cost of PV output deviation in the first and second stage. Without support from the gas system, case 8 yields 4.7% more cost than case 3. It is because the generation cost from natural gas sources is lower than that of traditional DGs and the pipeline capacity is set enough for large gas flow.

B. Studies on Voltage Profile

The voltage profiles of 33 buses in 24 time periods for cases 3, 6 and 7 with different capacity of PV systems are shown in Fig. 6-2. The red dotted curve is the mean voltage profile among all buses for clearer presentation and comparison. In case 3, with the

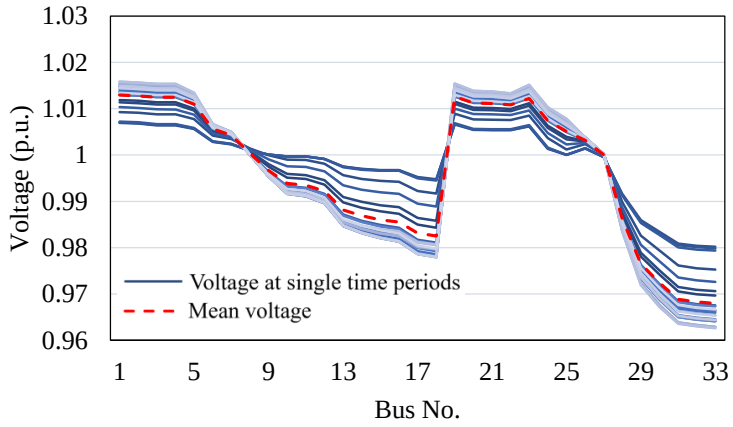

Fig. 6-2. Expected real-time voltage profiles for case 3.

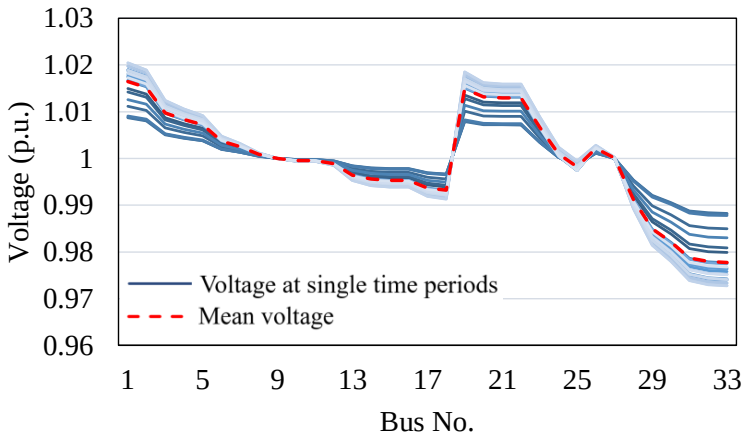

Fig. 6-3. Expected real-time profiles for case 6.

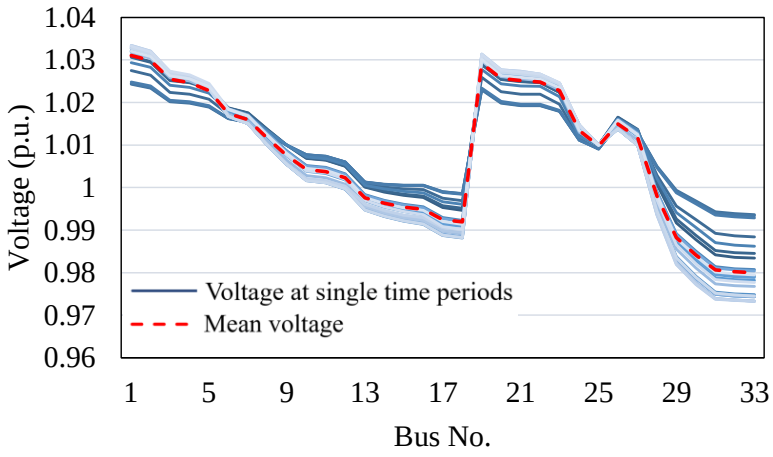

Fig. 6-4. Expected real-time profiles for case 7.

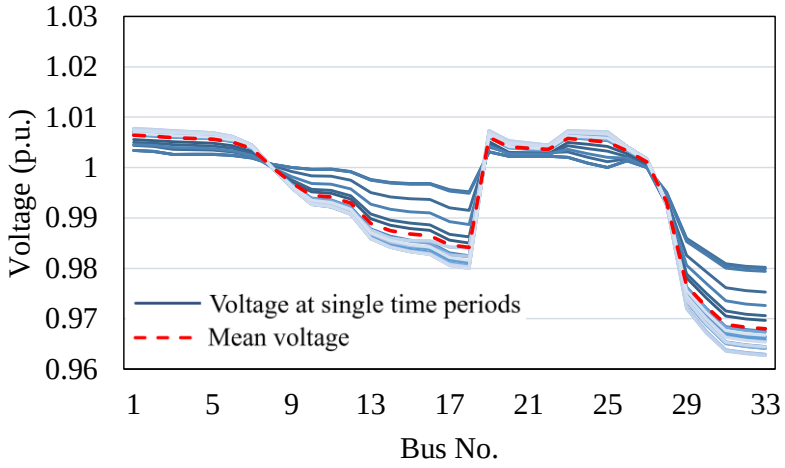

Fig. 6-5. Expected real-time voltage profiles for case 8.

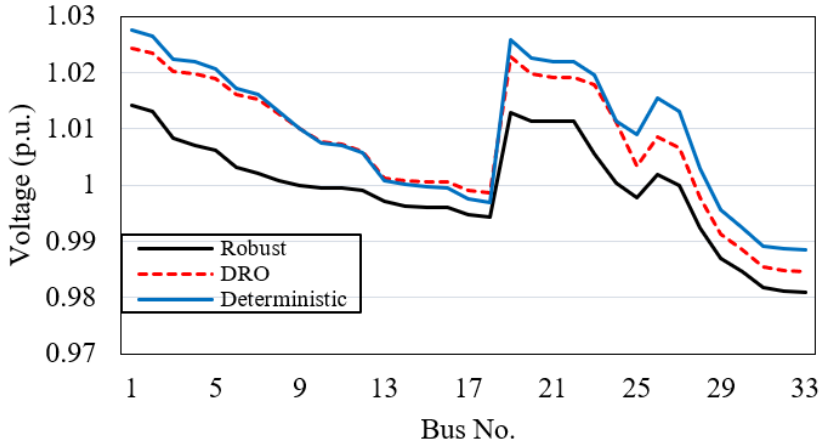

Fig. 6-6. Voltage profiles for case 1,2 and 3 at 20th time period.

least PV capacity connected, the voltage level ranges from 0.963 p.u. to 1.016 p.u.. With the higher PV connection in case 6, i.e., 200kVA more capacity of each PV, the voltage profile has been improved by 1%. In case 7, the voltage level reaches up to 1.032 p.u. when the PV capacity is 800kVA, which causes voltage improvement by 1.5% compared with case 3. The comparison between cases 3, 6 and 7 shows the increase of voltage level for all buses with the increasing PV penetration. The PV systems not only provide active power support but reactive power support, which will lead to the reduction of power losses in the real world. In Fig. 6-5, without connecting the gas system, the voltage profile of case 8 ranges between 0.96 p.u. and 1.00 p.u., which is lower than in case 3.

Cases 3, 6, 7 and 8 are used to study the impact of PV uncertainty on voltage deviations with different methods. In Fig. 6-6, voltage profile from the deterministic optimization is the highest, whilst that from RO is the lowest. The voltage difference is approximately 0.01 p.u., i.e., 0.13kV. Compared with the deterministic approach, DRO

leads to a more conservative result. Compared with RO, DRO mitigates the conservatism by 0.008 p.u., which considers the worst uncertainty distribution instead of the worst-case PV uncertainty of RO.

C. Studies on OLTC

The OLTC tap position for 24 time periods is given in Fig. 6-7. With the highest PV capacity connected, the OLTC tap position remains the highest in case 7, which starts from +10 position and maintains at +11 position from the 8th hour to 24th hour. With lower PV capacity, OLTC tap position in cases 3 and 6 are at relatively lower level since the system voltage level is low and can be maintained in an acceptable range without a large deviation from nominal voltage. In case 8, the tap position ranges from +1 to +3 and the maximum tap position deviation is 1, i.e., from +1 to +2 or +2 to +3. The reason is without the gas system connected, there is no power support converted from the gas flow, which will not raise the voltage level.

6.5.2 Studies on the 69-bus-20-node IEGS

The scalability study is conducted in the modified IEEE 69-bus system as given in Fig. 6-8. There are 6 PV systems connected at buses 9, 23, 26, 34, 44 and 58, respectively. The 12 capacitor banks and transformer are used to compensate the reactive power. The 20-node gas system contains two natural gas sources and two gas turbines, which are connected between the gas and electricity system.

A. Studies on Voltage Profile

In Fig. 6-9, the voltage profiles of cases 1, 6 and 8 are studied to investigate the impact from gas system connection. In case 1, it can be seen that the voltage level is decreasing along the main branch from bus 5 to bus 28. And the voltage level remains approximately the same value between bus 28 and bus 50 at 1.02 p.u.. With two gas turbines connected, the voltage level ranges from 0.952 p.u. to 1.020 p.u.. With only one connection with gas system, the voltage level is lower than that of case 1, which ranges from 0.952 p.u. to 1.007 p.u.. Compared with case 1, when no gas turbines equipped, the voltage profile decreases by 0.8% in case 8. The comparison between cases 1, 6 and 8 shows the increase of the voltage level for all buses with the addition of gas system connection.

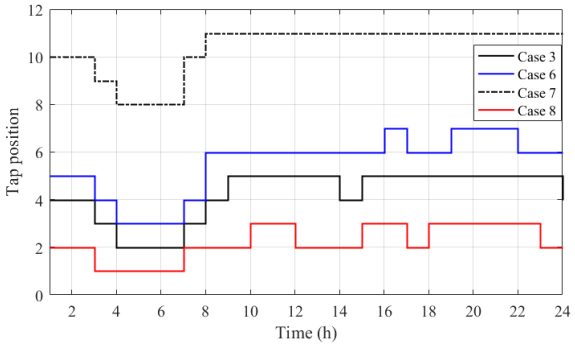

Fig. 6-7. OLTC tap position for cases 3,6,7 and 8.

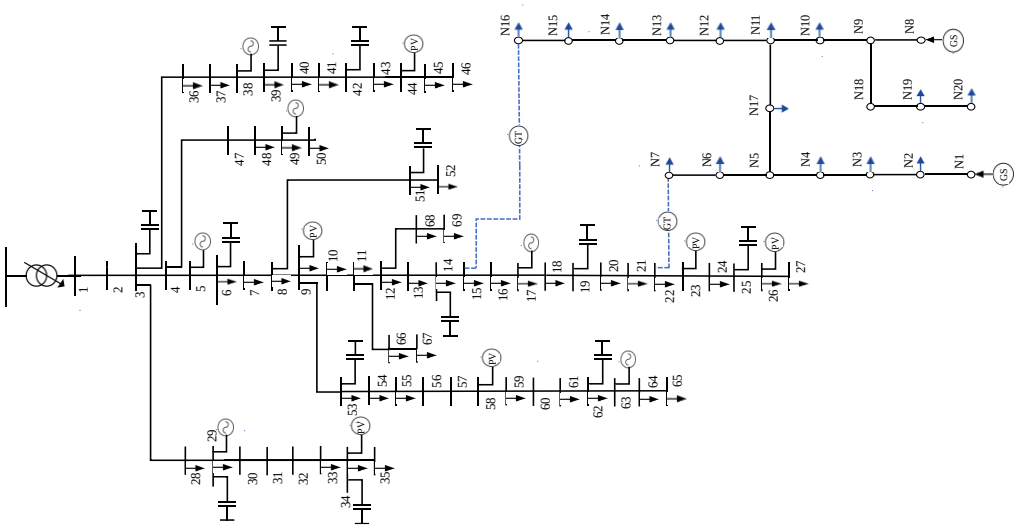

Fig. 6-8. A modified IEEE 69-bus system with a 20-node gas system.

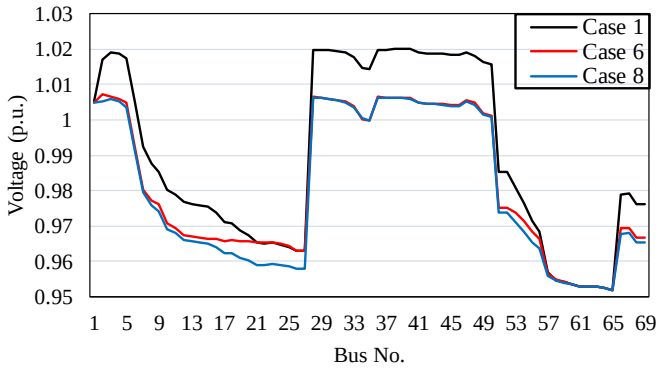

Fig. 6-9. Expected real-time voltage profile s for cases 1, 6 and 8.

B. Studies on Reactive Power Compensators

This subsection studies the scheduling and impact of capacitor banks and PV systems when regulating the voltage magnitude through reactive power support. The reactive power output of capacitor banks in cases 1, 4, 5 and 8 on selected buses is given in Fig. 6-10. The reactive power of case 4 is the highest since the capacity of capacitor banks

is twice compared with case 1. At buses 25, 29, 34, 39 and 42, the reactive power output is scheduled in the relatively low level. Since the load level is low with the less requirement of voltage regulation.

The reactive power output of PV systems is given in Figs. 6-11 - 6-14. Overall, the total PV reactive power output follows the trend of the reactive power load curve, where it peaks at 20:00 and the lowest level occurs at 4:00. The reactive power output from PV at bus 23 contributes the most while the PV at bus 34 contributes the least. The potential reason is that bus 34 is connected to both a PV system and a capacitor bank. Accordingly, the requirement of reactive power from PV system is not much. Case 5 has the highest level of PV reactive power output due to the case setting. The reactive power output ranges from 0.14MVar to 0.21MVar. By contrast, the reactive power output from PV systems in case 4 is the lowest since the total capacity of capactor banks is the highest in all cases, which reduces the reactive power support from PV systems.

6.6 Chapter Summary

This paper proposes a multi-objective optimization for minimizing both operation cost and voltage deviation of IES considering renewable power uncertainty. A two-stage data-driven DRO approach is used to solve the TS-VCO with dual and SDP formulations to ensure computational tractability. The reformulated TS-VCO is solved by CGA with master and subproblems. The key findings from the case studies are :

- Based on a large amount of moment information, DRO produces less conservative results compared with RO, more effective for maintaining voltage deviation and reducing operation cost considering renewable power uncertainty.
- The interdependency between electricity and gas systems reduces 4.7% of operation cost and a significant rise in the voltage profile.
- The proposed TS-VCO is effective in maintaining voltage and saving operation cost considering PV uncertainty.

This work can benefit integrated system operators with powerful operation tool to manage the systems with fewer costs but integrate more renewable energy.

Chapter 7

Distributionally Robust Operation for Integrated Energy Systems with Hydrogen Injection and Gas Quality Improvement

This chapter develops a new gas quality management scheme for hydrogen injection into natural gas systems produced from excessive wind power. It introduces four gas quality indices for the integrated electricity and gas system measuring gas quality, considering the coordinated operation of tightly coupled infrastructures.

Statement of Authorship

This declaration concerns the article entitled:			
Distributionally Robust Operation for Integrated Energy Systems with Hydrogen Injection and Gas Quality Improvement			
Publication status: Accepted			
Publication details (reference)	P. Zhao, C. Gu, Z. Hu, D. XIE, I. Hernando-Gil and Y. Shen, "Distributionally Robust Hydrogen Optimization with Ensured Security and Multi-Energy Couplings," in ***IEEE Transactions on Power Systems***, doi: 10.1109/TPWRS.2020.3005991.		
Candidate's contribution to the paper	The candidate and the second author jointly proposed the idea of the paper, and they designed the methodology. The candidate designed the case studies, and executed most of the coding to derive the experimental results. The third author helped the candidate with the format of the paper, and improvement of academic writing. The percentage of the candidate did compared with the whole work is indicated as follows: Formulation of ideas: 70% Design of methodology: 80% Experimental work: 90% Presentation of data in journal format: 70%		
Statement from candidate	This paper reports on original research I conducted during the period of my Higher Degree by Research candidature.		
Signed	Pengfei Zhao	Date	04/04/2020

7.1 Abstract

Power-to-gas (P2G) can convert excessive renewable energy into hydrogen via electrolysis, which can then be transported by natural gas systems to bypass constrained electricity systems. However, the injection of hydrogen could impact gas quality since gas composition fundamentally changes, adversely affecting the combustion, safety and lifespan of appliances.

This paper develops a new gas quality management scheme for hydrogen injection into natural gas systems produced from excessive wind power. It introduces four gas quality indices for the integrated electricity and gas system (IEGS) measuring gas quality, considering the coordinated operation of tightly coupled infrastructures. To maintain gas quality under an acceptable range, the gas mixture of nitrogen and liquid petroleum gas with hydrogen is adopted to address the gas quality violation caused by hydrogen injection. A distributionally robust optimization (DRO) modelled by Kullback-Leibler (KL) divergence-based ambiguity set is applied to flexibly control the robustness to capture wind uncertainty. The KL divergence-based ambiguity set defines the uncertainties within a measured space which limits the shape of probability distributions. Case studies demonstrate that wind power is maximally utilized and gas mixture is effectively managed, thus improving both gas quality and performance of IEGS. The work can benefit system operators with i) ensured gas quality under hydrogen injection ii) low system operation cost and iii) high renewable energy penetration.

7.2 Nomenclature

Indices and sets

t, T	Index and set for time periods.
n, N	Index and set for nodes in gas system.
i_e, I_e	Index and set for traditional distributed generators (DG).
i_g, I_g	Index and set for natural gas sources.
j, J	Index and set for wind turbines.
l_e, L_e	Index and set for power lines.
l_g, L_g	Index and set for gas pipelines.
k_e, K_e	Index and set for electric loads.
k_g, K_g	Index and set for gas loads.
k_h, K_h	Index and set for heating loads.

Parameters

η_e	Electrical efficiency for electrolyser.
$\eta_{hy-ca}, \eta_{hy-me}$	Reaction coefficients for required carbon dioxide and methanation output.
$G_{i_g,max}, G_{i_g,min}$	Maximum and minimum output of natural gas source i_g at time t.
$Pr_{l_g,max}, Pr_{l_g,min}$	Maximum and minimum gas pressure of gas pipeline l_g.
γ_{l_g}	Weymouth constant for pipeline l_g.
$f_{l_g,max}$	Maximum gas flow of pipeline l_g.
CF_{l_g}	Compressor's compression factor at pipeline l_g.
η_{GT}	Conversion efficiency of gas turbine.
$\Omega_{hy}, \Omega_{LPG}, \Omega_{ni}, \Omega_{me},$ Ω_{mix}	Gross calorific value (GCV) for hydrogen, liquid petroleum gas (LPG), nitrogen, methane and mixed natural gas.
$\rho_{hy}, \rho_{LPG}, \rho_{ni}, \rho_{me}$	Gas density of hydrogen, liquid petroleum gas, nitrogen and methane.
$E_{hy}, E_{LPG}, E_{ni}, E_{me}$	Combustion potential index (CPI) of hydrogen, liquid petroleum gas, nitrogen and methane.
O_i	Oxygen index.
$\Omega_{max}^{mix}, SG_{max}^{mix},$ $WI_{max}^{mix}, CP_{max}^{mix}$	Maximum limit for GCV, specific gravity, wobbe index (WI) and Combustion Potential (CP) of mixed gas.
$\Omega_{min}^{mix}, SG_{min}^{mix},$ $WI_{min}^{mix}, CP_{min}^{mix}$	Minimum limit for GCV, specific gravity (SG), WI and CP of mixed gas.
$\Delta\varphi_{n,max}^{hy\_me}, \Delta\varphi_{n,max}^{hy\_d},$ $\Delta\varphi_{n,max}^{LPG}, \Delta\varphi_{n,max}^{ni},$ $\Delta\varphi_{n,max}^{me}$	Maximum volume deviation for hydrogen producing methane, direct used hydrogen, LPG, nitrogen and methane.
$\varphi_{n,max}^{mix}, \varphi_{n,min}^{mix}$	Maximum and minimum volume for mixed gas at node n.
Θ	Constant in Boyle's law.
$G_{k_g,t}, G_{k_h,t}$	Gas and heating load at time *t*.
$P_{sub,max}, Q_{sub,max}$	Maximum active and reactive power injection at substation from upper level market.
$P_{i_e,max}, P_{i_e,min}$	Maximum and minimum output of traditional DG i_e.
x_{l_e}, r_{l_e}	Resistance and reactance of power line l_e.
$f_{l_e,max}^a, f_{l_e,max}^r$	Maximum active and reactive power flow of power line l_e.
$P_{k_e,t}, P_{k_g,t}$	Power and gas load at time *t*.
$\lambda_{i_e}^a, \lambda_{i_e}^b, \lambda_{i_e}^c$	Cost coefficients for of traditional DG i_e.
$\lambda_{sub}, \lambda_{i_g}$	Cost coefficients for electricity purchase at substation and natural gas source i_g.
λ_N, λ_{LPG}	Cost coefficients for nitrogen and liquid petroleum gas.

$\omega_{j,t}^{f}$	Forecasted output of wind turbine *j* at time *t*.
Variables	
$P_{n,t}^{P2G}$	Power consumed by the electrolyser.
$G_{n,t}^{hy}$, $G_{n,t}^{hy\_me}$, $G_{n,t}^{hy\_d}$, $G_{n,t}^{me}$	Gas output for overall P2G process, direct hydrogen injection, hydrogen during methanation process and methanation.
$G_{n,t}^{ca}$	Required gas of carbon dioxide during methanation process.
$G_{i_g,t}$	Output of natural gas source i_g at time *t*.
$Pr_{l_g,t}^{ini}$, $Pr_{l_g,t}^{ter}$	Gas pressure of initial and terminal nodes of pipeline l_g at time *t*.
$f_{l_g,t}$	Gas flow of pipeline l_g at time *t*.
$f_{l_g,t}^{GT,ini}$, $f_{l_g,t}^{GT,ter}$	Gas flow at initial and terminal nodes of gas turbine.
$\varphi_{n,t}^{hy\_me}$, $\varphi_{n,t}^{hy\_d}$, $\varphi_{n,t}^{LPG}$, $\varphi_{n,t}^{ni}$, $\varphi_{n,t}^{mix}$	Volume for hydrogen with methanation process, direct use, LPG, nitrogen, methane and mixed natural gas.
$\Omega_{n,t}^{mix}$, $SG_{n,t}^{mix}$, $WI_{n,t}^{mix}$, $CP_{n,t}^{mix}$	CGV, SG, WI and CP for mixed gas of node n at time *t*.
$f_{l_g,t}^{ini}$, $f_{l_g,t}^{ter}$	Gas flow from initial node and to terminal node of pipeline l_g at time *t*.
$P_{sub,t}$, $Q_{sub,t}$	Electricity purchase of substation at time *t*.
$P_{i_e,t}$, $Q_{i_e,t}$	Traditional DG active and reactive power output of i_e at time *t*.
$f_{l_e,t}^{a}$, $f_{l_e,t}^{r}$	Active and reactive power flow of power line l_e at time *t*.
$f_{l_g,t}^{ini}$, $f_{l_g,t}^{ter}$	Gas flow from initial node and to terminal node of pipeline l_g at time *t*.

7.3 Introduction

The increasing penetration of renewable energy is effective for revolutionising energy mix and addressing the climate crisis. In the U.S., 275 TWh wind power was generated in 2018 while 6 TWh wind energy was curtailed and wasted [146]. The main reason is that i) the fluctuating and uncertain characteristics of wind power cause unbalancing issues and ii) wind power cannot be fully consumed in local areas but cannot be transported to other areas due to network constraints.

As a promising solution to enable excessive renewable energy integration, power-to-gas (P2G) enables the conversion from electrical energy to hydrogen and synthetic natural gas. Accordingly, the bidirectional energy flow is achieved for tighter couplings between integrated energy systems (IES). P2G has been extensively investigated in

existing research, particularly in network planning and operation problems [29, 54, 55, 147-150].

One major research area is P2G planning in IES. A robust co-optimization model is presented in [147] to determine the optimal investment plan for installing investment candidates including P2Gs and gas compressors. Wind uncertainties and reliability are considered for economic and reliable solutions. Paper [148] proposes a bi-level multi-stage stochastic programming to minimize planning and operation cost of an integrated electricity and gas system (IEGS) with P2G. A real options model is designed for IEGS including P2Gs to determine the optimal investment timing and capacity of P2G [149]. The operating cost uncertainty is considered and the decision can be made immediately or postponed waiting for the operation opportunity based on real options.

P2G operation has also been well investigated to reduce operation cost and carbon emissions and maximise profits [29, 54, 55, 150]. Paper [54] designs a decentralized IEGS with P2G technologies and wind energy to save daily operation cost. A linearized transient-state gas flow model is developed and the alternating direction multiplier method is used to solve the proposed problem. A stochastic optimization (SO) based day-ahead economic dispatch model for IEGS considering renewable uncertainties and contingencies is proposed in [55]. A second-order cone relaxation is developed to address the nonconvexity caused by uncertain gas flow direction. Paper [29] aims to reduce CO_2 emissions and optimally utilize surplus renewable energy. To maximize the expected profit of P2G facilities to a gas grid, a distributed supply coordination is proposed [150], which is a two-layer optimization problem and solved by a model predictive control method.

Hydrogen is produced by electrolysers of P2G and then injected into gas systems, which can inevitably affect gas composition. The variation in gas composition will impact the security of gas pipelines, gas engine performance, emissions as well as the gas quality of end-users [151]. The changes in the safety and performance of domestic gas appliances are assessed in [152] with natural gas-hydrogen mixtures. Paper [153] proposes a steady-state analysis method with the injection of alternative gases at different locations. Both centralized and decentralized injection of hydrogen and biogas are studied and results show that the optimal management of diversified gas components can help reduce carbon emissions. Paper [154] investigates the impact on gas quality standards in terms of heating value indices, Wobbe indices and relative gas

density when hydrogen is injected to gas systems with variation between 1 and 10 vol%. In gas distribution systems, Wobbe index (WI) is the most common parameter in the existing literature to measure gas quality [21, 152-156]. Paper [152] analyses gas interchangeability using WI on domestic appliances. The results demonstrate that WI associated with flashback and thermal output are important constraints to consider. A distributed injection of alternative gas with a steady-state method is presented in [153] and the paper also assesses the impact of utilizing various gas supply sources by WI. A small-scale renewable hydro methane production system is designed in [155] considering WI as a key security index. Paper [156] investigates the effect of different hydrogen injection levels on gas quality based on WI for both distribution and transmission gas networks. Paper [21] studies P2G operation in IEGS considering using WI and Combustion Potential (CP). Through optimally managing gas mixture, hydrogen injection is maximized by using robust optimization (RO), effectively hedging wind power uncertainties.

The utilization of renewable as the source for P2G is influenced by the uncertain characteristics and existing research mainly uses SO [54, 55] and RO [21, 157]. SO assumes the decision making is either based on an explicit distribution knowledge or a large number of samples. The former solution is not always practical and the latter is prone to errors since it is difficult to estimate the accurate probability distribution when the dataset is not sufficiently large. Alternatively, RO finds the optimal solution under the worst-case scenario based on the uncertainty set, which is over-conservative. To overcome their shortcomings, distributionally robust optimization (DRO) is developed to balance the deficiencies of SO and RO with minor robustness guaranteed through partial distribution information. A risk-based optimal gas-power flow is presented and solved by DRO [56]. Paper [57] designs an economic dispatch model for IEGS considering renewable and load uncertainty. An IES at the building level is proposed considering PV output uncertainty and DRO is used to mitigate the conservatism [158]. In summary, existing research has extensively assessed the gas quality of hydrogen-gas admixture but the coordinated operation of energy infrastructures in IES is ignored. There is also a lack of an effective method to model renewable uncertainty.

Similar to the uncertainty set of RO, the ambiguity set of DRO is used to characterize uncertainties with certain known information of distributions. Constructing a proper ambiguity set is crucial to DRO, which must be sufficiently rich to accommodate the real distribution and small enough to exclude distributions that may cause over-

conservatism. So far, moment-based ambiguity set is the most common type due to its tractability and easy second-order cone program (SOCP) or semidefinite program (SDP) reformulations, e.g., Markov ambiguity set and Chebyshev ambiguity set that depend on first and second-moment information. Nevertheless, the moment information is not abundant enough to shape the real distribution compared with discrepancy-based ambiguity set which measures the discrepancy between the candidate distribution and the reference distribution. The discrepancy can be controlled by the decision-maker to either decrease or increase the conservatism depending on the reliability requirement of the optimization.

To fill the research gap, this paper designs new co-optimization for both gas quality and system operation in an IEGS. Kullback-Leibler (KL) divergence is used to measure the distance between two distributions. Renewable uncertainty is captured by DRO approach with KL divergence-based ambiguity set to ensure both robustness and tractability. The key indices to quantify gas quality, including gross calorific value (GCV), specific gravity (SG), WI, and CP, are included in the model. Apart from ensuring standard satisfaction, the injected gas from P2G is mixed with nitrogen and Liquid Petroleum Gas (LPG) to maintain overall gas quality. The uncertainty of wind power output is handled by KL divergence-based DRO, which can be transformed into a tractable deterministic model.

The main contributions of this paper are as follows:

1) Four key indices are used in the economic operation of IEGS to quantify the impact of hydrogen injection from P2G on gas quality.

2) A novel co-optimization model is developed to both minimize system operation costs and maintain gas quality within an acceptable range, achieved by a mixture of nitrogen and LPG.

3) A KL divergence based DRO is developed to model renewable uncertainties. Compared to SO and RO, it is less data-dependent and conservative. Compared to moment-based DRO, the robustness of the proposed ambiguity set can be controlled by adjusting divergence tolerance in the algorithm.

The remainder of this paper is organized as follows. Section 7.4 proposes the modelling for the gas quality indices. Section 7.5 presents the objective function and constraints for IEGS including P2G facility modelling and gas quality management. The KL divergence-based DRO methodology regarding and associated reformulations

are given in Section 2.2.2. Section 7.6 demonstrates case studies and performance of the problem. Finally, section 7.7 concludes the paper.

7.4 Gas Quality

To assess gas quality, gas adaptability and interchangeability are the two most significant indexes. The adaptability of gas is referred to as the ability of the gas-fired appliances to work properly when the gas composition is changed due to gas injection. The gas interchangeability refers to that, during the mix of various gas compositions, the operational performance of gas equipment is still acceptable in terms of safety, efficiency and emissions. For gas turbines and pipelines, only limited change of gas composition is tolerated.

Calorific value is defined as the amount of released heat during combustion. GCV represents the amount of released heat by unit volume of fuel when the temperature of the gas is equal before and after the combustion, which means the water vapour is entirely condensed and heat recovered during the combustion. GCV must be within a range which determines the available amount of energy. The GCV for hydrogen is given in (7-1), where Ω_{g} and Ω_{hy} are the GCV for the mixed gas and hydrogen and φ_{hy} is the volume of hydrogen.

$$\Omega = \Omega_g + \left(\Omega_{hy} - \Omega_g\right)\varphi_{hy} \tag{7-1}$$

SG is the ratio of gas density to air density at the same pressure and temperature. It is used for limiting hydrocarbon content, which is given in (7-2), where ρ_{g}, ρ_{hy} and ρ_{air} denote the density of gas, hydrogen and air. A high hydrocarbon content will cause serious combustion problems, e.g., engine knock, carbon monoxide emissions and spontaneous ignition of gas turbines, etc.

$$SG = \frac{\rho_g + \left(\rho_{hy} - \rho_g\right)\varphi_{hy}}{\rho_{air}} \tag{7-2}$$

The WI for gas equipment can vary within a small range, which is defined by (7-3).

$$WI = \frac{\Omega}{\sqrt{SG}} \tag{7-3}$$

The most frequent used WI in the world is set within 5-10% of the standard setpoint. Otherwise, non-optimal gas combustion appears, which will lead to inefficient and unstable equipment working conditions and high greenhouse gas emissions. A

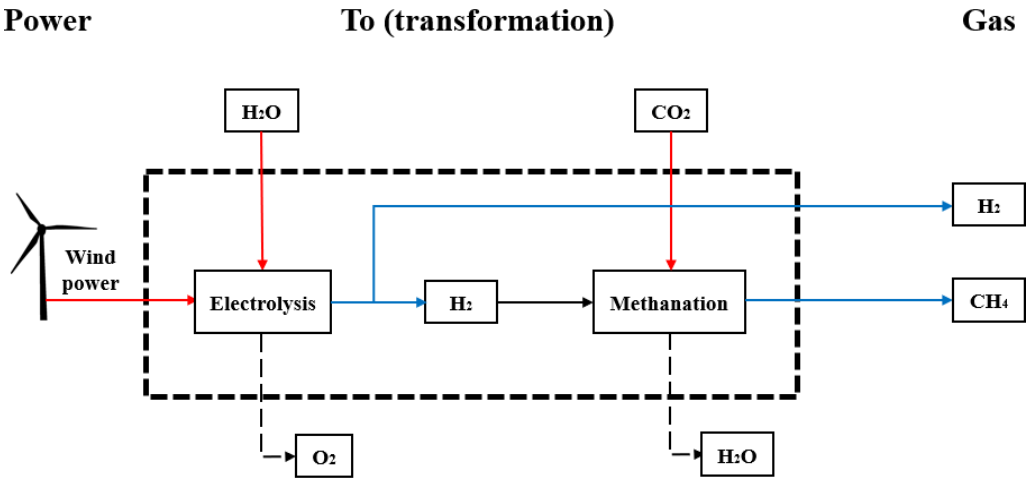

Fig. 7-1. Flowchart of constrained generation algorithm

significant change of WI can even result in emergency shutdowns of gas turbines due to the adverse impact on control issues, affecting the lifespan. In addition, the combustion performance is also influenced by the varying gas composition, e.g., flame stability, ignition properties and flashback. Ensuring equal WI can obtain the same energy input under the same gas pressure. CP is used to measure gas combustion stability, which can reflect combustion characteristics, including combustion flame and yellow flame, etc. CP is one important index for interchangeability of gas admixture that requires the CPs of mixed gases are close. Equation (7-4) defines CP.

$$CP = O_i \frac{\varphi_{hy} + 0.6(\varphi_{cm} + \varphi_{hc}) + 0.3\varphi_{me}}{\sqrt{SG}} \tag{7-4}$$

Where φ_{cm}, φ_{hc} and φ_{me} represent the volume of carbon monoxide, hydrocarbon except methane and methane.

7.5 IEGS Modelling

This section models P2G facility and IEGS, followed by the operation objective function. It is assumed that the entire IEGS is owned by a single system company, who has the full control of DGs, power lines, wind generators, gas sources, pipelines, P2G facility, compressors and other equipment.

7.5.1 P2G Modelling

P2G facility enables redundant wind power to be recovered and transported by the gas system. The P2G process is given in Fig. 7-1. Firstly, electrolysers split the water (H_2O) into hydrogen (H_2) and oxygen (O_2) by using excessive wind power. Then with

the interaction with carbon dioxide (CO_2), methane (CH_4) can be obtained through methanation. Meanwhile, the produced H_2 from the first step can be directly transported by the gas system. The relationship between the input and output of electrolyser is described in (7-5). According to Sabatier reaction factors [159], equations (7-6)-(7-8) present the requirement of CO_2 and production of CH_4 in the process of methanation.

$$G_{n,t}^{hy} = \eta_e \frac{P_{n,t}^{P2G}}{\Omega_{hy}} \tag{7-5}$$

$$G_{n,t}^{hy\_me} + G_{n,t}^{hy\_d} = G_{n,t}^{hy} \tag{7-6}$$

$$G_{n,t}^{ca} = \eta_{hy-ca} G_{n,t}^{hy\_me} \tag{7-7}$$

$$G_{n,t}^{me} = \eta_{hy-me} G_{n,t}^{hy\_me} \tag{7-8}$$

7.5.2 Modelling of Electricity and Gas Systems

The modelling of natural gas system is presented from (7-9) to (7-24). Equation (7-9) limits the gas production by natural gas source i_g. Gas pressure is limited in (7-10) and (7-11). It is noted that the pressure of initial gas nodes is always higher than that of terminal nodes in distribution gas systems. Weymouth gas flow equation is used to describe the relationship between gas pressure and flow in (7-12). Equation (7-13) limits gas flow. The inlet and outlet gas pressures of the compressor are constrained in (7-14). Equations (7-1)-(7-4) describing the gas quality with hydrogen are modified considering the mix of methane, LPG and nitrogen, which are given in (7-15)-(7-18). Equation (7-19) is used to ensure all gas quality indices are within a certain range for each gas node. The volume deviation between two consecutive time periods cannot be too big due to gas travelling speed in pipelines, which is presented in constraint (7-20). The total gas volume and its limit are given in (7-21) and (7-22). Constraint (7-23) presents the relationship between gas pressure and volume based on Boyle's law [160]. The nodal gas balance constraint is presented in (7-24).

$$G_{i_g,min} \leq G_{i_g,t} \leq G_{i_g,max} \tag{7-9}$$

$$Pr_{l_g,min}^2 \leq Pr_{l_g,t}^{^2} \leq Pr_{l_g,max}^2 \tag{7-10}$$

$$Pr_{l_g,t}^{ini} \geq Pr_{l_g,t}^{ter} \tag{7-11}$$

$$f_{l_g,t}{}^2 = \gamma_{l_g}\left(Pr_{l_g,t}^{ini\,2} - Pr_{l_g,t}^{ter\,2}\right) \tag{7-12}$$

$$0 \le f_{l_g,t} \le f_{l_g,max} \tag{7-13}$$

$$Pr_{l_g,t}^{ter} \le CF_{l_g} Pr_{l_g,t}^{ini} \tag{7-14}$$

$$\Omega_{n,t}^{mix} = \Omega_{hy}\left(\varphi_{n,t}^{hy,me} + \varphi_{n,t}^{hy,d}\right) + \Omega_{LPG}\varphi_{n,t}^{LPG} + \Omega_{ni}\varphi_{n,t}^{ni} + \Omega_{me}\varphi_{n,t}^{me} \tag{7-15}$$

$$\begin{aligned} SG_{n,t}^{mix} = \big[&\rho_{hy}\left(\varphi_{n,t}^{hy\_me} + \varphi_{n,t}^{hy\_d}\right) + \rho_{LPG}\varphi_{n,t}^{LPG} + \rho_{ni}\varphi_{n,t}^{ni} \\ &+ \rho_{me}\varphi_{n,t}^{me}\big]\left(\varphi_{n,t}^{hy,me} + \varphi_{n,t}^{hy,d} + \varphi_{n,t}^{LPG} + \varphi_{n,t}^{ni} + \varphi_{n,t}^{me}\right) \end{aligned} \tag{7-16}$$

$$WI_{n,t}^{mix} = \Omega_{n,t}^{mix} / \sqrt{SG_{n,t}^{mix}} \tag{7-17}$$

$$CP_{n,t}^{mix} = O_i \frac{E_{hy}\left(\varphi_{n,t}^{hy\_me} + \varphi_{n,t}^{hy\_d}\right) + E_{LPG}\varphi_{n,t}^{LPG} + E_{ni}\varphi_{n,t}^{ni} + E_{me}\varphi_{n,t}^{me}}{\sqrt{SG_{n,t}^{mix}}} \tag{7-18}$$

$$\{\cdot\}_{min} \le \{\cdot\} \le \{\cdot\}_{max}, \tag{7-19}$$

$$\{\cdot\} = \Omega_{n,t}^{mix}, SG_{n,t}^{mix}, WI_{n,t}^{mix}, CP_{n,t}^{mix}$$

$$-\Delta\varphi_{n,max}^{\{\cdot\}} \le \varphi_{n,t}^{\{\cdot\}} - \varphi_{n,t-1}^{\{\cdot\}} \le \Delta\varphi_{n,max}^{\{\cdot\}} \tag{7-20}$$

$$\{\cdot\} = hy\_me, hy\_d, LPG, ni, me$$

$$\varphi_{n,t}^{hy,me} + \varphi_{n,t}^{hy,d} + \varphi_{n,t}^{LPG} + \varphi_{n,t}^{ni} + \varphi_{n,t}^{me} = \varphi_{n,t}^{mix} \tag{7-21}$$

$$\varphi_{n,min}^{mix} \le \varphi_{n,t}^{mix} \le \varphi_{n,max}^{mix} \tag{7-22}$$

$$\varphi_{n,t}^{mix} = \frac{\Theta}{Pr_{n,t}} \tag{7-23}$$

$$\begin{aligned} &\sum_{i_g \in I_g} G_{i_g,t} + \sum_{n \in N} G_{n,t}^{hy} + \sum_{l_g \in L_g} f_{l_g,t}^{s,ini} - \sum_{l_g \in L_g} f_{l_g,t}^{s,ter} \\ &= \sum_{k_g \in K_g} G_{k_g,t} + \sum_{k_h \in K_h} G_{k_h,t} \end{aligned} \tag{7-24}$$

The electricity distribution system is modelled from (7-25) to (7-30). Equation (7-25) is the constraint for the active and reactive power of substations. The generation limits for traditional DGs are presented in (7-26). In the distribution system, the DistFlow equation is used with the linearization as presented from (7-27) to (7-28). In (7-29) and

(7-30), the power balance constraints for active and reactive power are given respectively.

$$0 \le \{\cdot\}_{sub,t} \le \{\cdot\}_{sub,max}, \{\cdot\} = P, Q \tag{7-25}$$

$$P_{i_e,min} \le P_{i_e,t} \le P_{i_e,max} \tag{7-26}$$

$$V_{b,t}^{ini} - V_{b,t}^{ter} = \left(f_{l_e,t}^{a} r_{l_e} + f_{l_e,t}^{r} x_{l_e}\right)/V_0 \tag{7-27}$$

$$0 \le f_{l_e,t}^{\{\cdot\}} \le f_{l_e,max}^{\{\cdot\}}, \{\cdot\} = a, r \tag{7-28}$$

$$\sum_{i_e \in I_e} P_{i_e,t} + \sum_{j \in J} \omega_{j,t}^{P} + \sum_{l_e \in L_e} f_{l_e,t}^{a,ini} - \sum_{l_e \in L_e} f_{l_e,t}^{a,ter} = \sum_{k_e \in K_e} P_{k_e,t} \tag{7-29}$$

$$\sum_{i_e \in I_e} Q_{i_e,t} + \sum_{l_e \in L_e} f_{l_e,t}^{r,ini} - \sum_{l_e \in L_e} f_{l_e,t}^{r,ter} = \sum_{k_e \in K_e} Q_{k_e,t} \tag{7-30}$$

7.5.3 Objective function

The injection of hydrogen into natural gas pipelines will inevitably change gas compositions and might cause gas quality issues, such as heat value, combustion potential pressure. In order to maintain the 4 gas quality indices within an acceptable statutory range, it is required to inject other gases with hydrogen into gas pipelines. Accordingly, the optimal gas mixture is required to determine the proper amount and timing of the injection of other gases. In this paper, LPG and nitrogen are used to blend with hydrogen to keep a satisfied gas quality. Nevertheless, the cost of purchase and injection of LPG are expensive compared with nitrogen. Accordingly, the key gas mixture process is to use the minimum LPG with gas quality satisfied. The objective in (7-31) is to minimize system operation cost while ensuring gas quality, considering the impact of uncertain wind power output.

$$\begin{aligned} min \ \ \Gamma = min \sum_{i_e \in I_e, i_g \in I_g, t \in T} & \lambda_{i_e}^{a} {P_{i_e,t}}^2 + \lambda_{i_e}^{b} P_{i_e,t} + \lambda_{i_e}^{c} + \lambda_{sub} P_{sub,t} \\ & + \lambda_{i_g} P_{i_g,t} + \lambda_N P_{N,t} + \lambda_{LPG} P_{LPG,t} \end{aligned} \tag{7-31}$$

The first three terms are the cost function for traditional DGs. The fourth term represents electricity purchased from the upper electricity market. The gas production cost of natural gas sources is shown as the fifth term. The last two terms are the cost for purchase and injection of LPG and nitrogen during gas mixture process.

7.6 Case Studies

The proposed gas quality management for IEGS is demonstrated on a modified IEEE 33-bus system with a 10-node gas system in Fig. 7-2. The gas system data is obtained from [14]. The temperature and pressure in the gas pipelines are of the standard level. The IEGS contains three traditional DGs, three renewable DGs and two natural gas sources. The wind DG at bus 10 is the power supply for the P2G facility with 1MW capacity. The parameters for natural gas sources and DGs in TABLEs 7-1 and 7-2 respectively. The ambiguity set is controlled by a divergence tolerance (η=2.3026 and β=0.1) for the DRO. The GCV and combustion potential index (CPI) for hydrogen, methane, LPG and nitrogen are given in TABLE 7-3. The gas composition of original natural gas and LPG is provided in TABLE 7-4, mainly consisting of methane, ethane,

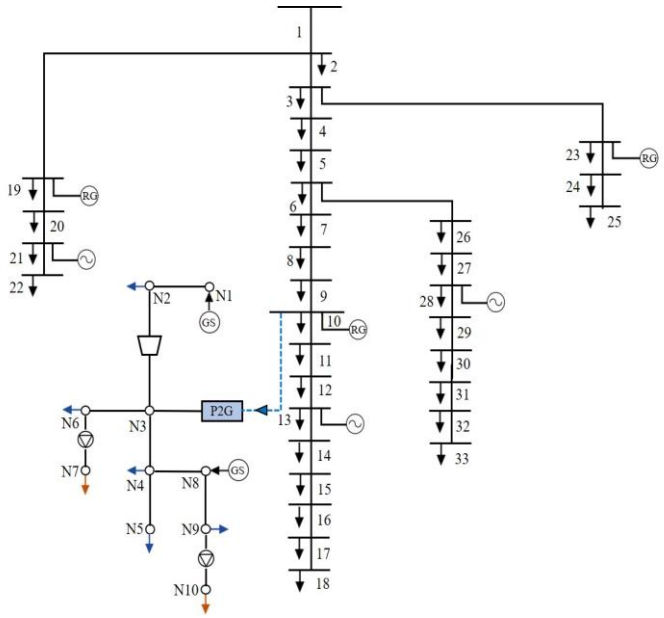

Fig. 7-2. The proposed IEGS test system.

TABLE 7-1 Parameters of natural gas sources

Node No.	$P_{ig,min}$ (kcf/h)	$P_{ig,max}$ (kcf/h)	λ_{ig} ($/kcf)
1	5	20	2.2
8	2	15	2

TABLE 7-2 Generator parameters

Bus No.	$P_{ie,max}$ (MW)	$P_{ie,min}$ (MW)	R_i^+, R_i^- (MW)	a_i ($/MW²)	b_i ($/MW)	c_i ($)
13	1.2	0.3	0.2	6000	7100	6200
21	1.2	0.3	0.2	4500	10500	4000
28	1.0	0.1	0.2	4500	10500	4000

TABLE 7-3 GCV AND CPI FOR DIFFERENT GASES

	H_2	CH_4	LPG	N_2
GCV	10	40	115	0
CPI	100	50	42	0

TABLE 7-4 GAS COMPOSITION (%)

	CH_4	C_2H_6	C_3H_8	C_4H_{10}	CO_2	Other
Natura gas	79.6	8.3	4.9	1.4	3.4	2.4
LPG	91.1	4.3	3.0	1.4	0	0.2

TABLE 7-5 CASE ILLUSTRATION

Case No.	Optimization method	Hydrogen injection	Gas mixture management
1	Robust	Yes	Yes
2	DRO	No	Yes
3	DRO	Yes	No
4	DRO	Yes	Yes

TABLE 7-6 Economic performance for all cases

Economic result	Case 1	Case 2	Case 3	Case 4
Power system operation cost ($)	479340	329065	337044	343630
Gas system operation cost ($)	133651	11443	845	243027
IEGS operation cost ($)	612991	340508	337889	586657
Purchase cost of nitrogen ($)	1266	1003	0	2424
Purchase cost of LPG ($)	120350	9760	0	240020
Cost for gas mixture management ($)	13301	10763	0	242444

TABLE 7-7 Economic performance under different confidence intervals

Confidence interval (β)	Divergence tolerance (η)	Case 2	Case 3	Case 4
0	1	337855	334510	583271
0.05	2.9957	339720	337025	585084
0.1	2.3026	340508	337889	586657
0.5	0.6065	343700	373179	594518
1	0.3679	345982	344221	596454

propane and butane. LPG has high GCV but low CPI, which is used to increase WI and decrease CP. By contrast, the GCV and CPI of nitrogen are both zero, which enables more flexible gas mixture. Four case studies in TABLE 7-5 are implemented based on optimization methods, hydrogen injection schemes, and gas mixture management strategies, which are presented.

7.6.1 Economic Performance

The economic results for all cases are investigated, including operation cost and gas mixture management cost, as is shown in TABLE 7-6. The IEGS operation cost is the sum of operation cost of power system and gas system. It shows that case 1 ($601922) has the highest IEGS operation cost and case 3 ($337889) has the lowest. The IEGS operation strategy for case 1 and 4 are the same which both consider hydrogen injection support for the gas system and gas mixture management for maintaining gas quality. Case 1 derives $135710 more operation cost in the power system since RO limits the uncertain wind power output with a higher degree of robustness, which, yields $120445 less gas system operation cost. The reason is that the hydrogen injection is strictly limited, which reduces the need for additional LPG and nitrogen to maintain acceptable gas quality indices. Overall, case 1 results in $15265 more IEGS operation cost compared with case 4.

Without considering hydrogen injection from the power system to the gas system, the two systems are operated separately in case 2. Accordingly, the power system only requires to supply electricity load in case 2 whose power system operation cost is 4.3% less than that of case 4. The purchase cost of nitrogen and LPG in case 2 are $1003 and $9760 respectively, which are $1421 and $230260 less than case 4. Since the original natural gas without hydrogen addition is more accessible to obtain acceptable gas quality. Due to the disconnection between power and gas systems, the overall operation cost of case 2 is $246149 less than case 4. In case 3, hydrogen injection is considered without gas mixture. The gas system operation cost, i.e., $845, is purely the generation cost of natural gas sources. Without the blend of LPG and nitrogen, the gas volume is less than case 4 and the gas pressure is higher than case 4, which reduces the hydrogen injection from P2G facility. Thus, the wind power provides more supply to the power system and the power system operation cost is reduced.

The divergence tolerance η is used to characterize the size of the ambiguity set which contains all the possible uncertainty distributions and is associated with the conservatism of numerical performance. According to [33], the divergence tolerance influences the confidence interval, i.e., ($\beta = e^{-\eta}$). The divergence tolerance η represents the radius of the ambiguity set, which affects the accuracy of estimating uncertainty distribution. The larger η leads to an ambiguity set with higher robustness

while the smaller η leads to less conservative numerical results. When the divergence tolerance is set as 0, the confidence interval turns into 100% and the candidate distribution is becoming the same as the reference distribution. Accordingly, the original DRO problem is equivalent to SO. With the variation of the confidence interval, the total operation cost for IEGS is depicted in TABLE 7-7. At the second column of the table, the divergence tolerance is determined based on selecting the confidence interval. Case 4 has the highest result with all the confidence intervals while case 3 remains the lowest. With the increase of the confidence interval, the total IEGS operation cost increases slowly. In case 4, when β = 0, the DRO degrades to SO and yields \$583271 total cost. The considered largest ambiguity set results in \$596454 with β = 1, which is 2.3% higher than the cost with the smallest ambiguity set.

7.6.2 Gas Quality Performance under Gas Quality Management

The resulting WI and CP with different P2G operation schemes are presented in this subsection. From Fig. 7-3 to Fig. 7-5, it can be seen that case 2 and 4 have a similar WI range and trend through the entire time period while case 3 shows a narrow range of WI. The WI of case 3 ranges from 32.65 to 32.75, which is 79% of the WI range of case 4. Besides, WI in case 3 does not fluctuate much while maintaining a smooth trend through the entire time period. The reason is that without the gas admixture of LPG and nitrogen, WI cannot be ensured in an acceptable range. In comparison with case 4, there is no hydrogen injection in case 2. Therefore, the gas quality management is implemented on the original environment based on the natural gas composition component given in TABLE 7-4. Compared with hydrogen and methane, nitrogen and LPG have higher CGV, which lead to higher WI in case 2 since case 2 has no hydrogen injected and the other gas components contribute to a higher WI. For case 2 and 4, the WI remains at a high level from 7:00 to 17:00 and peak at 49 in both cases. The WI of N3 and N8 are maintained smoothly around 42. For N6, the WI remains around 41 before 15:00 and then decreases dramatically.

The CP for all cases at 12:00 is provided in TABLE 7-8. Case 3 yields the highest CP and case 4 has the lowest. Since nitrogen and LPG have low CPI, which results in low CP. Without the blend of nitrogen and LPG, the CP in case 3 is relatively high considering only hydrogen and methane as the gas composition. On the contrary, without the hydrogen injection, case 2 has low CP. Compared with case 4, the CP of

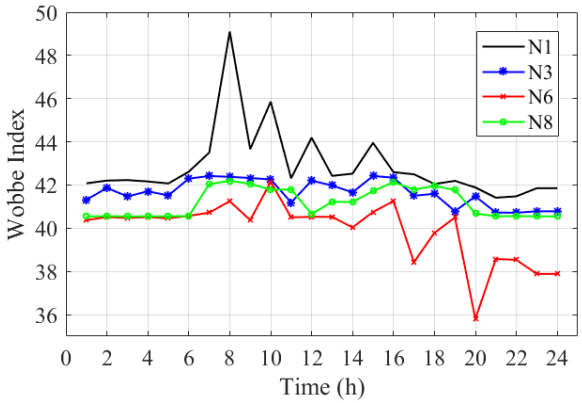

Fig. 7-3. Wobbe index for case 2.

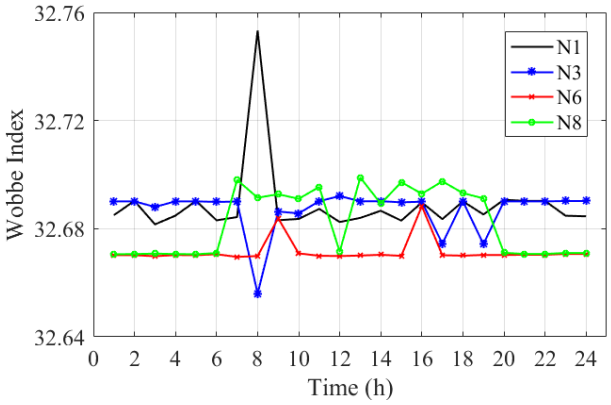

Fig. 7-4. Wobbe index for case 3.

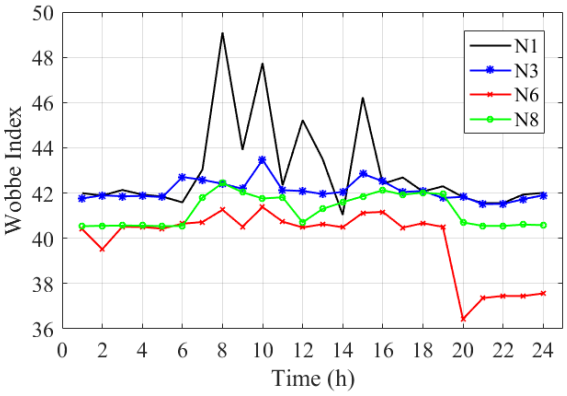

Fig. 7-5. Wobbe index for case 4.

N1 in case 2 is 30% less. In case 2, CP is slightly lower than case 4 when solved by RO since the higher degree of robustness leads to less P2G power output. Accordingly, the hydrogen is produced less and the resulting CP is lower.

7.6.3 Pressure Performance under Gas Quality Management

The nodal gas pressure for case 2-4 is given from Fig. 7-6 to Fig. 7-8. Overall, it can be seen that the pressure of N1 is the highest and N6 is the lowest. When the node is

close to the gas source, e.g., N1 and N6, the gas pressure is relatively high. Passing through the gas compressor between N2 and N3, the gas pressure of N3 is pumped up. As the base case with both hydrogen injection and gas mixture management considered, case 4 shows an increasing trend from 1:00 to 10:00 and a decrease from 11:00 to 14:00, followed by another pressure peak at 16:00. Connected to the main gas source, the pressure of N1 peaks at 1.2 Psig and the lowest is 0.6 Psig. At N3, with the hydrogen

TABLE 7-8 Combustion potential for all cases

Gas node	Case 1	Case 2	Case 3	Case 4
N1	50.4	49.4	75.0	50.9
N3	54.5	52.4	75.0	55.2
N6	56.0	55.7	75.0	57.6
N8	56.9	55.8	75.0	57.8

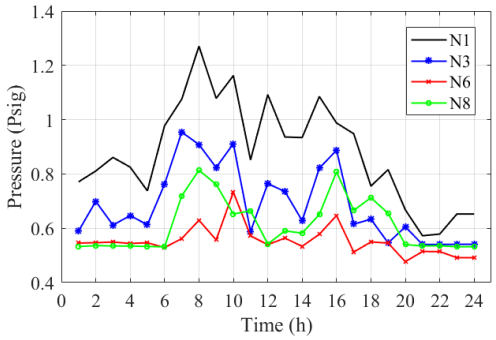

Fig. 7-6. Gas pressure for case 2.

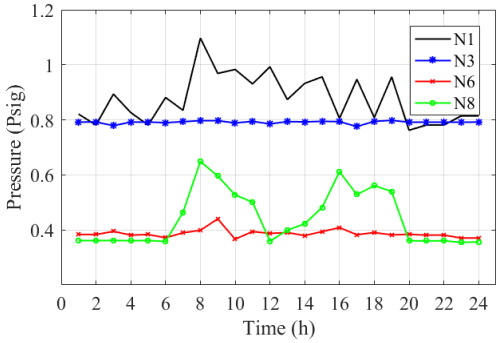

Fig. 7-7. Gas pressure for case 3.

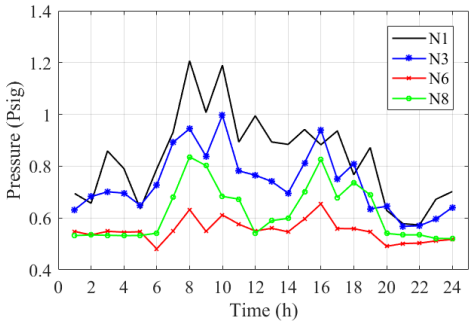

Fig. 7-8. Gas pressure for case 4.

injection from P2G facility and pumped pressure by from N2, the gas pressure of N3 reaches 1.0 Psig at 10:00.

Compared with case 4, case 2 shows similar pressure profile. However, the average pressure level of N1 in case 2 is 6% higher than in case 4. The reason is that without the power supply by hydrogen, the natural gas source on N1 needs to provide more gas supply to the gas system which results in higher gas pressure. In case 3, without gas

quality management, the gas volume is not limited. This leads to the large pressure deviation between nodes which are close to the sources and the nodes far from the sources. For instance, the average 0.4 Psig pressure deviation between N3 and N6 can provide large gas flow. Taking advantage of the unlimited gas quality and volume, case 3 enables large gas flow with different gas pressure profile compared with other cases.

7.7 Chapter Summary

A coordinated optimization for gas quality management and operation of IEGS in the presence of wind uncertainty is proposed. The wind uncertainty is handled by DRO with KL divergence for controlling the conservatism of numerical performance. A tractable deterministic formulation is obtained and the resulted linear programming model can be efficiently solved. Through the extensive case studies, the key findings are:

- Considering the four gas quality indices, i.e, GCV, SG, WI and CP, are necessary. The gas quality is not acceptable under the relative international standard without gas quality management.
- The P2G facility is useful for maximally utilizing the excessive wind power and economically effective for reducing the operation cost of IEGS.
- DRO provides less conservative results than RO in terms of economic performance.
- Through applying KL divergence, the size of the ambiguity set can be flexibly controlled based on confidence interval set by decision-makers for risk concerns.

The proposed co-optimization for IEGS ensures both the economic performance and gas quality via coordinating traditional DGs, natural gas resources and P2G facility, which can benefit system operators with economic benefits through saving operation cost and secure gas distribution with gas quality guaranteed.

Chapter 8

Conclusion

This chapter summarises the thesis by outlining the major contributions and findings from the research.

IEGS provides a powerful concept to advise system operators in terms of planning, dispatching and converting multi-energy infrastructures to achieve a coordinated optimal condition among power and gas systems. However, the renewable integration, natural disasters, cybersecurity issues, voltage fluctuation and gas quality issues have unignorable impacts on the secure and economic operation of IEGS. In consequence, this paper extensively investigates the solutions to counteract the aforementioned problems, which attempts to fill the research gaps of the existing literature.

Mean-Risk Distributionally Robust Co-Optimization of District Integrated Electricity-Gas-Water Systems

A mean-risk coordinated optimization for an IES in the water-energy nexus with enormous interdependencies is proposed in this paper. The tight couplings and interactions between each subsystem enable the reliable and economic operation for the entire IES. Renewable uncertainty is captured by mean-risk DRO. The coherent risk measure, CVaR provides the trade-off to system operators with flexible alternatives on choosing between economic efficiency and risk. A tractable Bender's decomposition is employed to solve the DR-IWENS problem.

Through the extensive case studies on the economic performance, scheduling of interdependent coupling devices and the risk management via adjusting parameters, the major contributions are tested:

- The coordination of each subsystem with the conversion technologies enhances energy efficiency.
- The water system is highly required to consider in the IES operation as the water is extensively consumed by energy conversions.

The mean-risk DRO applied in IES operation problem provides system operators with not only economic but risk concerns.

Resilience Enhancement and Emergency Response for Integrated Energy Systems against Seismic Attacks: A Data-Driven Approach

In this paper, a two-stage DRO method is developed to enhance the resilience of an IES under seismic attacks with combined planning and operation strategies. The proposed method provides optimal hardening plans for specific power lines and gas

pipelines under different seismic intensity levels and investment budgets. Through extensive case study demonstrations, the key findings are as follows: i) In the first stage, DR-SIP effectively determines the most vital lines to harden. In the second stage, DR-SIP optimally shed loads to keep system balanced and minimize the system operation cost; ii) With RO that considers the most extreme event and serious damage, the proposed DRO provides less conservative results for both planning and operation stages with 13% less cost; iii) Investment plan with a higher budget is more likely to yield a reliable IES with high resilient performance; iv) The optimal hardening plan is effective for protecting transmission lines and loads and IES is more resilient than electricity network against seismic attacks.

This method can help system operators to make economical hardening and operation strategies to improve the resilience of the integrated energy system under seismic attacks.

Two-Stage Coordinated Risk Mitigation Strategy for Integrated Electricity and Gas Systems under Malicious False Data Injections

A risk mitigation scheme for IEGS against FDIA is proposed in this paper with a two-stage DRO model. The hierarchical two-stage framework can determine both day-ahead and real-time system optimal operation schemes considering the impact of FDIA and renewable uncertainties on electricity load, gas load and gas density. A tractable SDP formulation is built for the original DR-FMS, which is solved by CGA in an iterative manner. Through the extensive case studies, the key findings are listed below:

- Considering all three types of FDIA, i.e., EL-FDIA, GL-FDIA and GD-FDIA, leads to higher economic results and more load shedding than considering two types or one type of FDIA.

- Load shedding is more sensitive to EL-FDIA than GD-FDIA or GL-FDIA.

- DRO provides less-conservative results than RO in terms of economic performance and load shedding.

- Renewable generation uncertainty is necessary to consider, which leads to 3.7% more operation cost.

The proposed DR-FMS ensures the economic performance of IEGS by providing a two-stage risk mitigation scheme via implementing efficient load shedding under FDIA and renewable uncertainty. The beneficiaries of this work inlcude: network operators can have powerful operation models, end customers will enjoy better supply security, and renewable can penetrate to the maximum level without much curtailment.

Voltage Management in Integrated Energy Systems Considering Interdependency and Renewable Uncertainty

This paper proposes a multi-objective optimization for minimizing both operation cost and voltage deviation of IES considering renewable power uncertainty. A two-stage data-driven DRO approach is used to solve the TS-VCO with dual and SDP formulations to ensure computational tractability. The reformulated TS-VCO is solved by CGA with master and subproblems. The key findings from the case studies are :

- Based on a large amount of moment information, DRO produces less conservative results compared with RO, more effective for maintaining voltage deviation and reducing operation cost considering renewable power uncertainty.

- The interdependency between electricity and gas systems reduces 4.7% of operation cost and a significant rise in the voltage profile.

- The proposed TS-VCO is effective in maintaining voltage and saving operation cost considering PV uncertainty.

This work can benefit integrated system operators with powerful operation tool to manage the systems with fewer costs but integrate more renewable energy.

Distributionally Robust Operation for Integrated Energy Systems with Hydrogen Injection and Gas Quality Improvement

A coordinated optimization for gas quality management and operation of IEGS in the presence of wind uncertainty is proposed. The wind uncertainty is handled by DRO with KL divergence for controlling the conservatism of numerical performance. A tractable deterministic formulation is obtained and the resulted linear programming model can be efficiently solved. Through the extensive case studies, the key findings are:

- Considering the four gas quality indices, i.e, GCV, SG, WI and CP, are necessary. The gas quality is not acceptable under the relative international standard without gas quality management.

- The P2G facility is useful for maximally utilizing the excessive wind power and economically effective for reducing the operation cost of IEGS.

- DRO provides less conservative results than RO in terms of economic performance.

- Through applying KL divergence, the size of the ambiguity set can be flexibly controlled based on confidence interval set by decision-makers for risk concerns.

The proposed co-optimization for IEGS ensures both the economic performance and gas quality via coordinating traditional DGs, natural gas resources and P2G facility, which can benefit system operators with economic benefits through saving operation cost and secure gas distribution with gas quality guaranteed.

Chapter 9

Future Work

This chapter presents the potential future work to enrich the optimisation methodologies for multi-carrier energy system, as well as the interaction with other smart grid technologies or frameworks.

Future work will continue to investigate the optimal operation of IEGS. Instead of progressing on the optimization approach, more effort will be made on the optimization scenarios and models, aiming to develop an economic, reliable and resilient IEGS framework. With the increasing integration of DGs, the application of microgrids and energy hubs are becoming wider. Accordingly, the first future work will establish a co-optimization framework for IEGS connected with multiple energy hubs. Moreover, based on the existing works of VVO and gas quality management, the combination of them is also practical and innovative. In addition, when cyber-attacks are launched on IES with more energy vectors and interdependencies, the cyber-resiliency faces more challenges as the attack on each sub-system will propagate to other ones. Thus, it is critically essential to investigate the impact and mitigation scheme against cyber-attacks in IES with more energy systems. Detailed future work is illustrated as follows.

IEGS Operation with Networked Energy Hubs

To facilitate energy efficiency, energy interdependency and conversion are also essential at the customers' side. Energy hubs feature micro-energy systems with multi-vector energy inputs and outputs. An IEGS in distribution level networked with multiple energy hubs further enhances the energy efficiency and energy system reliability. A hierarchical optimization framework for IEGS networked with energy hubs will be considered. A two-stage DRO model will be utilized to handle extensive renewable uncertainty. This work will benefit the system operators of both IEGS and energy hubs on minimizing the daily operation cost with enriched energy flexibility.

VVO with Gas Quality Management

VVO is a powerful management scheme in distribution systems to manage the voltage magnitudes within acceptable limits under the high renewable penetration era. This is further complicated by the growing interdependencies between power and gas systems. Meanwhile, the emerging P2G poses gas quality problems with hydrogen injection into gas pipelines.

To overcome the voltage and gas quality problems, this future work will propose a coordinated volt-VAR-pressure (VVP) optimization of IEGS for limiting voltage

magnitudes and gas pressure considering renewable uncertainties. Due to the effective energy conversion to handle surplus renewable generation, P2G operation can be utilized as a mitigation strategy for VVO problems. As a consequence, the optimal set of management actions of voltage regulating devices and P2G facilities is determined. Meanwhile, the gas quality issues caused by the hydrogen injection via P2G is handled by the proposed gas quality management scheme. A two-stage mean-risk distributionally robust optimization (TSMR-DRO) is developed to model the coordinated optimization problem considering risk measures for the objective function. The proposed VVP provides a guideline to IEGS operators with an efficient and economic operation scheme to effectively manage the voltage profile and gas quality with fewer operation costs and higher integration of renewable energy.

Mitigate Cyber-Attacks in IES

The wide implementation of ICT causes power system operations exposed to cyber-attacks. Meanwhile, the tendency of integrated multi-energy vectors has worsened this issue with multiple energy coupled.

This future work will propose a two-stage risk-averse mitigation strategy for IES, incorporating power, natural gas and water systems against FDIA under water-energy nexus. The FDIA on individual sub-systems is modelled through hampering false data integrity to the systems. An innovative two-stage risk-averse distributionally robust optimization (RA-DRO) is proposed to mitigate uneconomic operation and provides a coordinated optimal load shedding scheme for the nexus system security. A coherent risk measure, Conditional Value-at-Risk is incorporated into the RA-DRO to model risk. A Benders decomposition method is used to solve the original NP-hard RA-DRO problem. This research provides IES operators with an economic system operation tool by optimally coordinating energy infrastructures and implementing reasonable load shedding to enhance cybersecurity.

Reference

[1] F. Urban and J. Nordensvärd, "Low carbon development: origins, concepts and key issues," in *Low Carbon Development*: Routledge, 2013, pp. 25-44.

[2] O. Edenhofer, *Climate change 2014: mitigation of climate change*. Cambridge University Press, 2015.

[3] J. Rogelj *et al.*, "Paris Agreement climate proposals need a boost to keep warming well below 2 C," *Nature*, vol. 534, no. 7609, pp. 631-639, 2016.

[4] C. Stark, M. Thompson, and C. C. Committee, "Net Zero The UK's contribution to stopping global warming," 2019.

[5] H. L. van Soest, M. G. den Elzen, and D. P. van Vuuren, "Net-zero emission targets for major emitting countries consistent with the Paris Agreement," *Nature communications*, vol. 12, no. 1, pp. 1-9, 2021.

[6] G. Von Wald, D. Cullenward, M. D. Mastrandrea, and J. Weyant, "Accounting for the Greenhouse Gas Emission Intensity of Regional Electricity Transfers," *Environmental Science & Technology*, 2021.

[7] N. Strachan, "UK energy policy ambition and UK energy modelling—fit for purpose?," *Energy Policy*, vol. 39, no. 3, pp. 1037-1040, 2011/03/01/ 2011, doi: https://doi.org/10.1016/j.enpol.2011.01.015.

[8] S. Safarzadeh, M. Rasti-Barzoki, and S. R. Hejazi, "A review of optimal energy policy instruments on industrial energy efficiency programs, rebound effects, and government policies," *Energy Policy*, vol. 139, p. 111342, 2020.

[9] B. Raybould, W. M. Cheung, C. Connor, and R. Butcher, "An investigation into UK government policy and legislation to renewable energy and greenhouse gas reduction commitments," *Clean Technologies and Environmental Policy*, vol. 22, no. 2, pp. 371-387, 2020.

[10] I. E. Agency, *World Energy Outlook 2019*. 2019.

[11] L. Kane and G. Ault, "A review and analysis of renewable energy curtailment schemes and Principles of Access: Transitioning towards business as usual," *Energy Policy*, vol. 72, pp. 67-77, 2014.

[12] S. Canbulat, K. Balci, O. Canbulat, and I. S. Bayram, "Techno-economic analysis of on-site energy storage units to mitigate wind energy curtailment: A case study in scotland," *Energies*, vol. 14, no. 6, p. 1691, 2021.

[13] J. Rifkin, *The third industrial revolution: how lateral power is transforming energy, the economy, and the world*. Macmillan, 2011.

[14] L. Tsoukalas and R. Gao, "From smart grids to an energy internet: Assumptions, architectures and requirements," in *2008 Third International Conference on Electric Utility Deregulation and Restructuring and Power Technologies*, 2008: IEEE, pp. 94-98.

[15] P. Geoffron and L. De Paoli, "Introduction: a critical overview of the European National Energy and Climate Plans," *Introduction: a critical overview of the European National Energy and Climate Plans.*, pp. 31-41, 2019.

[16] Z. Yan and J. Hu, "Energy internet in the Yangtze River Delta: opportunities, challenges, and suggestions," *Frontiers in Energy*, vol. 12, no. 4, pp. 484-492, 2018.

[17] P. Zhao, C. Gu, and D. Huo, "Two-Stage Coordinated Risk Mitigation Strategy for Integrated Electricity and Gas Systems under Malicious False Data Injections," *IEEE Transactions on Power Systems*, pp. 1-1, 2020, doi: 10.1109/TPWRS.2020.2986455.

[18] Z. Yi, Y. Xu, J. Hu, M. Chow, and H. Sun, "Distributed, Neurodynamic-Based Approach for Economic Dispatch in an Integrated Energy System," *IEEE Transactions on Industrial Informatics*, vol. 16, no. 4, pp. 2245-2257, 2020, doi: 10.1109/TII.2019.2905156.

[19] Y. Li, Z. Li, F. Wen, and M. Shahidehpour, "Privacy-Preserving Optimal Dispatch for an Integrated Power Distribution and Natural Gas System in Networked Energy Hubs," *IEEE Transactions on Sustainable Energy*, vol. 10, no. 4, pp. 2028-2038, 2019, doi: 10.1109/TSTE.2018.2877586.

[20] Z. Wu, W. Gu, R. Wang, X. Yuan, and W. Liu, "Economic optimal schedule of CHP microgrid system using chance constrained programming and particle swarm optimization," in *2011 IEEE Power and Energy Society General Meeting*, 24-29 July 2011 2011, pp. 1-11, doi: 10.1109/PES.2011.6038921.

[21] C. Gu, C. Tang, Y. Xiang, and D. Xie, "Power-to-gas management using robust optimisation in integrated energy systems," *Applied Energy,* vol. 236, pp. 681-689, 2019/02/15/ 2019, doi: https://doi.org/10.1016/j.apenergy.2018.12.028.
[22] X. Lu, K. W. Chan, S. Xia, X. Zhang, G. Wang, and F. Li, "A Model to Mitigate Forecast Uncertainties in Distribution Systems Using the Temporal Flexibility of EVAs," *IEEE Transactions on Power Systems,* vol. 35, no. 3, pp. 2212-2221, 2020, doi: 10.1109/TPWRS.2019.2951108.
[23] C. M. Correa-Posada and P. Sánchez-Martín, "Integrated Power and Natural Gas Model for Energy Adequacy in Short-Term Operation," *IEEE Transactions on Power Systems,* vol. 30, no. 6, pp. 3347-3355, 2015, doi: 10.1109/TPWRS.2014.2372013.
[24] A. Nikoobakht, J. Aghaei, M. Shafie-khah, and J. P. S. Catalão, "Continuous-Time Co-Operation of Integrated Electricity and Natural Gas Systems with Responsive Demands Under Wind Power Generation Uncertainty," *IEEE Transactions on Smart Grid,* pp. 1-1, 2020, doi: 10.1109/TSG.2020.2968152.
[25] S. Pye, N. Sabio, and N. Strachan, "An integrated systematic analysis of uncertainties in UK energy transition pathways," *Energy Policy,* vol. 87, pp. 673-684, 2015.
[26] G. Harrison. "ARIES: Adaptation and Resilience in Energy Systems." https://www.eng.ed.ac.uk/research/projects/aries-adaptation-and-resilience-energy-systems (accessed.
[27] "MAGNITUDE – Bringing flexibility provided by multi energy carrier integration to a new MAGNITUDE." https://www.magnitude-project.eu/ (accessed.
[28] X. Xing, J. Lin, Y. Song, and Q. Hu, "Maximum Production Point Tracking of a High-Temperature Power-to-Gas System: A Dynamic-Model-Based Study," *IEEE Transactions on Sustainable Energy,* vol. 11, no. 1, pp. 361-370, 2020, doi: 10.1109/TSTE.2019.2891296.
[29] J. Yang, N. Zhang, Y. Cheng, C. Kang, and Q. Xia, "Modeling the Operation Mechanism of Combined P2G and Gas-Fired Plant With CO2 Recycling," *IEEE Transactions on Smart Grid,* vol. 10, no. 1, pp. 1111-1121, 2019, doi: 10.1109/TSG.2018.2849619.
[30] E. Delage and Y. Ye, "Distributionally robust optimization under moment uncertainty with application to data-driven problems," *Operations research,* vol. 58, no. 3, pp. 595-612, 2010.
[31] J. Goh and M. Sim, "Distributionally robust optimization and its tractable approximations," *Operations research,* vol. 58, no. 4-part-1, pp. 902-917, 2010.
[32] G. A. Hanasusanto, D. Kuhn, S. W. Wallace, and S. Zymler, "Distributionally robust multi-item newsvendor problems with multimodal demand distributions," *Mathematical Programming,* vol. 152, no. 1-2, pp. 1-32, 2015.
[33] Z. Hu and L. J. Hong, "Kullback-Leibler divergence constrained distributionally robust optimization," *Available at Optimization Online,* 2013.
[34] D. Bertsimas, X. V. Doan, K. Natarajan, and C.-P. Teo, "Models for minimax stochastic linear optimization problems with risk aversion," *Mathematics of Operations Research,* vol. 35, no. 3, pp. 580-602, 2010.
[35] D. Bertsimas and I. Popescu, "Optimal inequalities in probability theory: A convex optimization approach," *SIAM Journal on Optimization,* vol. 15, no. 3, pp. 780-804, 2005.
[36] Y. Chen, W. Wei, F. Liu, and S. Mei, "Distributionally robust hydro-thermal-wind economic dispatch," *Applied Energy,* vol. 173, pp. 511-519, 2016/07/01/ 2016, doi: https://doi.org/10.1016/j.apenergy.2016.04.060.
[37] J. Blanchet, F. He, and K. Murthy, "On distributionally robust extreme value analysis," *Extremes,* pp. 1-31, 2020.
[38] R. T. Rockafellar and S. Uryasev, "Optimization of conditional value-at-risk," *Journal of risk,* vol. 2, pp. 21-42, 2000.
[39] S. Zhu and M. Fukushima, "Worst-case conditional value-at-risk with application to robust portfolio management," *Operations research,* vol. 57, no. 5, pp. 1155-1168, 2009.
[40] S. Dempe, "Directional differentiability of optimal solutions under Slater's condition," *Mathematical Programming,* vol. 59, no. 1-3, pp. 49-69, 1993.
[41] A. Ruszczyński and A. Shapiro, "Optimality and duality in stochastic programming," *Handbooks in Operations Research and Management Science,* vol. 10, pp. 65-139, 2003.
[42] R. Yadav, S. Raj, and A. K. Pradhan, "Real-Time Event Classification in Power System With Renewables Using Kernel Density Estimation and Deep Neural Network," *IEEE Transactions on Smart Grid,* vol. 10, no. 6, pp. 6849-6859, 2019, doi: 10.1109/TSG.2019.2912350.
[43] E. A. M. Ceseña and P. Mancarella, "Energy Systems Integration in Smart Districts: Robust Optimisation of Multi-Energy Flows in Integrated Electricity, Heat and Gas Networks," *IEEE*

Transactions on Smart Grid, vol. 10, no. 1, pp. 1122-1131, 2019, doi: 10.1109/TSG.2018.2828146.
[44] Y. Wang *et al.*, "Optimal Scheduling of the Regional Integrated Energy System Considering Economy and Environment," *IEEE Transactions on Sustainable Energy,* vol. 10, no. 4, pp. 1939-1949, 2019, doi: 10.1109/TSTE.2018.2876498.
[45] N. Liu, J. Wang, and L. Wang, "Hybrid Energy Sharing for Multiple Microgrids in an Integrated Heat–Electricity Energy System," *IEEE Transactions on Sustainable Energy,* vol. 10, no. 3, pp. 1139-1151, 2019, doi: 10.1109/TSTE.2018.2861986.
[46] Y. Cheng, N. Zhang, B. Zhang, C. Kang, W. Xi, and M. Feng, "Low-Carbon Operation of Multiple Energy Systems Based on Energy-Carbon Integrated Prices," *IEEE Transactions on Smart Grid,* pp. 1-1, 2019, doi: 10.1109/TSG.2019.2935736.
[47] S. Shin *et al.*, "A systematic review of quantitative resilience measures for water infrastructure systems," *Water,* vol. 10, no. 2, p. 164, 2018.
[48] V. M. Leiby and M. E. Burke, *Energy efficiency best practices for North American drinking water utilities*. WRF, 2011.
[49] A. S. Zamzam, E. Dall'Anese, C. Zhao, J. A. Taylor, and N. D. Sidiropoulos, "Optimal Water–Power Flow-Problem: Formulation and Distributed Optimal Solution," *IEEE Transactions on Control of Network Systems,* vol. 6, no. 1, pp. 37-47, 2019, doi: 10.1109/TCNS.2018.2792699.
[50] K. Oikonomou and M. Parvania, "Optimal Coordination of Water Distribution Energy Flexibility With Power Systems Operation," *IEEE Transactions on Smart Grid,* vol. 10, no. 1, pp. 1101-1110, 2019, doi: 10.1109/TSG.2018.2824308.
[51] Q. Li, S. Yu, A. S. Al-Sumaiti, and K. Turitsyn, "Micro Water–Energy Nexus: Optimal Demand-Side Management and Quasi-Convex Hull Relaxation," *IEEE Transactions on Control of Network Systems,* vol. 6, no. 4, pp. 1313-1322, 2019, doi: 10.1109/TCNS.2018.2889001.
[52] L. Ji, B. Zhang, G. Huang, and P. Wang, "A novel multi-stage fuzzy stochastic programming for electricity system structure optimization and planning with energy-water nexus - A case study of Tianjin, China," *Energy,* vol. 190, p. 116418, 2020/01/01/ 2020, doi: https://doi.org/10.1016/j.energy.2019.116418.
[53] C. Wang, N. Gao, J. Wang, N. Jia, T. Bi, and K. Martin, "Robust Operation of a Water-Energy Nexus: A Multi-energy Perspective," *IEEE Transactions on Sustainable Energy,* pp. 1-1, 2020, doi: 10.1109/TSTE.2020.2971259.
[54] F. Qi, M. Shahidehpour, F. Wen, Z. Li, Y. He, and M. Yan, "Decentralized Privacy-Preserving Operation of Multi-Area Integrated Electricity and Natural Gas Systems with Renewable Energy Resources," *IEEE Transactions on Sustainable Energy,* pp. 1-1, 2019, doi: 10.1109/TSTE.2019.2940624.
[55] F. Liu, Z. Bie, and X. Wang, "Day-Ahead Dispatch of Integrated Electricity and Natural Gas System Considering Reserve Scheduling and Renewable Uncertainties," *IEEE Transactions on Sustainable Energy,* vol. 10, no. 2, pp. 646-658, 2019, doi: 10.1109/TSTE.2018.2843121.
[56] C. Wang, R. Gao, W. Wei, M. Shafie-khah, T. Bi, and J. P. S. Catalão, "Risk-Based Distributionally Robust Optimal Gas-Power Flow With Wasserstein Distance," *IEEE Transactions on Power Systems,* vol. 34, no. 3, pp. 2190-2204, 2019, doi: 10.1109/TPWRS.2018.2889942.
[57] L. Wu, C. He, X. Zhang, and T. Liu, "Distributionally Robust Scheduling of Integrated Gas-Electricity Systems with Demand Response," *IEEE Transactions on Power Systems,* pp. 1-1, 2019, doi: 10.1109/TPWRS.2019.2907170.
[58] Y. Chen, Q. Guo, H. Sun, Z. Li, W. Wu, and Z. Li, "A Distributionally Robust Optimization Model for Unit Commitment Based on Kullback–Leibler Divergence," *IEEE Transactions on Power Systems,* vol. 33, no. 5, pp. 5147-5160, 2018, doi: 10.1109/TPWRS.2018.2797069.
[59] Z. Li, W. Wu, B. Zhang, and X. Tai, "Kullback–Leibler divergence-based distributionally robust optimisation model for heat pump day-ahead operational schedule to improve PV integration," *IET Generation, Transmission & Distribution,* vol. 12, no. 13, pp. 3136-3144, 2018, doi: 10.1049/iet-gtd.2017.2062.
[60] M. Asensio and J. Contreras, "Stochastic Unit Commitment in Isolated Systems With Renewable Penetration Under CVaR Assessment," *IEEE Transactions on Smart Grid,* vol. 7, no. 3, pp. 1356-1367, 2016, doi: 10.1109/TSG.2015.2469134.
[61] C. Peng, Y. Hou, N. Yu, and W. Wang, "Risk-Limiting Unit Commitment in Smart Grid With Intelligent Periphery," *IEEE Transactions on Power Systems,* vol. 32, no. 6, pp. 4696-4707, 2017, doi: 10.1109/TPWRS.2017.2672939.

[62] L. Yang, J. Jian, Y. Xu, Z. Dong, and G. Ma, "Multiple Perspective-Cuts Outer Approximation Method for Risk-Averse Operational Planning of Regional Energy Service Providers," *IEEE Transactions on Industrial Informatics*, vol. 13, no. 5, pp. 2606-2619, 2017, doi: 10.1109/TII.2017.2710055.

[63] T. Haktanır and M. Ardıçlıoğlu, "Numerical modeling of Darcy–Weisbach friction factor and branching pipes problem," *Advances in Engineering Software*, vol. 35, no. 12, pp. 773-779, 2004.

[64] X. Lu, K. W. Chan, S. Xia, B. Zhou, and X. Luo, "Security-Constrained Multiperiod Economic Dispatch With Renewable Energy Utilizing Distributionally Robust Optimization," *IEEE Transactions on Sustainable Energy*, vol. 10, no. 2, pp. 768-779, 2019, doi: 10.1109/TSTE.2018.2847419.

[65] W. Wei, F. Liu, and S. Mei, "Distributionally Robust Co-Optimization of Energy and Reserve Dispatch," *IEEE Transactions on Sustainable Energy*, vol. 7, no. 1, pp. 289-300, 2016, doi: 10.1109/TSTE.2015.2494010.

[66] I. I. o. T. Electrical and Computer Engineering Department. "Index of /data." motor.ece.iit.edu/data/ (accessed.

[67] P. Zhao, C. Gu, D. Huo, Y. Shen, and I. Hernando-Gil, "Two-Stage Distributionally Robust Optimization for Energy Hub Systems," *IEEE Transactions on Industrial Informatics*, vol. 16, no. 5, pp. 3460-3469, 2020, doi: 10.1109/TII.2019.2938444.

[68] D. COHEN, U. SHAMIR, and G. SINAI, "Optimal operation of multi-quality water supply systems-II: The QH model," *Engineering Optimization+ A35*, vol. 32, no. 6, pp. 687-719, 2000.

[69] J. C. Araneda, H. Rudnick, S. Mocarquer, and P. Miquel, "Lessons from the 2010 Chilean earthquake and its impact on electricity supply," in *2010 international conference on power system technology*, 2010: IEEE, pp. 1-7.

[70] J. Eidinger, "Wenchuan earthquake impact to power systems," in *TCLEE 2009: Lifeline Earthquake Engineering in a Multihazard Environment*, 2009, pp. 1-12.

[71] S. J. Brandenberg *et al.*, "Preliminary report on engineering and geological effects of the July 2019 Ridgecrest earthquake sequence," Geotechnical Extreme Event Reconnaissance Association, 2019.

[72] W. Yuan, J. Wang, F. Qiu, C. Chen, C. Kang, and B. Zeng, "Robust Optimization-Based Resilient Distribution Network Planning Against Natural Disasters," *IEEE Transactions on Smart Grid*, vol. 7, no. 6, pp. 2817-2826, 2016, doi: 10.1109/TSG.2015.2513048.

[73] S. Ma, B. Chen, and Z. Wang, "Resilience Enhancement Strategy for Distribution Systems Under Extreme Weather Events," *IEEE Transactions on Smart Grid*, vol. 9, no. 2, pp. 1442-1451, 2018, doi: 10.1109/TSG.2016.2591885.

[74] N. R. Romero, L. K. Nozick, I. D. Dobson, N. Xu, and D. A. Jones, "Transmission and Generation Expansion to Mitigate Seismic Risk," *IEEE Transactions on Power Systems*, vol. 28, no. 4, pp. 3692-3701, 2013, doi: 10.1109/TPWRS.2013.2265853.

[75] C. Shao, M. Shahidehpour, X. Wang, X. Wang, and B. Wang, "Integrated Planning of Electricity and Natural Gas Transportation Systems for Enhancing the Power Grid Resilience," *IEEE Transactions on Power Systems*, vol. 32, no. 6, pp. 4418-4429, 2017, doi: 10.1109/TPWRS.2017.2672728.

[76] C. He, C. Dai, L. Wu, and T. Liu, "Robust Network Hardening Strategy for Enhancing Resilience of Integrated Electricity and Natural Gas Distribution Systems Against Natural Disasters," *IEEE Transactions on Power Systems*, vol. 33, no. 5, pp. 5787-5798, 2018, doi: 10.1109/TPWRS.2018.2820383.

[77] S. Moslehi and T. A. Reddy, "Sustainability of integrated energy systems: A performance-based resilience assessment methodology," *Applied Energy*, vol. 228, pp. 487-498, 2018/10/15/ 2018, doi: https://doi.org/10.1016/j.apenergy.2018.06.075.

[78] C. Wang, R. Gao, W. Wei, M. Shafie-khah, T. Bi, and J. P. S. Catalao, "Risk-based Distributionally Robust Optimal Gas-Power Flow With Wasserstein Distance," *IEEE Transactions on Power Systems*, pp. 1-1, 2018, doi: 10.1109/TPWRS.2018.2889942.

[79] Y. Zhang, J. Le, F. Zheng, Y. Zhang, and K. Liu, "Two-stage distributionally robust coordinated scheduling for gas-electricity integrated energy system considering wind power uncertainty and reserve capacity configuration," *Renewable Energy*, vol. 135, pp. 122-135, 2019/05/01/ 2019, doi: https://doi.org/10.1016/j.renene.2018.11.094.

[80] T. Datta, "Seismic response of buried pipelines: a state-of-the-art review," *Nuclear Engineering and Design*, vol. 192, no. 2-3, pp. 271-284, 1999.

[81] D. J. Wald, V. Quitoriano, T. H. Heaton, and H. Kanamori, *Relationships between Peak Ground Acceleration, Peak Ground Velocity, and Modified Mercalli Intensity in California*. 1999, pp. 557-564.
[82] K. Poljanšek, F. Bono, and E. Gutiérrez, *GIS-based method to assess seismic vulnerability of interconnected infrastructure: A case of EU gas and electricity networks*. Office for Official Publications of the European Communities, 2010.
[83] F. E. M. Agency, "HAZUS-MH multi-hazard loss estimation methodology, earthquake model, technical manual," ed: FEMA Washington, DC, 2003.
[84] Y. Shen, C. Gu, X. Yang, and P. Zhao, "Impact Analysis of Seismic Events On Integrated Electricity and Natural Gas Systems," *IEEE Transactions on Power Delivery*, pp. 1-1, 2020, doi: 10.1109/TPWRD.2020.3017050.
[85] G. Huang, J. Wang, C. Chen, J. Qi, and C. Guo, "Integration of Preventive and Emergency Responses for Power Grid Resilience Enhancement," *IEEE Transactions on Power Systems*, vol. 32, no. 6, pp. 4451-4463, 2017, doi: 10.1109/TPWRS.2017.2685640.
[86] P. Hoffman, W. Bryan, M. Farber-DeAnda, M. Cleaver, C. Lewandowski, and K. Young, "Hardening and Resiliency, US Energy Industry Response to Recent Hurricane Seasons," *Office of Electricity Delivery and Energy Reliability, US Department of Energy, OE/ISER Final Report*, 2010.
[87] A. Mahmood, N. Javaid, and S. Razzaq, "A review of wireless communications for smart grid," *Renewable and sustainable energy reviews*, vol. 41, pp. 248-260, 2015.
[88] G. Liang, J. Zhao, F. Luo, S. R. Weller, and Z. Y. Dong, "A Review of False Data Injection Attacks Against Modern Power Systems," *IEEE Transactions on Smart Grid*, vol. 8, no. 4, pp. 1630-1638, 2017, doi: 10.1109/TSG.2015.2495133.
[89] G. Liang, S. R. Weller, J. Zhao, F. Luo, and Z. Y. Dong, "The 2015 ukraine blackout: Implications for false data injection attacks," *IEEE Transactions on Power Systems*, vol. 32, no. 4, pp. 3317-3318, 2016.
[90] L. Che, X. Liu, Z. Li, and Y. Wen, "False Data Injection Attacks Induced Sequential Outages in Power Systems," *IEEE Transactions on Power Systems*, vol. 34, no. 2, pp. 1513-1523, 2019, doi: 10.1109/TPWRS.2018.2871345.
[91] A. Tajer, "False Data Injection Attacks in Electricity Markets by Limited Adversaries: Stochastic Robustness," *IEEE Transactions on Smart Grid*, vol. 10, no. 1, pp. 128-138, 2019, doi: 10.1109/TSG.2017.2733346.
[92] R. Deng, P. Zhuang, and H. Liang, "False Data Injection Attacks Against State Estimation in Power Distribution Systems," *IEEE Transactions on Smart Grid*, vol. 10, no. 3, pp. 2871-2881, 2019, doi: 10.1109/TSG.2018.2813280.
[93] A. Ashok, M. Govindarasu, and V. Ajjarapu, "Online Detection of Stealthy False Data Injection Attacks in Power System State Estimation," *IEEE Transactions on Smart Grid*, vol. 9, no. 3, pp. 1636-1646, 2018, doi: 10.1109/TSG.2016.2596298.
[94] X. Wang, X. Luo, Y. Zhang, and X. Guan, "Detection and Isolation of False Data Injection Attacks in Smart Grids via Nonlinear Interval Observer," *IEEE Internet of Things Journal*, pp. 1-1, 2019, doi: 10.1109/JIOT.2019.2916670.
[95] Y. Yuan, Z. Li, and K. Ren, "Modeling Load Redistribution Attacks in Power Systems," *IEEE Transactions on Smart Grid*, vol. 2, no. 2, pp. 382-390, 2011, doi: 10.1109/TSG.2011.2123925.
[96] Y. Yuan, Z. Li, and K. Ren, "Quantitative Analysis of Load Redistribution Attacks in Power Systems," *IEEE Transactions on Parallel and Distributed Systems*, vol. 23, no. 9, pp. 1731-1738, 2012, doi: 10.1109/TPDS.2012.58.
[97] L. Che, X. Liu, and Z. Li, "Mitigating False Data Attacks Induced Overloads Using a Corrective Dispatch Scheme," *IEEE Transactions on Smart Grid*, vol. 10, no. 3, pp. 3081-3091, 2019, doi: 10.1109/TSG.2018.2817515.
[98] H. Shayan and T. Amraee, "Network Constrained Unit Commitment Under Cyber Attacks Driven Overloads," *IEEE Transactions on Smart Grid*, pp. 1-1, 2019, doi: 10.1109/TSG.2019.2904873.
[99] Z. Li, W. Wu, M. Shahidehpour, J. Wang, and B. Zhang, "Combined Heat and Power Dispatch Considering Pipeline Energy Storage of District Heating Network," *IEEE Transactions on Sustainable Energy*, vol. 7, no. 1, pp. 12-22, 2016, doi: 10.1109/TSTE.2015.2467383.
[100] Y. Zhou, W. Hu, Y. Min, and Y. Dai, "Integrated Power and Heat Dispatch Considering Available Reserve of Combined Heat and Power Units," *IEEE Transactions on Sustainable Energy*, vol. 10, no. 3, pp. 1300-1310, 2019, doi: 10.1109/TSTE.2018.2865562.

[101] S. Massucco, A. Pitto, and F. Silvestro, "A Gas Turbine Model for Studies on Distributed Generation Penetration Into Distribution Networks," *IEEE Transactions on Power Systems*, vol. 26, no. 3, pp. 992-999, 2011, doi: 10.1109/TPWRS.2010.2091290.
[102] R. Rigo-Mariani, C. Zhang, A. Romagnoli, M. Kraft, K. V. Ling, and J. Maciejowski, "A Combined Cycle Gas Turbine Model for Heat and Power Dispatch Subject to Grid Constraints," *IEEE Transactions on Sustainable Energy*, vol. 11, no. 1, pp. 448-456, 2020, doi: 10.1109/TSTE.2019.2894793.
[103] Y. Li *et al.*, "Optimal Stochastic Operation of Integrated Low-Carbon Electric Power, Natural Gas, and Heat Delivery System," *IEEE Transactions on Sustainable Energy*, vol. 9, no. 1, pp. 273-283, 2018, doi: 10.1109/TSTE.2017.2728098.
[104] Y. He, M. Shahidehpour, Z. Li, C. Guo, and B. Zhu, "Robust Constrained Operation of Integrated Electricity-Natural Gas System Considering Distributed Natural Gas Storage," *IEEE Transactions on Sustainable Energy*, vol. 9, no. 3, pp. 1061-1071, 2018, doi: 10.1109/TSTE.2017.2764004.
[105] Y. Li, Z. Li, F. Wen, and M. Shahidehpour, "Minimax-Regret Robust Co-Optimization for Enhancing the Resilience of Integrated Power Distribution and Natural Gas Systems," *IEEE Transactions on Sustainable Energy*, vol. 11, no. 1, pp. 61-71, 2020, doi: 10.1109/TSTE.2018.2883718.
[106] P. Zhao, H. Wu, C. Gu, and I. H. Gil, "Optimal Home Energy Management under Hybrid PV-Storage Uncertainty: A Distributionally Robust Chance-Constrained Approach," *IET Renewable Power Generation*, p. 9, 2019.
[107] C. Wang, R. Gao, F. Qiu, J. Wang, and L. Xin, "Risk-Based Distributionally Robust Optimal Power Flow With Dynamic Line Rating," *IEEE Transactions on Power Systems*, vol. 33, no. 6, pp. 6074-6086, 2018, doi: 10.1109/TPWRS.2018.2844356.
[108] T. Ding, C. Li, Y. Yang, J. Jiang, Z. Bie, and F. Blaabjerg, "A Two-Stage Robust Optimization for Centralized-Optimal Dispatch of Photovoltaic Inverters in Active Distribution Networks," *IEEE Transactions on Sustainable Energy*, vol. 8, no. 2, pp. 744-754, 2017, doi: 10.1109/TSTE.2016.2605926.
[109] H. Gao, J. Liu, and L. Wang, "Robust Coordinated Optimization of Active and Reactive Power in Active Distribution Systems," *IEEE Transactions on Smart Grid*, vol. 9, no. 5, pp. 4436-4447, 2018, doi: 10.1109/TSG.2017.2657782.
[110] M. Qadrdan, J. Wu, N. Jenkins, and J. Ekanayake, "Operating Strategies for a GB Integrated Gas and Electricity Network Considering the Uncertainty in Wind Power Forecasts," *IEEE Transactions on Sustainable Energy*, vol. 5, no. 1, pp. 128-138, 2014, doi: 10.1109/TSTE.2013.2274818.
[111] B. Odetayo, J. MacCormack, W. D. Rosehart, and H. Zareipour, "A sequential planning approach for Distributed generation and natural gas networks," *Energy*, vol. 127, pp. 428-437, 2017/05/15/ 2017, doi: https://doi.org/10.1016/j.energy.2017.03.118.
[112] R. Mageshvaran and T. Jayabarathi, "Steady state load shedding to mitigate blackout in power systems using an improved harmony search algorithm," *Ain Shams Engineering Journal*, vol. 6, no. 3, pp. 819-834, 2015/09/01/ 2015, doi: https://doi.org/10.1016/j.asej.2014.12.014.
[113] A. S. Musleh, G. Chen, and Z. Y. Dong, "A Survey on the Detection Algorithms for False Data Injection Attacks in Smart Grids," *IEEE Transactions on Smart Grid*, pp. 1-1, 2019, doi: 10.1109/TSG.2019.2949998.
[114] R. J. Kuo and C. C. Huang, "Application of particle swarm optimization algorithm for solving bi-level linear programming problem," *Computers & Mathematics with Applications*, vol. 58, no. 4, pp. 678-685, 2009/08/01/ 2009, doi: https://doi.org/10.1016/j.camwa.2009.02.028.
[115] S. Sengupta, S. Basak, and R. A. Peters, "Particle Swarm Optimization: A survey of historical and recent developments with hybridization perspectives," *Machine Learning and Knowledge Extraction*, vol. 1, no. 1, pp. 157-191, 2019.
[116] R. J. Kuo and Y. S. Han, "A hybrid of genetic algorithm and particle swarm optimization for solving bi-level linear programming problem – A case study on supply chain model," *Applied Mathematical Modelling*, vol. 35, no. 8, pp. 3905-3917, 2011/08/01/ 2011, doi: https://doi.org/10.1016/j.apm.2011.02.008.
[117] D. E. Kvasov and M. S. Mukhametzhanov, "Metaheuristic vs. deterministic global optimization algorithms: The univariate case," *Applied Mathematics and Computation*, vol. 318, pp. 245-259, 2018/02/01/ 2018, doi: https://doi.org/10.1016/j.amc.2017.05.014.
[118] B. Zeng, "Solving two-stage robust optimization problems by a constraint-and-column generation method," *University of South Florida, FL, Tech. Rep*, 2011.

[119] B. L. Gorissen, İ. Yanıkoğlu, and D. den Hertog, "A practical guide to robust optimization," *Omega,* vol. 53, pp. 124-137, 2015.
[120] B. A. d. Souza and A. M. F. d. Almeida, "Multiobjective Optimization and Fuzzy Logic Applied to Planning of the Volt/Var Problem in Distributions Systems," *IEEE Transactions on Power Systems,* vol. 25, no. 3, pp. 1274-1281, 2010, doi: 10.1109/TPWRS.2010.2042734.
[121] H. Ahmadi, J. R. Martí, and H. W. Dommel, "A Framework for Volt-VAR Optimization in Distribution Systems," *IEEE Transactions on Smart Grid,* vol. 6, no. 3, pp. 1473-1483, 2015, doi: 10.1109/TSG.2014.2374613.
[122] A. Padilha-Feltrin, D. A. Q. Rodezno, and J. R. S. Mantovani, "Volt-VAR Multiobjective Optimization to Peak-Load Relief and Energy Efficiency in Distribution Networks," *IEEE Transactions on Power Delivery,* vol. 30, no. 2, pp. 618-626, 2015, doi: 10.1109/TPWRD.2014.2336598.
[123] R. Zafar, J. Ravishankar, J. E. Fletcher, and H. R. Pota, "Optimal Dispatch of Battery Energy Storage System using Convex Relaxations in Unbalanced Distribution Grids," *IEEE Transactions on Industrial Informatics,* pp. 1-1, 2019, doi: 10.1109/TII.2019.2912925.
[124] K. Kumar, S. Satsangi, and G. B. Kumbhar, "Extension of life of distribution transformer using Volt-VAr optimisation in a distribution system," *IET Generation, Transmission & Distribution,* vol. 13, no. 10, pp. 1777-1785, 2019, doi: 10.1049/iet-gtd.2018.5746.
[125] D. Jin, H. Chiang, and P. Li, "Two-Timescale Multi-Objective Coordinated Volt/Var Optimization for Active Distribution Networks," *IEEE Transactions on Power Systems,* pp. 1-1, 2019, doi: 10.1109/TPWRS.2019.2914923.
[126] T. Niknam, M. Zare, and J. Aghaei, "Scenario-Based Multiobjective Volt/Var Control in Distribution Networks Including Renewable Energy Sources," *IEEE Transactions on Power Delivery,* vol. 27, no. 4, pp. 2004-2019, 2012, doi: 10.1109/TPWRD.2012.2209900.
[127] F. U. Nazir, B. C. Pal, and R. A. Jabr, "A Two-Stage Chance Constrained Volt/Var Control Scheme for Active Distribution Networks With Nodal Power Uncertainties," *IEEE Transactions on Power Systems,* vol. 34, no. 1, pp. 314-325, 2019, doi: 10.1109/TPWRS.2018.2859759.
[128] D. Choeum and D. Choi, "OLTC-Induced False Data Injection Attack on Volt/VAR Optimization in Distribution Systems," *IEEE Access,* vol. 7, pp. 34508-34520, 2019, doi: 10.1109/ACCESS.2019.2904959.
[129] A. D. Le, M. A. Kashem, M. Negnevitsky, and G. Ledwich, "Minimising voltage deviation in distribution feeders by optimising size and location of distributed generation," *Australian Journal of Electrical and Electronics Engineering,* vol. 3, no. 2, pp. 147-155, 2007/01/01 2007, doi: 10.1080/1448837X.2007.11464155.
[130] J. A. Sa'ed, N. Ismail, S. Favuzza, M. G. Ippolito, and F. Massaro, "Effect of voltage deviations on power distribution losses in presence of DG technology," in *2015 International Conference on Renewable Energy Research and Applications (ICRERA)*, 22-25 Nov. 2015 2015, pp. 766-771, doi: 10.1109/ICRERA.2015.7418515.
[131] Y. P. Agalgaonkar, B. C. Pal, and R. A. Jabr, "Stochastic Distribution System Operation Considering Voltage Regulation Risks in the Presence of PV Generation," *IEEE Transactions on Sustainable Energy,* vol. 6, no. 4, pp. 1315-1324, 2015, doi: 10.1109/TSTE.2015.2433794.
[132] T. Ding, S. Liu, W. Yuan, Z. Bie, and B. Zeng, "A Two-Stage Robust Reactive Power Optimization Considering Uncertain Wind Power Integration in Active Distribution Networks," *IEEE Transactions on Sustainable Energy,* vol. 7, no. 1, pp. 301-311, 2016, doi: 10.1109/TSTE.2015.2494587.
[133] A. Martinez-Mares and C. R. Fuerte-Esquivel, "A Unified Gas and Power Flow Analysis in Natural Gas and Electricity Coupled Networks," *IEEE Transactions on Power Systems,* vol. 27, no. 4, pp. 2156-2166, 2012, doi: 10.1109/TPWRS.2012.2191984.
[134] C. Unsihuay-Vila, J. W. Marangon-Lima, A. C. Z. d. Souza, I. J. Perez-Arriaga, and P. P. Balestrassi, "A Model to Long-Term, Multiarea, Multistage, and Integrated Expansion Planning of Electricity and Natural Gas Systems," *IEEE Transactions on Power Systems,* vol. 25, no. 2, pp. 1154-1168, 2010, doi: 10.1109/TPWRS.2009.2036797.
[135] C. He, L. Wu, T. Liu, and M. Shahidehpour, "Robust Co-Optimization Scheduling of Electricity and Natural Gas Systems via ADMM," *IEEE Transactions on Sustainable Energy,* vol. 8, no. 2, pp. 658-670, 2017, doi: 10.1109/TSTE.2016.2615104.
[136] Q. Bian, H. Xin, Z. Wang, D. Gan, and K. P. Wong, "Distributionally Robust Solution to the Reserve Scheduling Problem With Partial Information of Wind Power," *IEEE Transactions on Power Systems,* vol. 30, no. 5, pp. 2822-2823, 2015, doi: 10.1109/TPWRS.2014.2364534.

[137] P. M. Esfahani and D. Kuhn, "Data-driven distributionally robust optimization using the Wasserstein metric: Performance guarantees and tractable reformulations," *Mathematical Programming*, vol. 171, no. 1-2, pp. 115-166, 2018.
[138] C. Duan, L. Jiang, W. Fang, and J. Liu, "Data-Driven Affinely Adjustable Distributionally Robust Unit Commitment," *IEEE Transactions on Power Systems*, vol. 33, no. 2, pp. 1385-1398, 2018, doi: 10.1109/TPWRS.2017.2741506.
[139] A. T. Davda, B. Azzopardi, B. R. Parekh, and M. D. Desai, "Dispersed Generation Enable Loss Reduction and Voltage Profile Improvement in Distribution Network—Case Study, Gujarat, India," *IEEE Transactions on Power Systems*, vol. 29, no. 3, pp. 1242-1249, 2014, doi: 10.1109/TPWRS.2013.2292117.
[140] A. G. Exposito, J. L. M. Ramos, J. L. R. Macias, and Y. C. Salinas, "Sensitivity-based reactive power control for voltage profile improvement," *IEEE Transactions on Power Systems*, vol. 8, no. 3, pp. 937-945, 1993, doi: 10.1109/59.260908.
[141] M. Zeraati, M. E. H. Golshan, and J. M. Guerrero, "Voltage Quality Improvement in Low Voltage Distribution Networks Using Reactive Power Capability of Single-Phase PV Inverters," *IEEE Transactions on Smart Grid*, vol. 10, no. 5, pp. 5057-5065, 2019, doi: 10.1109/TSG.2018.2874381.
[142] J. Vanishree and V. Ramesh, "Voltage profile improvement in power systems - A review," in *2014 International Conference on Advances in Electrical Engineering (ICAEE)*, 9-11 Jan. 2014 2014, pp. 1-4, doi: 10.1109/ICAEE.2014.6838533.
[143] F. Mancilla–David, A. Angulo, and A. Street, "Power Management in Active Distribution Systems Penetrated by Photovoltaic Inverters: A Data–Driven Robust Approach," *IEEE Transactions on Smart Grid*, pp. 1-1, 2019, doi: 10.1109/TSG.2019.2951086.
[144] M. B. Liu, C. A. Canizares, and W. Huang, "Reactive Power and Voltage Control in Distribution Systems With Limited Switching Operations," *IEEE Transactions on Power Systems*, vol. 24, no. 2, pp. 889-899, 2009, doi: 10.1109/TPWRS.2009.2016362.
[145] M. E. Baran and F. F. Wu, "Network reconfiguration in distribution systems for loss reduction and load balancing," *IEEE Transactions on Power Delivery*, vol. 4, no. 2, pp. 1401-1407, 1989, doi: 10.1109/61.25627.
[146] E. Home, I. General, S. Business, N. F. Act, and W. Protection, "2018 Wind Technologies Market Report."
[147] C. He, L. Wu, T. Liu, and Z. Bie, "Robust Co-Optimization Planning of Interdependent Electricity and Natural Gas Systems With a Joint N-1 and Probabilistic Reliability Criterion," *IEEE Transactions on Power Systems*, vol. 33, no. 2, pp. 2140-2154, 2018, doi: 10.1109/TPWRS.2017.2727859.
[148] Q. Zeng, B. Zhang, J. Fang, and Z. Chen, "A bi-level programming for multistage co-expansion planning of the integrated gas and electricity system," *Applied Energy*, vol. 200, pp. 192-203, 2017/08/15/ 2017, doi: https://doi.org/10.1016/j.apenergy.2017.05.022.
[149] Z. Yang, C. Gao, and M. Zhao, "The Optimal Investment Strategy of P2G based on Real Option Theory," *IEEE Access*, pp. 1-1, 2019, doi: 10.1109/ACCESS.2019.2910259.
[150] D. Alkano and J. M. A. Scherpen, "Distributed Supply Coordination for Power-to-Gas Facilities Embedded in Energy Grids," *IEEE Transactions on Smart Grid*, vol. 9, no. 2, pp. 1012-1022, 2018, doi: 10.1109/TSG.2016.2574568.
[151] I. Union, "Petroleum B. guidebook to gas interchangeability and gas quality," 2011.
[152] H. de Vries, A. V. Mokhov, and H. B. Levinsky, "The impact of natural gas/hydrogen mixtures on the performance of end-use equipment: Interchangeability analysis for domestic appliances," *Applied Energy*, vol. 208, pp. 1007-1019, 2017/12/15/ 2017, doi: https://doi.org/10.1016/j.apenergy.2017.09.049.
[153] M. Abeysekera, J. Wu, N. Jenkins, and M. Rees, "Steady state analysis of gas networks with distributed injection of alternative gas," *Applied Energy*, vol. 164, pp. 991-1002, 2016/02/15/ 2016, doi: https://doi.org/10.1016/j.apenergy.2015.05.099.
[154] M. Deymi-Dashtebayaz, A. Ebrahimi-Moghadam, S. I. Pishbin, and M. Pourramezan, "Investigating the effect of hydrogen injection on natural gas thermo-physical properties with various compositions," *Energy*, vol. 167, pp. 235-245, 2019/01/15/ 2019, doi: https://doi.org/10.1016/j.energy.2018.10.186.
[155] L. de Santoli, G. Lo Basso, and D. Bruschi, "A small scale H2NG production plant in Italy: Techno-economic feasibility analysis and costs associated with carbon avoidance," *International Journal of Hydrogen Energy*, vol. 39, no. 12, pp. 6497-6517, 2014/04/15/ 2014, doi: https://doi.org/10.1016/j.ijhydene.2014.02.003.

[156] I. A. Gondal, "Hydrogen integration in power-to-gas networks," *International Journal of Hydrogen Energy*, vol. 44, no. 3, pp. 1803-1815, 2019/01/15/ 2019, doi: https://doi.org/10.1016/j.ijhydene.2018.11.164.
[157] A. R. Sayed, C. Wang, J. Zhao, and T. Bi, "Distribution-level Robust Energy Management of Power Systems Considering Bidirectional Interactions with Gas Systems," *IEEE Transactions on Smart Grid*, pp. 1-1, 2019, doi: 10.1109/TSG.2019.2947219.
[158] P. Zhao, C. Gu, D. Huo, Y. Shen, and I. Hernando-Gil, "Two-Stage Distributionally Robust Optimization for Energy Hub Systems," *IEEE Transactions on Industrial Informatics*, pp. 1-1, 2019, doi: 10.1109/TII.2019.2938444.
[159] C. Toro and E. Sciubba, "Sabatier based power-to-gas system: Heat exchange network design and thermoeconomic analysis," *Applied Energy*, vol. 229, pp. 1181-1190, 2018/11/01/ 2018, doi: https://doi.org/10.1016/j.apenergy.2018.08.036.
[160] J. Qiu, J. Zhao, H. Yang, D. Wang, and Z. Y. Dong, "Planning of solar photovoltaics, battery energy storage system and gas micro turbine for coupled micro energy grids," *Applied Energy*, vol. 219, pp. 361-369, 2018/06/01/ 2018, doi: https://doi.org/10.1016/j.apenergy.2017.09.066.